

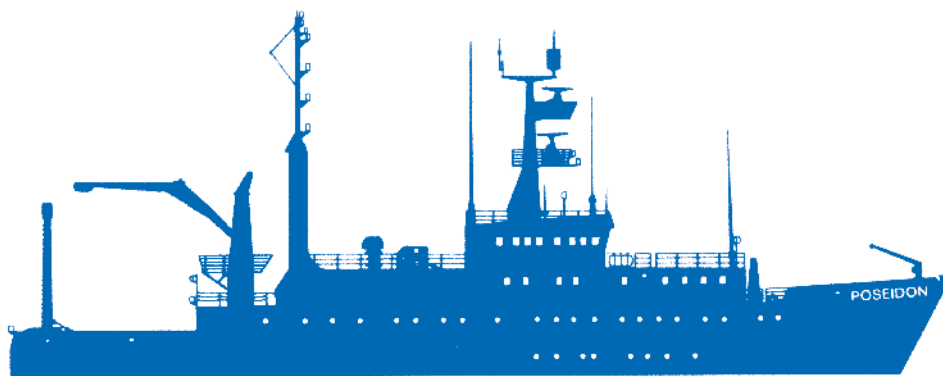


Helmholtz-Zentrum für Ozeanforschung Kiel

RV POSEIDON Fahrtbericht / Cruise Report POS524

GrimseyEM: Geophysical and geological investigations in the vicinity of the Grimsey Hydrothermal Field offshore Northern Iceland for the assessment of the geothermal potential and the exploration for potential mineralizations within the seafloor

Reykjavik (Iceland) – Bergen (Norway)
7.6 - 26.6.2018



Berichte aus dem GEOMAR
Helmholtz-Zentrum für Ozeanforschung Kiel

Nr. 44 (N. Ser.)

October 2018

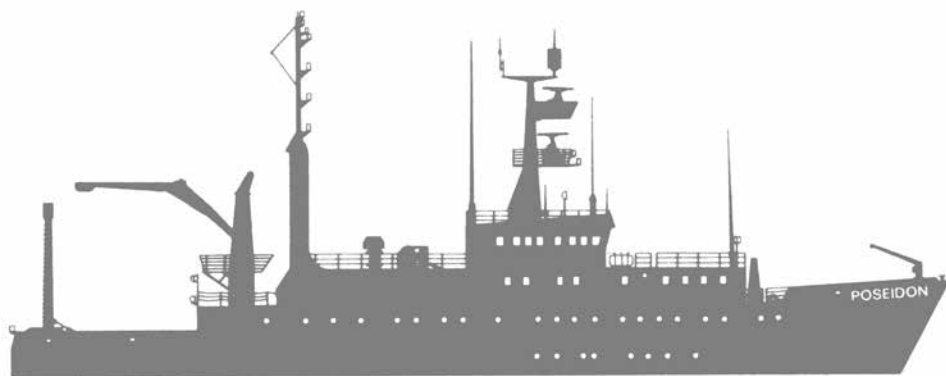


Helmholtz-Zentrum für Ozeanforschung Kiel

RV POSEIDON Fahrtbericht / Cruise Report POS524

GrimseyEM: Geophysical and geological investigations in the vicinity of the Grimsey Hydrothermal Field offshore Northern Iceland for the assessment of the geothermal potential and the exploration for potential mineralizations within the seafloor

Reykjavik (Iceland) – Bergen (Norway)
7.6 - 26.6.2018



Berichte aus dem GEOMAR
Helmholtz-Zentrum für Ozeanforschung Kiel

Nr. 44 (N. Ser.)

October 2018

Das GEOMAR Helmholtz-Zentrum für Ozeanforschung Kiel
ist Mitglied der Helmholtz-Gemeinschaft
Deutscher Forschungszentren e.V.

The GEOMAR Helmholtz Centre for Ocean Research Kiel
is a member of the Helmholtz Association of
German Research Centres

Herausgeber / Editor:
Sebastian Hölz and Sofia Martins

GEOMAR Report
ISSN Nr. 2193-8113, DOI 10.3289/GEOMAR_REP_NS_44_2018

Helmholtz-Zentrum für Ozeanforschung Kiel / Helmholtz Centre for Ocean Research Kiel
GEOMAR
Dienstgebäude Westufer / West Shore Building
Düsternbrooker Weg 20
D-24105 Kiel
Germany

Helmholtz-Zentrum für Ozeanforschung Kiel / Helmholtz Centre for Ocean Research Kiel
GEOMAR
Dienstgebäude Ostufer / East Shore Building
Wischhofstr. 1-3
D-24148 Kiel
Germany

Tel.: +49 431 600-0
Fax: +49 431 600-2805
www.geomar.de

Table of Contents

1. Summary - Zusammenfassung.....	2
2. Participants.....	6
3. Research Program.....	7
3.1. General.....	7
3.2. Geological Target.....	8
4. Narrative of Cruise.....	11
5. Applied Methods & Preliminary Results.....	15
5.1. Electric and Electromagnetic Instruments & Experiments.....	15
5.1.1. MARTEMIS Coil System – TEM Measurements.....	17
5.1.2. Coil2Dipole.....	23
5.1.3. Dual Polarization CSEM.....	27
5.1.4. Selfpotential.....	29
5.2. Heatflow.....	30
5.3. Gravity Coring.....	32
5.4. CTD.....	36
6. Data and Sample Storage and Availability.....	37
7. Acknowledgments.....	37
8. References.....	38
9. Appendix.....	40
9.1. Station Log.....	40
9.2. Station Protocol Heatflow.....	47
9.3. Core Descriptions.....	48
9.4. Pore Fluid Samples.....	69

1. Summary - Zusammenfassung

In the marine environment elevated electrical conductivities may be caused by sulfide mineralizations within the seafloor as well as hot saline pore fluids. Such conductive targets may be studied with suitable electromagnetic systems like the novel coil-system MARTEMIS¹, which we previously used to investigate a known zone of sediment covered mineralization at the Palinuro Seamount (cruises POS483 & POS509) and in the vicinity of the TAG hydrothermal mound at the Mid Atlantic Ridge (cruise JC138). Both the Palinuro site as well as the sites in the vicinity of the TAG hydrothermal mound (Shinkai, Double Mound, MIR) are hydrothermally inactive and, thus, allowed to study, how the responses of an inductive EM system is influenced and shaped by mineralizations within the seafloor without having to consider the effect of heated pore fluids. In the interpretation of the collected data at these inactive sites we learned that the MARTEMIS system is able to detect conductivity anomalies in the vicinity of mineralizations.

The main objective of cruise POS524 to the Grimsey Vent Field (GVF), to the North of Iceland, which is presented in this report, was to study the suitability of the MARTEMIS system (as well as other EM systems / configurations) for the characterization of an active hydrothermal system. The hydrothermal system had previously been studied during several GEOMAR cruises in the late 90s to early 2000s (POS229, POS253, POS291), during which high temperature venting was observed – temperatures between 200 – 250°C were reported by Botz et al. (1999) – but no massive sulfide mineralization, which would be expected to some degree in such a geotectonic setting, were found (e.g. Hannington et al., 2001). Thus, as second objective it was projected that EM investigations would not only give insight into the hydrothermal structure, but could potentially also reveal covered mineralizations at depth. To facilitate interpretations, EM investigations were accompanied by geophysical (heat probe) and geological (gravity core) measurements for ground truthing and to gain further structural insight.

During cruise POS524 successful measurements with the MARTEMIS coil system were carried out covering the hydrothermally active area as defined in Hannington et al. (2001) with about 15km of profiles. Additional measurements were carried out along 2.5km of profile around a second site of interest to the north of the hydrothermal field and, additionally, along a 2.5km long profile connecting the two working areas, which most likely cover background sediments. Signals transmitted with the MARTEMIS coil were also recorded by 12 stationary, remote OBEM receivers, which had been installed prior to the first experiment. This “Coil2Dipole” experiment with a moving coil as transmitter and stationary OBEMs as receivers, has an increased depth of penetration (~100m) as compared to the pure MARTEMIS coil measurements (~30m) and will hopefully yield complementary information for the EM interpretation. As part of these experiment, measurements of the self-potential (... actually of the ambient horizontal electric field ...) were also carried out. Additionally, we performed a novel EM experiment (working title: “Dual Polarization”), in which the coil frame of the MARTEMIS system was used to carry two perpendicular pairs of transmitter electrodes, thus, allowing for a CSEM experiment with two independent transmitter dipole polarizations, which will yield an increased depth of investigation (~250m). The Dual Polarization experiment was carried out along a 3.7km long W ↔ E profile crossing the active hydrothermal vent field. Transmitted signals were recorded by 9 stationary OBEM receivers along the profile. Active EM experiments were concluded by running a second MARTEMIS experiment along 20km of profiles. A first review of the

1 Marine transient electromagnetic induction system

coil data revealed some problems caused by a damaged cable of the receiver coil and it is not clear if it will be possible to use this MARTEMIS data set. However, the data measured with the remote OBEM receivers during this last deployment, will yield an additional Coil2Dipole data set.

EM investigations were accompanied by measurements with a 2.2m long heat probe. They may yield valuable data for the interpretation of EM data, potentially aiding in distinguishing between anomalies in the EM data caused by hydrothermal activity or anomalies caused by mineralizations. Successful temperature measurements were acquired at a total of 14 stations, at 8 of these stations thermal conductivity data was also acquired.

Finally, geological samples were collected with a 3m long gravity corer for ground truthing and to gain further structural insight. In total about 20m of core material was collected at 8 stations. Temperature measurements were directly performed on deck and sampling of the pore fluids will help in the interpretation of EM data by yielding in situ salinities of fluids taken from the active field as well as fluids taken in background areas.

The combination of experiments proved to be convenient in terms of handling on the ship, as EM experiments on the one hand and measurements with heat probe and gravity coring on the other hand were usually performed in an alternating manner each other day. This alternating style of experiments gave each method time for adjustments and repairs as well as time to take a first look at measurements.

In summary, the following first results were obtained during the cruise:

1. Highly elevated temperatures ($>60^{\circ}\text{C}$) were measured with the heat-flow probe to the east of the previously depicted area (station HF04). This indicates that the extent of the active area is larger than previously known. In a gravity core which we tried to take at the same location (GC06), only 31.5°C were measured at deck in the core catcher. This seems to indicate that temperature varies significantly over short distances. This observation, distinct temperature measurement in a very short distance, points to a strong tectonic control in hydrothermal influence, with faults acting as fluid pathways.
2. Increases in temperature and thermal conductivity towards the north (HF14) as well as strong H_2S smell and elevated temperatures in cores (GC04 & GC05) at the – up to date – most northerly sampled sites from the GVF show that the hydrothermal influence extent more than 2.5 km north of the main hydrothermal mound along an inferred N-S fault.
3. Calibration measurements with the MARTEMIS system show that improvements to the mechanical setup of the system, which were implemented after the 2017 cruise to Palinuro, were successful in the sense that previous distortions in measurements, which had been caused by metal parts on the coil frame, are now completely absent.
4. A first interpretation of the MARTEMIS coil data shows systematically increased, anomalous amplitudes above and around the previously mapped hydrothermal area. Additional anomalies were detected further to the east, either showing that the active area is larger than previously known or, potentially giving a first speculative indication towards hidden massive sulfides.

Upcoming work will aim to further integrate results of all methods into a joint interpretation, which will guide investigations to be carried out during the approved cruise POS535 in June 2019.

Im marinen Umfeld können erhöhte elektrische Leitfähigkeiten sowohl durch Vererzungen als auch durch heiße, saline Fluide verursacht werden. Solche leitfähigen Untersuchungsziele können mit geeigneten elektromagnetischen Systemen wie dem am GEOMAR entwickelten Spulensystem MARTEMIS untersucht werden. Mit diesem System hatten wir bereits marine Massivsulfide untersucht, z.B. eine sedimentbedeckte Mineralisierung am Palinuro Seamount (Ausfahrten POS483 & POS509) und geologische Ziele in der Nähe des TAG Hydrothermalfeldes am Mittelatlantischen Rücken (Ausfahrt JC138). Sowohl Palinuro als auch die Mounds in der Nähe des TAG-Hydrothermalfeldes (Shinkai, Double Mound, MIR) sind hydrothermal inaktiv und erlauben somit zu untersuchen, wie Messungen eines induktiven EM-Systems durch Mineralisierungen beeinflusst werden, ohne die Wirkung von erhitzten Porenfluiden berücksichtigen zu müssen. Bei der Interpretation der gesammelten Daten an diesen inaktiven Standorten haben wir festgestellt, dass das MARTEMIS-System in der Lage ist, Leitfähigkeitsanomalien in der Umgebung von Mineralisierungen zu detektieren.

Das Hauptziel der Ausfahrt POS524 zum Grimsey Hydrothermalfeld nördlich von Island, das in diesem Bericht vorgestellt wird, war die Untersuchung der Eignung des MARTEMIS Systems (sowie anderer EM-Systeme / Konfigurationen) für die Charakterisierung eines aktiven hydrothermalen Systems. Das Hydrothermalfeld wurde bereits während mehrerer Ausfahrten des GEOMARs in den späten 90ern bis frühen 2000ern untersucht (POS229, POS253, POS291). Während dieser Ausfahrten wurde eine substantielle hydrothermale Aktivität beobachtet (Temperaturen zwischen 200 - 250°C in Botz et al., 1999). Es wurden jedoch keine Massivsulfide gefunden, die zu einem gewissen Grad in einer solchen geotektonischen Umgebung zu erwarten wären (s. z. B. Hannington et al., 2001). Zweites Ziel der EM-Untersuchungen war somit nicht nur Einblicke in die hydrothermale Struktur zu erhalten, sondern weiterhin auch Hinweise auf verdeckte Mineralisierungen in der Tiefe zu erhalten. Um die Interpretation zu erleichtern, wurden EM-Untersuchungen mit geophysikalischen (Wärmesonde) und geologischen (Schwerelot) Messungen kombiniert, um die Interpretation der EM Daten zu unterstützen und weitere strukturelle Einblicke zu gewinnen.

Während der Ausfahrt POS524 wurden erfolgreiche Messungen mit dem MARTEMIS Spulensystem durchgeführt, die den hydrothermal aktiven Bereich (s. Hannington et al., 2001) mit Profilen mit einer Gesamtlänge von ca. 15km abdecken. Zusätzliche Messungen wurden entlang eines Profils von 2,5km Länge an einer zweiten auffälligen Struktur nördlich des hydrothermalen Feldes und zusätzlich entlang eines 2,5km langen Profils durchgeführt, das die zwei Arbeitsbereiche verbindet. Signale, die mit der MARTEMIS Senderspule gesendet wurden, wurden außerdem von 12 stationären, OBEM Empfängern aufgezeichnet, die vor dem ersten Experiment installiert worden waren. Dieses "Coil2Dipole" Experiment mit einer beweglichen Spule als Sender und stationären OBEMs als Empfänger hat eine erhöhte Eindringtiefe (~ 100 m) im Vergleich zu den reinen MARTEMIS Spulenmessungen (~ 30 m) und wird komplementäre Informationen für die EM-Interpretation liefern. Im Rahmen dieses Experiments wurden auch Messungen des Eigenpotentials (... eigentlich des natürlichen horizontalen elektrischen Feldes ...) durchgeführt. Zusätzlich führten wir ein neuartiges EM-Experiment durch (Arbeitstitel: "Dual Polarization"), bei dem am Spulenrahmen des MARTEMIS Systems zwei orthogonale Senderelektrodenpaaren befestigt wurden, was ein CSEM Experiment mit zwei unabhängigen Senderdipolpolarisationen ermöglicht, die eine erhöhte Ein-

dringtiefe erlauben (~300m). Das "Dual Polarization"-Experiment wurde entlang eines 3.7 km langen W-E-Profils durchgeführt, welches das aktive hydrothermale Feld kreuzt. Die ausgesendeten Signale wurden von 9 stationären OBEM Empfängern entlang des Profils aufgezeichnet. Die aktiven EM-Experimente wurden mit einem zweiten MARTEMIS Experiment entlang von Profilen mit einer Gesamtlänge von 20km abgeschlossen. Eine erste Überprüfung der Spulendaten zeigt hier aber Probleme, die offensichtlich durch ein beschädigtes Kabel der Empfängerspule verursacht wurden. Es ist nicht klar, ob es möglich sein wird, diesen MARTEMIS Datensatz zu verwenden. Die Daten, die während dieser letzten Implementierung mit den entfernten OBEM Empfängern gemessen wurden, können jedoch als zusätzlichen Coil2Dipol-Datensatz ausgewertet werden.

EM-Untersuchungen wurden von Messungen mit einer 2,2m langen Wärmesonde begleitet. Diese können wertvolle Daten für die Interpretation von EM-Daten sowie Hinweise darauf liefern, ob eine Anomalien in den EM-Daten durch hydrothermale Aktivität oder durch Mineralisierungen verursacht wird. Erfolgreiche Temperaturmessungen wurden an insgesamt 14 Stationen durchgeführt, an 8 dieser Stationen wurden auch Messungen der thermischen Leitfähigkeit durchgeführt.

Weiterhin wurden Proben mit einem 3m langen Schwerelot gesammelt, die weitere strukturelle Einblicke ermöglichen. Insgesamt wurde an 8 Stationen ca. 20m Kernmaterial gewonnen und Temperaturmessungen wurden direkt an Deck durchgeführt. Die Probenahme von Porenfluiden erlaubt die in-situ Bestimmung von Salinitäten und liefert somit einen wichtigen Parameter für die Interpretation der EM-Daten.

Die Kombination der Experimente erwies sich im Einsatz auf dem Schiff als sehr gut abgestimmt, da durch den täglichen Wechsel der Methoden – EM Experimente an einem Tag, Wärmelanze und Schwerelot am nächsten Tag – den einzelnen Arbeitsgruppen jeweils genug Zeit blieb um Arbeiten an den Systemen durchzuführen und außerdem erste Ergebnisse zu produzieren, die dann wiederum zu einer zielgerichteten Einsatzplanung verwendet werden konnten.

Zusammenfassend wurden die folgenden ersten Erkenntnisse während der Fahrt gewonnen:

1. Stark erhöhte Temperaturen ($> 60^{\circ}\text{C}$) wurden mit der Wärmelanze östlich des zuvor bekannten aktiven Gebiets (Station HF04) gemessen. Dies zeigt, dass das Ausmaß des aktiven Bereichs größer ist als zuvor bekannt. In einem Sedimentkern, der an der gleichen Stelle genommen wurde (GC06), wurden jedoch nur $31,5^{\circ}\text{C}$ an Deck gemessen. Dies deutet darauf hin, dass die Temperatur über kurze Distanzen stark variiert. Diese Beobachtung einer deutlichen Variation der Temperatur über kurze Entfernungen deutet auf eine tektonische Kontrolle des hydrothermalen Systems hin, wobei Störungen als Pfade für den Fluidtransport wirken.
2. Anstieg der Temperatur und Wärmeleitfähigkeit nach Norden (HF14) sowie starker H_2S -Geruch und erhöhte Temperaturen in Kernen (GC04 & GC05) an den - aktuell - nördlichsten beprobten Lokationen im GVF zeigen, dass der hydrothermal beeinflusste Bereich mehr als 2,5km nördlich des hydrothermalen Mounds nachgewiesen werden kann, woraus eine potentielle existierende N-S-Verwerfung abgeleitet werden kann.
3. Kalibrierungsmessungen mit dem MARTEMIS-System zeigen, dass Verbesserungen am mechanischen Aufbau des Systems, die nach der Ausfahrt nach Palinuro 2017 durchgeführt wurden, erfolg-

reich waren. Bei früheren Messungen vorhandene unerwünschte Verzerrungen in den Messungen, die durch Metallteile auf der Spule verursacht wurden, sind nicht mehr vorhanden.

4. Eine erste Interpretation der MARTEMIS Spulendaten zeigt systematisch erhöhte, anomale Amplituden über und in der Umgebung des bisher bekannten hydrothermalen Feldes. Weitere Anomalien wurden weiter östlich entdeckt, was entweder darauf hindeutet, dass die aktive Fläche größer ist als bisher bekannt, oder möglicherweise einen ersten spekulativen Hinweis auf verborgene massive Sulfide gibt.

Weiterführende Arbeiten werden sich auf die Integration der gewonnenen Datensätze in eine gemeinsame Interpretation konzentrieren, anhand welcher die Untersuchungen für die genehmigten Ausfahrt POS535 im Juni 2019 geplant werden können.

2. Participants

	Name	Position (Affiliation)	Function on board
1	Sebastian Hölz	Senior Scientist (GEOMAR)	chief scientist, marine EM
2	Sofia Martins	Senior Scientist (GEOMAR)	co-chief scientist, GC, heatflow
3	Amir Haroon	Scientist (GEOMAR)	marine EM
4	Konstantin Reeck	PhD-student (GEOMAR)	marine EM
5	Gesa Franz	PhD-student (GEOMAR)	marine EM
6	Shuangmin Duan	PhD-student (GEOMAR)	marine EM
7	Martin Wollatz-Vogt	Technician (GEOMAR)	marine EM
8	Patrick Schröder	Technician (GEOMAR)	gravity core, heatflow
9	Anna Jegen	Bachelor student (CAU)	gravity core, heatflow

3. Research Program

3.1. General

Hydrothermal circulation is driven by heat and occurs mainly at marine plate boundaries such as mid ocean ridges, volcanic arcs and at back arc basins where heat is supplied by increased magmatic activity. In Iceland the occurrences of high-temperature hydrothermal systems is clearly linked to the neovolcanic zone (Fig. 1), which crosses the island from the SW to the NNE. The neovolcanic zone is an expression of the Mid-Atlantic Rift system crossing the Iceland hot spot (Hannington et al., 2001). As part of the rift system, the neovolcanic zone extends into the submarine domain to the SW along the Reykjanes Ridge and to the NNE along the Kolbeinsey Ridge.

Investigations of geothermal settings on and around Iceland are of special interest for two main reasons:

1. At present, geothermal heat is already of major importance for Iceland's economy and infrastructure since 25% of the country's electricity production, 66% of the primary energy use and about 90% of heating for households stem from geothermal energy (Orkustofnun, 2017)². At present this hydrothermal potential is mainly exploited on the main island, but the potential of offshore reservoirs for smaller islands like Grimsey is investigated e.g. by Atkins & Audunsson (2013). For the Grimsey Vent Field (GVF), which is the geological target of this proposal, the authors state: *“Although it has by far been the most extensively surveyed offshore resource around Iceland, only very limited information is available on reservoirs temperature, size, and energy content.”* This demonstrates that the economical interest for these offshore resources is at present not matched by adequate knowledge about the true potential, which demonstrates the need for fundamental research.
1. Hydrothermal circulation of seawater is a prerequisite for the formation of seafloor massive sulfides (SMS). Hot fluids leach out metal bearing ores from the host rocks at depth and the mineral rich fluid rises towards the seafloor. When cooling, e.g. in contact with cold seawater metals may precipitate to form SMS deposits. Depending on the structure of the seafloor and the overall build up of hydrothermal circulation, the cooling of hydrothermal fluids may occur within the seafloor, in which case deposits may form at depth or within the water column, in which case venting of high-temperature fluids may build up chimney structures such as black smokers. Along oceanic plate boundaries

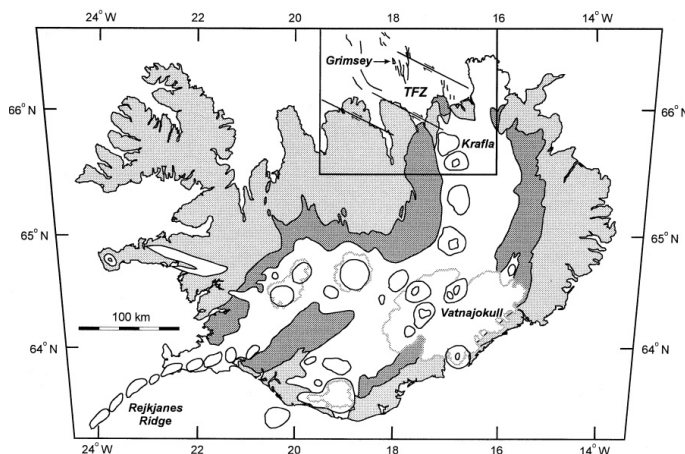


Fig. 1: Map of Iceland (from Hannington et al., 2001) showing the neovolcanic zone (white) with offshore extensions to the SW along the Reykjanes Ridge and to the NNE in the Tjörnes Fracture Zone (TFZ) and the Kolbeinsey Ridge. The proposed study area (Fig. 7) to the E of the Grimsey island is part of the TFZ.

² <http://www.nea.is/geothermal/> (Orkustofnun – National Energy Authority of Iceland, accessed 10.2.2017)

approximately 330 vent sites have been observed at the seafloor. Of these sites, a majority of 237 contain massive sulfide mineralization (Beaulieu et al., 2015; Monecke et al., 2016) and an estimate of the global potential yields a total accumulated volume of 600 million tons of SMS containing 30 million tons of copper and zinc are present in the immediate vicinity of the oceanic plate boundaries (Hannington et al., 2010 & 2011). Due to the fact that SMS are compact (i.e. localized) structures close to the seafloor with potentially high ore grades, the possibility of mining such massive sulfide deposits has gained much attention on a national and international level (Boschen et al., 2013). However, in the case of the GVF no massive occurrences of have been reported, even though some indications for the existence of sulfides was found in cores (Hannington et al., 2001). This poses the question, if SMS are simply not present in the proposed working area or if they simply have not been found so far, because they are hidden underneath a sediment blanket.

3.2. Geological Target

The Grimsey Vent Field (GVF) is located on the eastern side of the Grimsey Graben on a 30 – 40m high. The graben is a pull-apart basin within the Tjörnes Fracture Zone, which is about 10km wide, 30 – 40km long and filled with glacial sediments from ice-fed rivers draining the northern coast of Iceland (Lackschewitz et al., 2006).

Since its discovery in 1997 (Stoffers et al., 1997), the GVF has been studied during several scientific cruises with *R/V Poseidon*. Hannington et al. (2001) identified three main areas of venting (Fig. 2):

1. A northern field composed of isolated mounds and solitary chimneys,
2. a central field consisting of coalesced anhydrite mounds, where the most active venting occurs along a 300m long and 200m wide ridge and
3. a small and older southern field, in the form of a coalesced mound with at least one active vent.

During cruise POS229 samples of chimneys, hydrothermal fluid and gas were collected using the submersible JAGO (Stoffers et al., 1997). In 1999, seventeen 3m and 5m gravity cores were recovered during POS253 along with samples collected by the submersible JAGO (Scholten et al., 2000). The GVF was again sampled in 2002 during POS291 recovering fifteen 6 – 9m long gravity cores, from which sediment and pore water samples were retrieved (Devey et al., 2002).

All the information collected within these cruises allowed for a comprehensive picture of the GVF, which is a shallow water (400m) system covering an area of at least 1km². It is characterized by hydrothermal

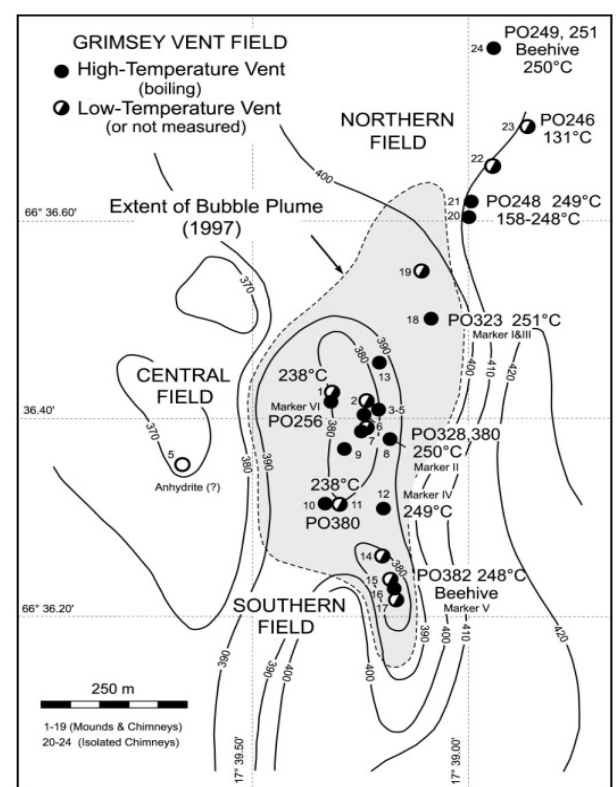


Fig. 2: Contour map of the Grimsey Vent Field (GVF) with locations of temperature measurements taken with the JAGO submersible and the deduced area of active, high-temperature venting (shaded area) (after Hannington et al., 2001).

anhydrite mounds comprising active and inactive anhydrite chimneys. Hannington et al. (2001) identified 24 mounds and chimneys in JAGO dives, of which 14 were characterized as high-temperature vents (boiling). They also observed acoustic scattering within the water column in echo-sounder profiles (their figure 5), which they used to map out the extent of the hydrothermal field (shaded area in Fig. 2).

Fluid analyses on core samples were reported with end-member chlorinity of 274mM, which is about half of seawater chlorinity (Lackschewitz et al., 2006). Even though sulfur smell was apparent on fresh chimney samples, the lack of smoke in the venting fluids and the only patchy distribution of bacteria mats on the surfaces of mounts suggests that neither sulfur nor metals are abundant at the surface. However, it remains unclear if accumulations of massive sulfides may exist at greater depth (Hannington et al., 2001).

Sediment coring results shows that the area is underlain by pelagic, clastic and hydrothermal altered sediment sequences. The cycle of formation, alteration, destruction and re-sedimentation of the anhydrite/talc chimneys is represented by debris flow, turbiditic and hemipelagic deposits (Scholten et al., 1999). Sulfide deposition was identified as disseminated occurrences, but also filling veins, fractures and vugs in hydrothermal altered sediments (Hannington et al., 2001).

Within the high temperature vents, many showed boiling, and phase separation was visually observed. Temperature measured by JAGO ranged from 248 to 251°C (Betz et al., 1999). The temperatures measured on deck, on the core catchers, reached 102°C in the central mound area and as low as 2°C in the more distal areas with background values sediments (Stoffers et al., 1997; Scholten et al., 2000).

Fig. 3 demonstrates how elevated temperatures of pore fluids are connected to a strong increase in the electrical conductivity. This relationship motivates the use of EM methods for the investigation of a hydrothermal system!

In a review of Icelandic geothermal areas Ármannsson (2016) lists 33 prospective high temperature geothermal systems, of which three are submarine. Of these submarine fields Atkins and Audunsson (2013) consider the

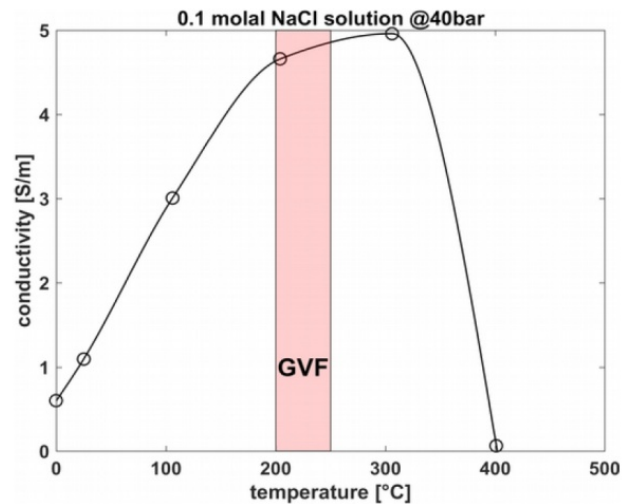


Fig. 3: Temperature - conductivity relationship for 0.1 molal NaCl solution at a pressure of 100bar (based on Fig. 10 in Quist and Marshal, 1968). The red area marks the temperature range observed in the GVF.

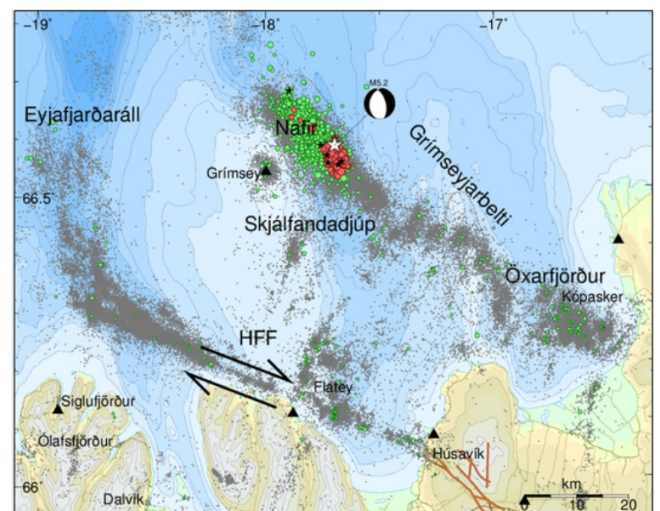


Fig. 4: Seismic activity offshore northern Iceland since 1994 with recent activity indicated by green (January 2018) and red points (since 19th of February). Magnitude larger 4 are shown as black stars, the white star indicates the location of a M5.2 earthquake (IMO, 2018b).

Grimsey field to be the most compelling site for offshore power production off Iceland due to the size of the field (comparable to geothermal areas on land) its temperature (at least 250°C) and its proximity to land (16km from Grimsey island and 50km from mainland Iceland). Their assessment for Grimsey seems to be mainly based on research results collected during *R/V Poseidon* cruises POS229, POS253 and POS291 (1997, 1999, 2002, respectively)

Seismic and geochemical investigations indicate high permeability in the deep crust which facilitates fluid and gas migration from the crust–mantle boundary to the seafloor (Riedel et al., 2001). Some additional data is presented by Magnúsdóttir et al. (2015) who show an E-W striking section of chirp seismic data, in which the GVF is associated with two separate, cone-shaped acoustic anomalies along a stretch of about 500m. This is a first indication that the vent field is actually wider / larger than depicted in Fig. 2 and may actually consist of several separate centers of strong hydrothermal activity. They also present some stratigraphy from the approximately 38m long drill core MD-75, which was taken at a location about 6km to the SW of the GVF. Additional information about this core can be found in Gudmundsdóttir et al. (2011).

Recent news have reported that the area around the GVF has been shaken by swarms of earthquakes starting in January 2018 (Fig. 14). The highest activity with about 2000 events was reported mid February³ (IMO, 2018a) and was centered in the Skajálfandadujúp submarine rift valley. The Icelandic Met Office (IMO, 2018b) reported the highest activity on February 19th with the largest earthquake (M5.2) located 14km ENE of Grimsey together with five smaller earthquakes (M4-4.9). Generally, such pattern of activity occur every few years with similar activity reported in May and September 1969, during the Christmas period in 1980, in September 1988 and April 2013. This activity was attributed to movements of the tectonic plates which can cause a change in geothermal and hydrothermal activity in the area.

3 <http://icelandreview.com/news/2018/02/19/magnitude-52-earthquake-near-grimsey>

4. Narrative of Cruise

6.6. - 8.6.2018

After a seamless mobilization on the 6th of June we left the harbor of Reykjavik (Iceland) on schedule the next morning. In the morning of the 7th of June, we were surprised by open pack ice to the NW of Iceland, which partially blocked the passage through the Greenland Strait. For the better part of the morning Captain Günther was busy trying to find a save passage, which delayed our transit by several hours. In the evening hours of the 8th of June we arrived in our working area, which is located about 15km to the West of the Island of Grimsey offshore Northern Iceland.

9.6.2018

To prepare experiments we first performed a pressure test of the releases and at the same time acquired a CTD-profile, which yielded data necessary for the calibration of the Posidonia USBL-system (sound-velocity profile) as well as for the later interpretation of the EM data (conductivity profile). The following installation and calibration of the Posidonia USBL-system was finished in the early afternoon. The calibration of the USBL system confirmed the correct operation of the system and yielded acceptable precision in the order of 5 – 8m. Later this afternoon, we deployed the first two OBEM receiver to locations, which were planned around the active hydrothermal field.

10.6.2018

Most of the day was spent on the deployment of seven additional OBEM receivers around the vent site and of three additional receivers to a site approximately 2.5km to the north of the vent field, which was identified as a point of potential hydrothermal activity in the bathymetric data. All OBEMs were lowered via the winch cable down to about 30m above the seafloor and then released and deployed to the predetermined positions.

The deployment of stations was finished ahead of schedule, which left just enough time for a first deployment of the gravity corer to the center of the active field. A full core (GC1) with high temperatures (84°C measured on deck) and abundant disseminated sulfides was recovered and during the evening analyzed and sampled in the wet lab.

11.6.2018

In order to minimize the necessary work on deck, work with the gravity corer was continued in the morning of the 11th. One gravity core (GC2) with full recovery was taken to the North of the vent field to recover some background sediments.

Since space in the wet lab was limited, work could be carried out on a maximum of two 3m cores at the same time. Thus, the scientific program was continued with six measurements with the heat-flow probe along a W→ E profile crossing the vent field. Measurements within the active zones of the vent field were avoided, since the probe only allows for measurements up to 60°C.

During measurements with the heat probe and gravity coring the MARTEMIS coil system was assembled and dry tested on aft deck. A first deployment in of the system in the afternoon started at around ~15:00h after measurements with the heat-flow probe had finished. During this first deployment the rigging of the

system, which connects the upper and the lower frame, did not open up correctly in the water. After recovery of the system the problems were analyzed and some adjustments to the rigging were made in the evening.

12.6.2018

Adjustments to the rigging and mechanical components of MARTEMIS system had to be continued in the morning hours. Therefore, it was decided to continue work by taking additional gravity cores, which recovered about 1m of hydrothermally altered material with strong H₂S smell (GC3) and 6m of background material in two additional cores (GC4, GC5).

After finishing work with the gravity corer, the MARTEMIS system was deployed for a second time. The applied adjustments to the rigging showed to have eliminated the problems encountered during the previous day. Consequently, the system was lowered to the seafloor to perform active measurements along a first profile to the west of the hydrothermal field (S0001 – S0245). Together with this active measurement, where the coil of the MARTEMIS system works as a transmitter and receiver at the same time (→ transient electromagnetic – TEM), measurements were also taken with the remote OBEM receivers (→ Coil2Dipole) and with two perpendicular pairs of electrodes attached to the coil frame, which allowed for the measurement of the self-potential during the transmitter off times.

After recovery of the system, a first quality check of acquired data was carried out in the evening hours. While the transmitter and receiver of the coil looked OK, it was evident that the coil's ranging system, which is used to measure the distance between the coil and the remote receivers for the Coil2Dipole experiment, did not work properly. A repair of the system was performed during the night.

13. - 14.6.2018

Measurements with the MARTEMIS system were started in the early morning hours around 6:00am. After measurements along a first profile (S0246 – S0404), a check showed that repair attempts during the night had not solved the problems with the ranging system. After bringing the system back to deck, a second repair attempt was started. After two hours it was decided to continue without a functioning ranging system, since TEM measurements with the MARTEMIS system do not require ranging measurements and the correct ranges for the Coil2Dipole experiment may still be reconstructed at a later stage from the USBL data. Starting at 11h00, measurements with the system were carried out until the next morning along about 18.5km of profile lines (S0405 - S1743), which cover the previously reported extent of the vent field, the second site of interest to the north and a ~2.5km long profile connecting the two.

14. - 15.6.2018

In the morning hours of the 14th wind and waves picked up considerably and measurements with the MARTEMIS system had to be stopped. After recovery of the system, the captain decided to take shelter for the next 48h in the Eyjafjörður Fjord.

The down time in the fjord was used to finally repair the ranging system of the MARTEMIS system and to prepare a novel experiment, which uses the coil frame of the MARTEMIS system as fixation for two perpendicular transmitter dipoles (→ Dual Polarization).

16.6.2018

After returning to the working area in the morning, measurements were continued with the heat-flow probe at three locations.

Since the main objective of EM experiments – a full coverage of the hydrothermal system with TEM measurements with the MARTEMIS system – had already been achieved on the 13th – 14th, preparations were started for the “Dual Polarization” experiment by re-deploying three of the OBEM receivers to new positions along a profile line crossing the hydrothermal field. To save time, receivers were not lowered via the winch cable but instead were deployed free falling.

17.6.2018

Preparations were continued in the morning by re-deploying two additional receivers to new positions along the new profile. The recovery of a 3rd receiver (RX11) had to be abandoned after the receiver seemingly released (according to acoustic signals) but never rose to the surface.

Scientific work in the morning was continued by taking another gravity core (GC6), which contained background sediments with strong H₂S smell and elevated temperatures (31.5°C measured on deck).

Starting at 10h00, the MARTEMIS system was deployed with the attached pair of transmitter electrodes to perform the dual polarization experiment, this time with a working ranging system. After measurements along a 3.7km long profile crossing the vent field from W → E the experiment was finished after recovery around 16h00.

Due to a bad weather forecast it was decided to again take shelter in the fjord.

18.6.2018

No work due to winds and waves.

19.6.2018

In the morning hours weather conditions improved and we were able to steam back to the working area.

Scientific work was continued with six heatflow measurements in the afternoon.

20.6.2018

In the morning, geological work in the working area was finished by taking two gravity cores (GC7, GC8) with recovery of 150cm and 291cm, respectively. Both cores showed elevated temperatures of 66°C and 45°C, respectively, on deck.

As final EM experiment, the MARTEMIS coil system (i.e. without the transmitter electrodes), was deployed to measure along a total of about 20km of profiles, which covered the surrounding of the vent field to the E and W. During measurements the ranging system was operational, thus, good data for the Coil2Dipole experiment should also be available from this experiment. Measurements were continued until the next morning.

21.6.2018

With the recovery of the MARTEMIS system at around 6:00h, the scientific program was finished.

After the recovery of the OBEM receivers, which lasted from 6h00 – 13h00, the rest of the day was dedicated to the attempt to rescue the missing receiver RX11, from which acoustic signals could still be received. A first search in the vicinity of the original drop position yielded strange ranging measurements indicating that the station was no longer at its original position. A “regional” triangulation with ranging measurements taken at three different positions in the working area yielded a position about 2km to the south of the original drop position.

22.6.2018

In the morning hours the upper frame of the MARTEMIS system, equipped with a camera and some steel hooks, was lowered to the previously determined new position. By using the MARTEMIS ranging system, which allows for direct ranging at the seafloor, we could perform a “local” triangulation and were indeed able to find the station within 45min on video. Subsequent tries to get the station onto the hooks did not succeed. Provided that we did not have dynamic positioning on the ship and no thrusters on the MARTEMIS frame, we were already quite happy to have found the station at its new position. Rescue attempts were aborted around noon.

23. - 26.6.2018

After four days of transfer we arrived at our final destination port in Bergen, Norway.

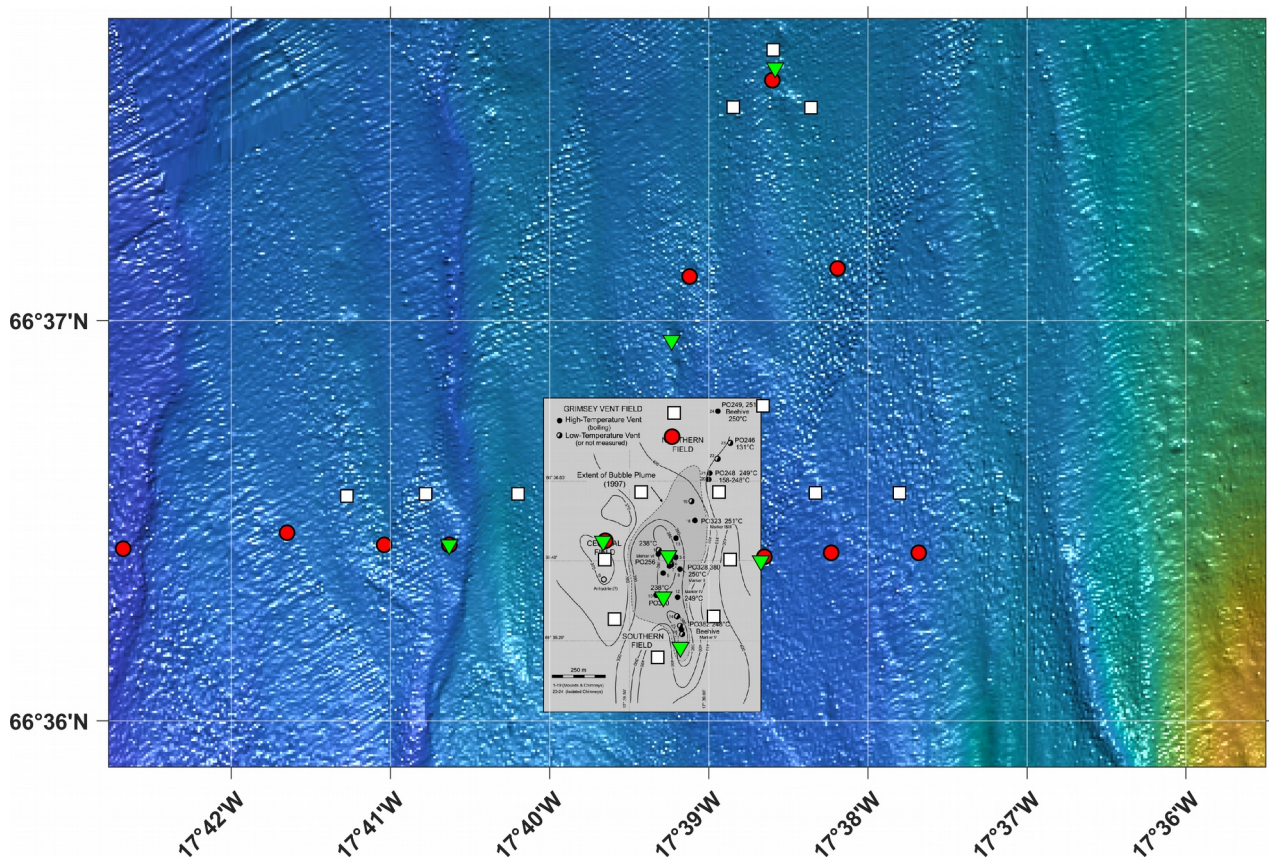


Fig. 5: Overview map with all deployed OBEM receivers (white squares), heatflow stations (red circles) and locations of gravity coring (green triangles). Detailed maps with station names can be found in the following sub-chapters. As reference, the map of Hannington et al. (2001) marks the position of the vent field and previous investigations (compare Fig. 2).

5. Applied Methods & Preliminary Results

In the following sub-chapters we will present the experiments conducted with the various methods. To give a first overview,

5.1. Electric and Electromagnetic Instruments & Experiments

In land-based exploration it has been common practice for several decades to use electromagnetic methods to detect and characterize massive sulfide deposits (i.e. Palacky, 1987). Investigations on marine samples indicate that conductive anomalies may also be expected in the marine environment (e.g. Iturrino et al., 2000). Consequently, it seems promising to use both passive and active EM methods for the investigation of SMS and the associated hydrothermal systems:

1. active experiments rely on the fact that the generated electromagnetic field couples to the conductive ore body and is distorted by the coupled current systems, which are channeled into the ore body,
1. passive self-potential (SP) measurements detects naturally occurring anomalies in electrical potential which can arise from buried conductive bodies (e.g., massive sulfides, graphite shear zones) or from streaming potentials caused by fluid flow (e.g., groundwater).

However, only a few electric and electromagnetic experiments have ever been conducted on marine SMS targets:

- The SP method has been shown to work in marine environments, where both graphite and massive sulfide bodies have been detected by marine SP systems (Brewitt-Taylor, 1975; Corwin, 1976; Von Herzen et al., 1996; Heinson et al., 1999, 2005; Beltenev et al., 2007; Cherkashov et al., 2010; Shilov et al., 2012; Cherkashev et al., 2013). However, prior to our study, the SP method had not been tested over a hydrothermally inactive SMS site which is buried under sediment.
- Cairns et al. (1997) report about an electromagnetic pilot study to image the TAG hydrothermal field (26°N, Mid-Atlantic Ridge) SMS deposit. However, at that time marine electromagnetic instrumentation was in its infancy and 3D modeling capabilities were just in development such that a 3D image of the sulfide deposit could not be derived
- Kowalczyk (2008) reports on a shallow penetration ROV based EM, which was used to map anomalies of the electrical conductivity at the Solwara site offshore Papua New Guinea. Later drilling confirmed that anomalous electrical conductivity anomalies were indeed associated with occurrences of SMS at or directly beneath the seafloor.

In 2012 our working group suggested to use a coil system for the detection of conductive features (Swidinsky et al., 2012). Starting in 2015, we have used the MARTEMIS system to perform investigations on the inactive Palinuro Seamount in the Tyrrhenian Sea (2015, 2017) and inactive mounds in the vicinity of the TAG hydrothermal field at the Mid-Atlantic Ridge (2016).

During cruise POS524, electric and electromagnetic measurements were carried out during four deployments of the MARTEMIS system (Fig. 6). A first test of the system was exclusively dedicated to familiarize the crew with the deployment of the system and to test the rigging between the upper and the lower frame. Since the rigging did not open up correctly, some adjustments had to be implemented after which all following deployments went smooth. In the following experiments, measurements with different transmitter and receiver configurations were performed along various profiles covering the working area. The deployments are summarized in the following table, details about the instruments and the performed experiments are given in the next sections.

Deployment (Stations)	Date	TEM	Coil2Dipole	Dual Polariza- tion	SP	Comment
Test 1	11.6.	x	x	x	x	Problems with rigging.
1 (Coil/S0001 - S0245)	12.6.	yes	yes (no ranging)	x	yes	TEM measurements, problems with ranging system
2 (Coil/S0246 - S1743)	13. - 14.6.	yes	yes (no ranging)	x	yes	TEM measurements, Problems with ranging system,
3 (DualPolarization/ S0001 - S0193)	17.6.	no	no	yes	no	Dual Polarization measurements along W → E profile
4 (Coil/S1744 - S3123)	20. - 21.6.	?	yes	no	?	TEM measurements, problems with RX coil cable?

5.1.1. MARTEMIS Coil System – TEM Measurements

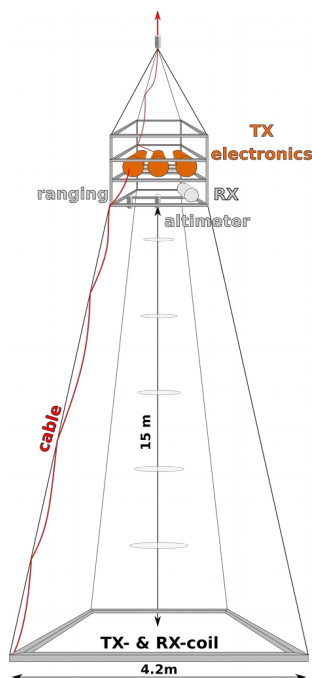


Fig. 6: MARTEMIS system.

Fig. 6 shows a sketch of the MARTEMIS system, which consists of two frames which are connected by a rigging.

The lower square frame holds cables of the coincident transmitter (TX) and the receiver (RX) coils. The frame is constructed from glass fiber reinforced tubes. In previous experiments (2015 – 17) we had used corner connectors made of stainless steel, which were identified as one cause of distortions in test measurements in late 2017. Therefore, during this cruise we used a new set of custom made corner connectors made from glass fiber reinforced plastic. Generally, the robust connector system allows for flexible loop sizes by simply using tubes with different lengths, which of course also requires a coil cable with a matching length. Thus, the system may be adjusted to the available deck space and the size of the ship's A-frame by up- or downsizing. For measurements on *R/V Poseidon* during this cruise we used a 4.2 x 4.2m² coil. Additionally, weights, a metal free attitude sensor and a small CTD – the only metal part on the lower frame – were mounted to the coil frame. For this experiment we used weights made from fluorite

for the first time. Similar to the corner connectors, the previously used weights had not been metal free and had been identified as the second major cause for distortions in past experiments.

The upper frame holds several pressure tubes with the receiver, the transmitter electronics and the power supply, an altimeter and a self build acoustic ranging system, which is used to measure the distance between the MARTEMIS system and the remote OBEM receivers (see chapter 5.1.2). The upper and lower frame are connected via a rigging, which connects the corners of upper and lower frame. Cables, which are attached to the rigging connect the transmitter and receiver coils as well as a downward looking attitude sensor to the associated counter parts within the pressure tubes in the upper frame. The reason for separating the two frames by a distance of about 15m is simply that all metal parts (e.g. pressure tubes, ...) and components, which create EM noise (e.g. transmitter electronics) should be kept as far away from the sensor (i.e. the receiver coil) as possible. After all, the MARTEMIS system is in a sense a metal detector.

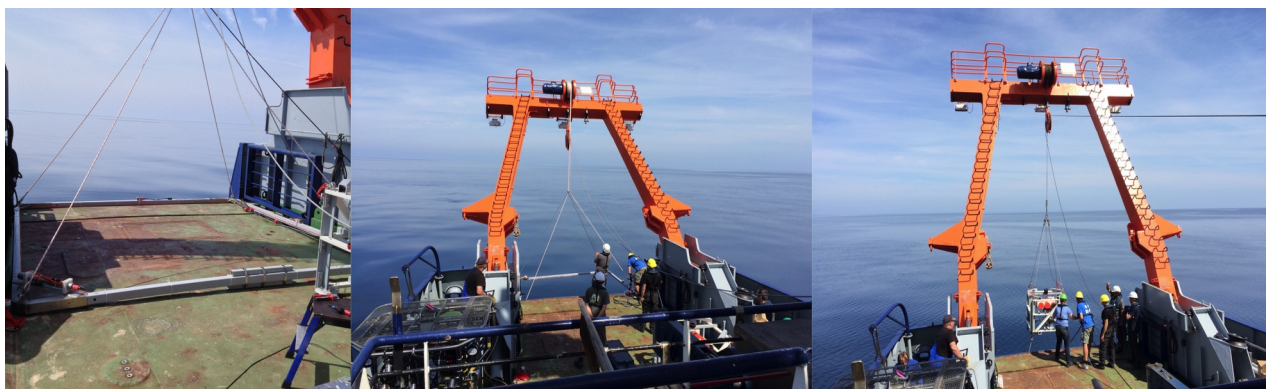


Fig. 7: Deployment of the MARTEMIS system on R/V Poseidon (pictures taken during cruise POS483).

The receiver unit has three input channel with 24bit resolution, which are sampled at a frequency of 10kHz and have a storage capacity to acquire about 48h of continuous data. For TEM experiments we used one of the channels connected to the receiver coil to record the transient responses at the highest gain setting. The two additional channels were used to measure the selfpotential (see chapter 5.1.4). Due to improvements to the system prior to the cruise, we were able to download data from the receiver units directly from the laboratory during the experiment. However, due to the coaxial link used, the data transfer was too slow to monitor the data in real-time and we only downloaded receiver data every other hour check, if the receiver was still recording data. For future experiments on ships with fiber optical link, we plan to download all data near real-time to establish a quasi online monitoring of all system components in the laboratory during experiments. Also, this would allow for real-time quality checking and evaluation of incoming data to allow for direct detection of conductivity anomalies, which would offer the possibility to adapt the survey plan in the course of an experiment.

We use the same transmitter, which was previously developed for the Sputnik CSEM system. The transmitter generates a bipolar square waveform with a 50% duty cycle. Repetition frequencies may be switched to 0.25Hz for CSEM measurements (see chapter 5.1.3) or 2.5Hz for TEM measurements (this chapter) and signal amplitudes can be selected to be 19A, 38A or 57A. The transmitter current is supplied and regulated through DC/DC converters, buffer batteries and a microprocessor controller unit. These units are housed in titanium cylinders, which are mounted to the upper frame.

Generally, for experiments the MARTEMIS system is assembled on the aft of the ship (Fig. 7, left). After assemblage, the coil frame is lowered into the water (Fig. 7, middle) and attached at a vertical distance of 15m beneath the upper frame (Fig. 7, right). After deployment the whole system is lowered towards the seafloor using the ship's winch cable and “flown” across the seafloor by moving the ship at a slow speed of approximately 0.5kn. By monitoring the altimeter, the position of the loop is kept at a close distance of about 5m above the seafloor by constantly adjusting the length of the winch cable (see Fig. 8).

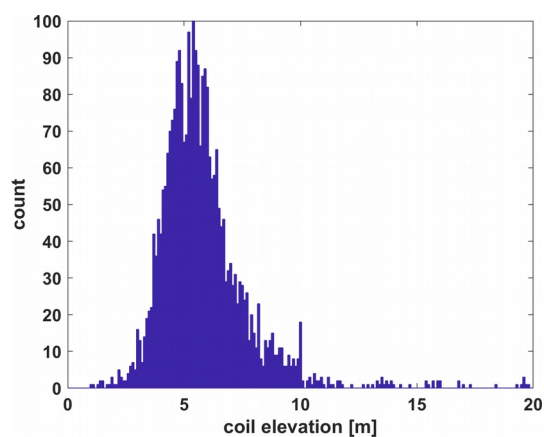


Fig. 8: Histogram of coil altitude during TEM experiment.

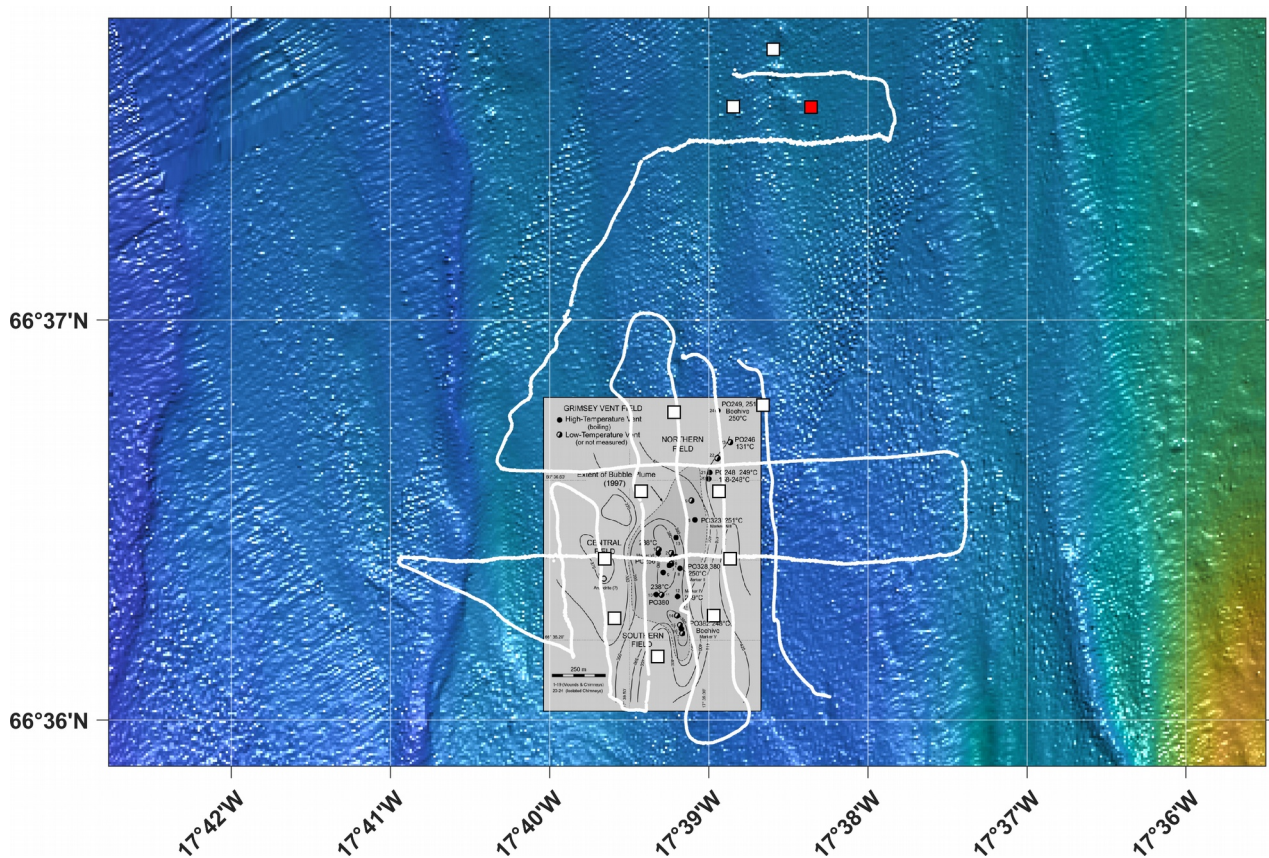


Fig. 9: Track of MARTEMIS system in experiments during the 2nd deployment. Squares mark the positions of the OBEM receivers during this experiment (red square = displaced OBEM). As reference, the map of Hannington et al. (2001) marks the position of the vent field and previous investigations (compare Fig. 2).

The main TEM experiment was carried out on June 13th – 14th (Fig. 9). General procedure for all measurements with the MARTEMIS system was to keep the coil at a distance of about 4-6m to the seafloor while measuring along profile lines. At the end of each profile line, the system was lifted to about 150m above the seafloor to perform calibration measurements and to collect additional data with the transmitter being turned off for the drift correction of the selfpotential data (see chapter 5.1.4).

After measurements along a first profile (stations S0246 – S0404), a check showed that the ranging system on the upper frame did not work properly. After a repair attempt on deck it was decided to continue the experiment without the ranging system, since TEM measurements with the MARTEMIS system do not require ranging measurements. Starting at 11h00, measurements with the system were carried out until the next morning along about 18.5km of profile lines (S0405 – S1743). Measurements were started in the SE and first covered the previously known extent of the vent field with six N ↔ S profiles followed by an W → E profile. Total length of these profiles was about 16km. Measurements were then continued along a 2.5km transfer profile to the NNE to a second area of interest, which was covered by another 2.5km of profiles. After about 18h and 45min the experiment was finished in the early morning hours of the 14th of June. Thus, the average acquisition speed during the experiment was about 1km/h.

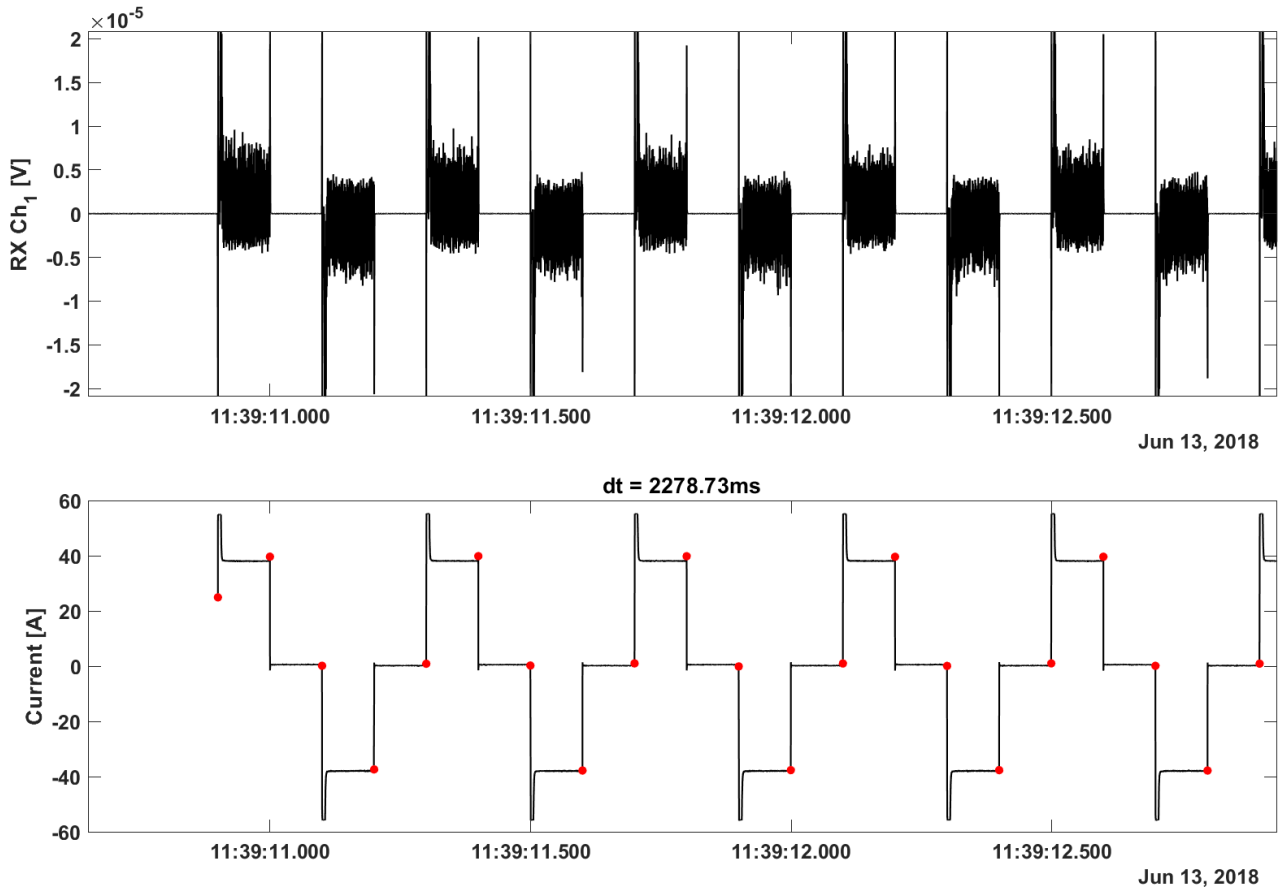


Fig. 10: Example of TEM raw data measured at station S0444. The receiver data (top) is noisy while the transmitter (bottom) is turned on and decays rapidly (not visible in linear time scale) as the transmitter is turned off. The red dots mark picked times when the transmitter was either turned on or off.

Generally, for active measurements, a regular cycle of measurements was performed as follows:

- ranging measurement needed for Coil2Dipole (chapter 5.1.2) and Dual Polarization (5.1.3) measurements (did not work during this TEM experiment),
- TX activation for 10s (50% duty-cycle, $I = 19\text{A}$, repetition frequency 2.5Hz), 10s pause,
- TX activation for 10s (50% duty-cycle, $I = 38\text{A}$, repetition frequency 2.5Hz), 10s pause.

Fig. 10 shows some typical TEM rawdata, which was acquired during the experiment. For the processing of data it is necessary to know the exact times of the TX turn-on and turn-off. As first step it is therefore necessary to determine these time points (red dots in Fig. 10, bottom), which is done by an automated picking routine, which still requires visual inspection of all picks and – where necessary – manual correction of possible mistakes. The second step for processing is then to assure the correct time-synchronization between the transmitter and receiver clock(s). With these two steps finished it is possible to perform a batch processing of the TEM data, which simply comprises the import of the RX data for the correct time-interval, stacking of successive transients and log-gating of the stacked transient (see Hölz et al., 2015 for details).

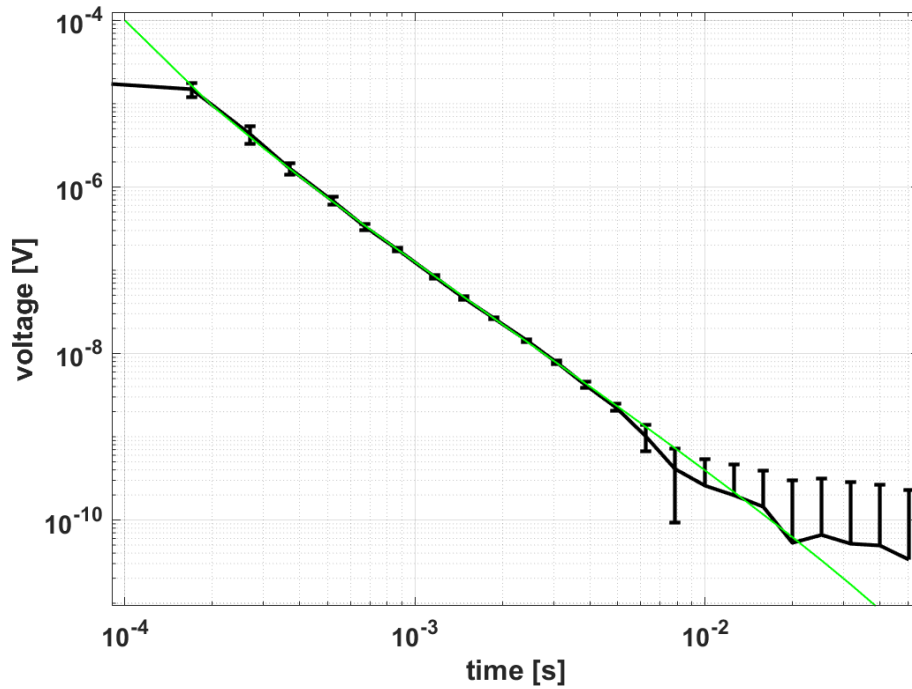


Fig. 11: Processing result of calibration measurement with the MARTEMIS system in the water column (black) and theoretical full-space response (green).

Since the first processing still require substantial work, data of only a few selected stations was performed directly after the recovery of the system. A first important result is shown in Fig. 11: the displayed processed transient with errorbars (black) was measured with the MARTEMIS system being elevated about 150m above the seafloor, i.e. halfway in the water column. Since the system has a limited detection range ($<50\text{m}$), such a measurement in the water column is perfectly suited to calibrate the system, since the surrounding conductivity structure is perfectly known from CTD measurements (... indeed, the measurement can be considered to be a measurement in a homogeneous fullspace !!!). The green line shows the to be expected theoretical response, which demonstrates that the MARTEMIS system is perfectly calibrated for the better part of the transient, at least in a time range between $\sim 200\mu\text{s}$ – 6ms. This is a huge improvement as compared to experiments during previous cruises, where metal parts (corner connectors, weights) had caused significant distortions to the measured transients.

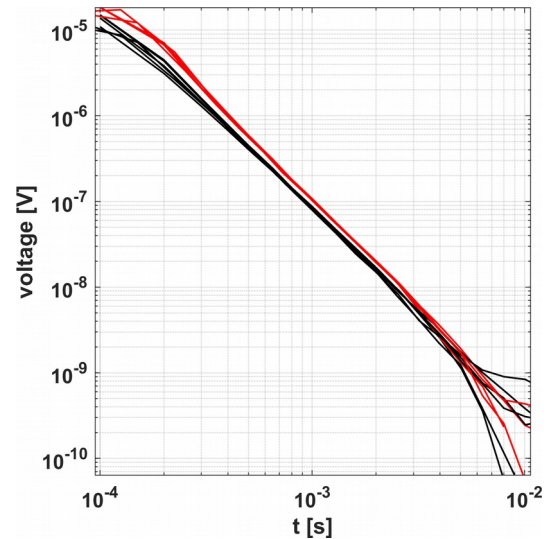


Fig. 12: Processed transients measured at stations over background geology (black) and above the vent field (red).

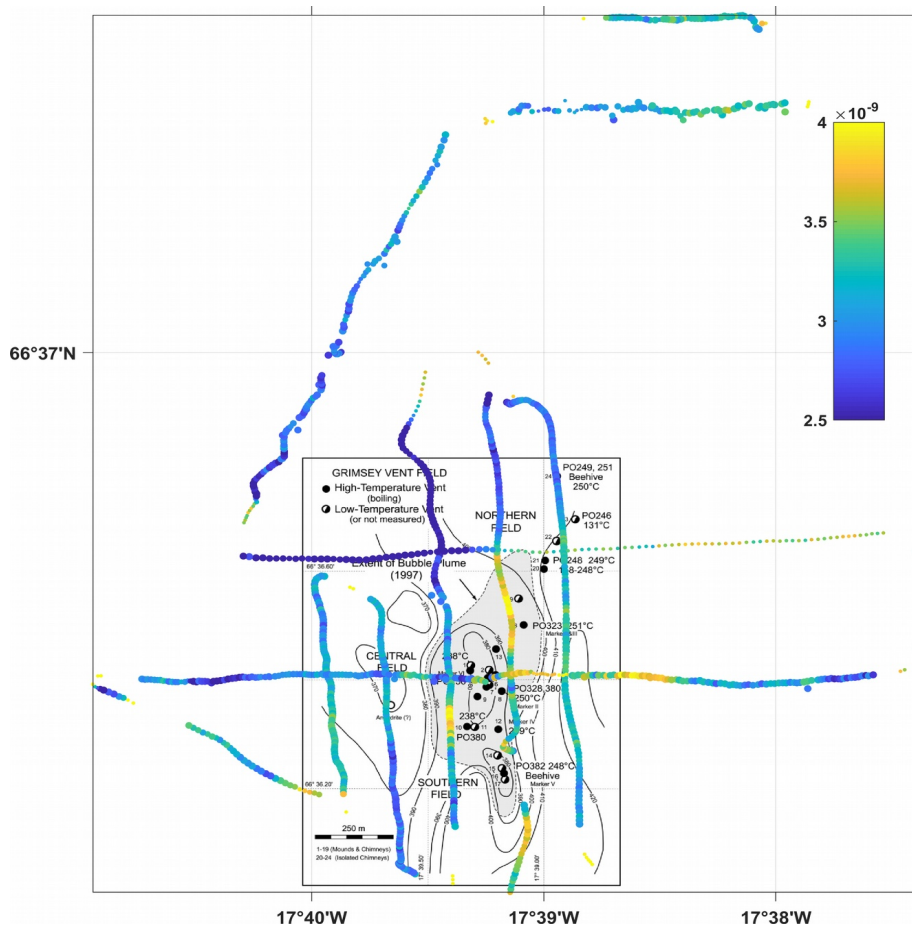


Fig. 13: Amplitude of transients (4ms) at stations with increased amplitudes evident above the GVF. As reference the map of Hannington et al. (2001) marks positions of the vent field and previous investigations (see Fig. 2).

As second result, Fig. 12 shows a comparison of processed transients, which were measured at stations in regions where we expect background geology (black lines) and at stations which were located above the previously mapped out active area (red lines). As expected, amplitudes are elevated, which points towards an elevated conductivity in the subsurface, which is a direct indicator for elevated temperatures (compare Fig. 3). Thus, this figure serves as a first prove of principle to use TEM measurements with the MARTEMIS system for the investigation of a hydrothermal system!

Data processing of the TEM data acquired along the profiles displayed in Fig. 9 was finished a couple of months after the cruise. We include a first map of the processed data to demonstrate that the detection of the hydrothermal system did not only work at selected stations – as shown by the increased amplitudes in Fig. 12 – but seemingly worked in the whole working area. In Fig. 13 we show the amplitudes of transients at all processed stations at a certain time (4ms) together with the map of Hannington et al. (2001). Elevated amplitudes in transients (yellow) – similar to the elevated amplitudes at a certain time depicted in Fig. 12 – are evident above the vent field, but also in an area to the east of the field along the E ↔ W profile in an area, which had not been investigated before. Displays of data for other times in the transients show similar results. Upcoming work will focus on creating apparent resistivity maps from the data (which is basically just a scaling) followed by 1D inversions of all data, which will give first insight into the distribution of the resistivities within and around the vent field.

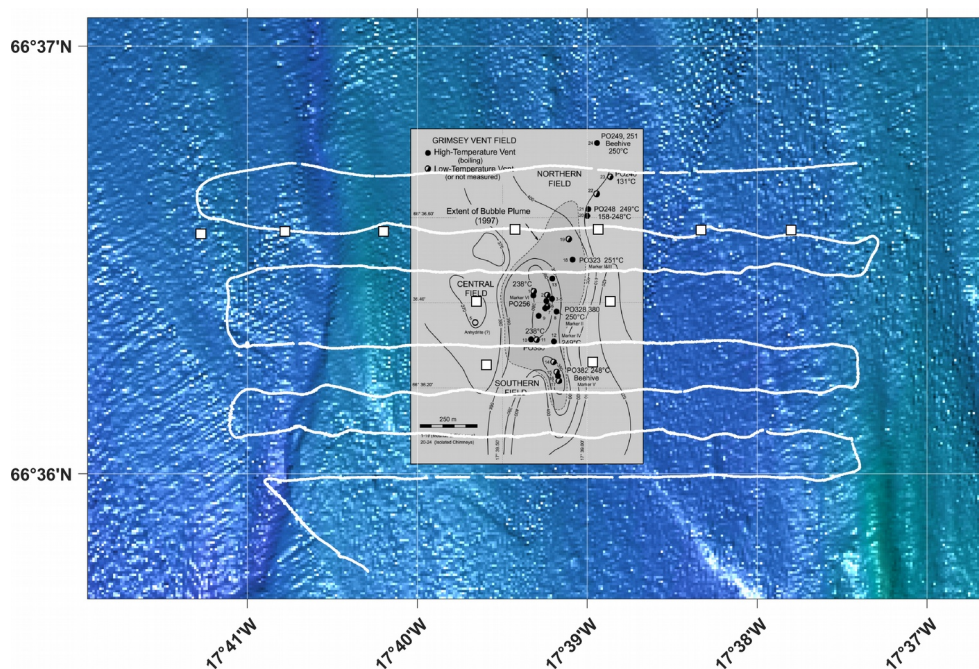


Fig. 14: Track of MARTEMIS system for the last experiment during the 4th deployment. Squares mark the positions of the OBEM receivers during this experiment. As reference, the map of Hannington et al. (2001) marks the position of the vent field and previous investigations (compare Fig. 2).

As final EM experiment, the MARTEMIS coil system, was deployed on the 20th of June for measurements along 20km of profiles, which covered the surrounding of the vent field to the E and W. Measurements were continued until the next morning. A first appraisal of the coil data indicated some data corruption, which might be related to a faulty connector or a broken cable or connector. At the moment it is not clear, if the coil data acquired during this deployment will be suitable for interpretation.

5.1.2. Coil2Dipole

With the configuration described in the previous sub-chapter, the MARTEMIS system was used for TEM measurements. However, by using remote receivers, which are placed stationary onto the seafloor, one can perform an additional EM experiment, which offers an increased depth of investigation, thus, adding valuable information about the deeper structure of the hydrothermal system. Stationary OBEM (ocean bottom electro-magnetic) receiver nodes (Fig. 15) are equipped with a three component fluxgate magnetometer, and can measure two components of the horizontal electric field. The components of the electric field are measured using Ag/AgCl-electrodes, which are attached at the end of four flexible arms. The total length of each receiver dipole is 11.2m. Additional sensors allow measurements of the attitude (pitch, roll) and the temperature. The receivers can either be used in MT-mode, in which

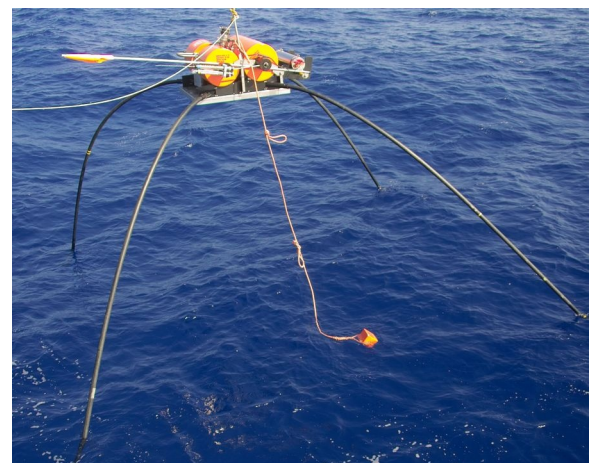


Fig. 15: OBEM receiver during deployment.

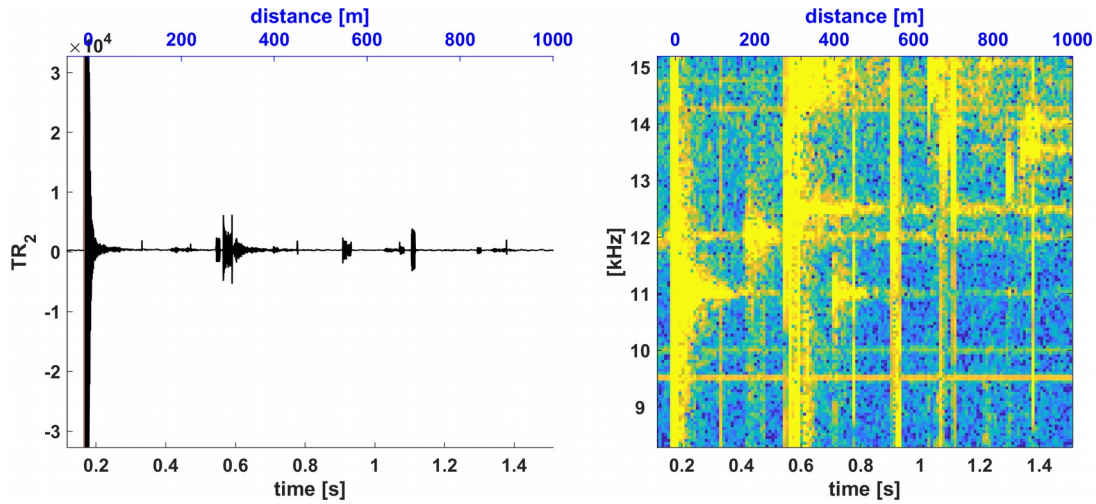


Fig. 16: Example of measurement with MARTEMIS ranging system with the acoustic waveform (left) and the associated spectrogram (right). The initial interrogation pulse (11kHz) with high amplitudes (@0m) is followed by several replies of transducers mounted to the remote OBEM receivers (e.g. ping of 12.0kHz @175m from OBEM11).

all sensors are logged at sampling rates of up to 10Hz, or switched into CSEM-mode, in which only two components of the E-field are recorded at a high sampling rate of 10kHz. This high frequency is necessary to acquire transient data at short offsets on the order of 100m and was used in this experiment. Generally, the switch from one mode to the other can be performed by using a preset timetable or alternatively by an external acoustic signal.

Since the MARTEMIS transmitter coil is used to transmit the signals which are picked up by the electric dipoles of the OBEM receivers, we call this experiment “Coil2Dipole”. Previously, we have conducted such an experiment at the Palinuro Seamount. Theoretical considerations for this type of experiment and first results from Palinuro can be found in Safipour et al. (2017a) and Safipour et al. (2018), respectively.

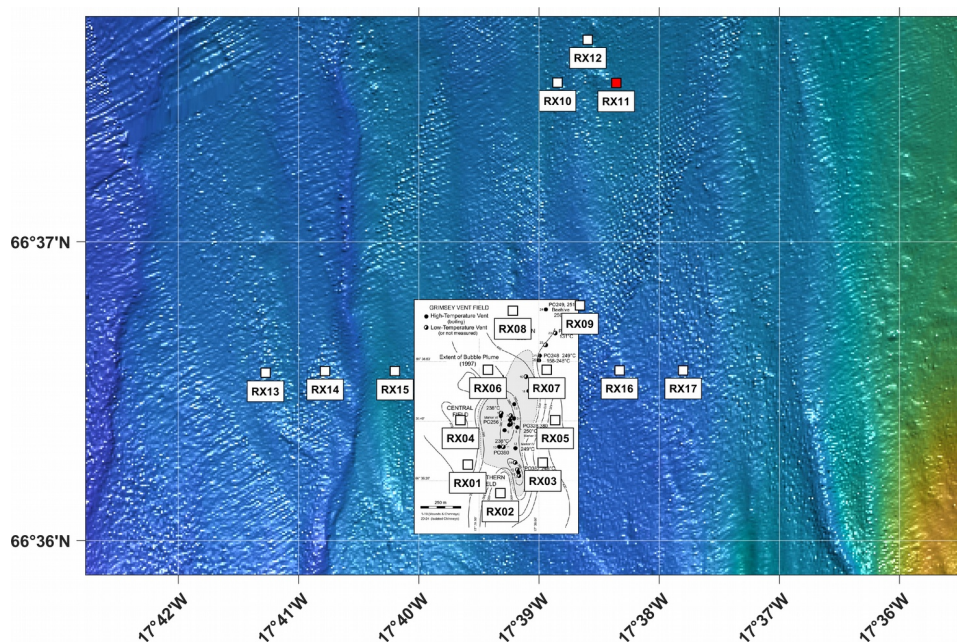


Fig. 17: Station map OBEM receivers (squares) with names. As reference, the map of Hannington et al. (2001) marks the position of the vent field and locations of previous investigations (compare Fig. 2).

We used 12 OBEMs (Fig. 15 & Fig. 17) for experiments, which were synchronized to GPS time prior to deployment and after recovery. On June 9th and 10th – before the first experiments – the receivers were lowered via the winch cable towards the seafloor being hooked onto a release with USBL beacon. At an altitude of approximately 30m above the seafloor the OBEMs were then released. Nine receivers were placed around the vent site and three additional receivers were deployed at a site approximately 2.5km to the north of the vent field, which was identified as a point of potential hydrothermal activity in the bathymetric data (see Fig. 9 for OBEM positions). Before the “Dual Polarization” experiment (see next chapter), some of the receivers were recovered and re-deployed free falling onto a W ↔ E profile line (see Fig. 14 for OBEM positions after re-deployment) on June 16th - 17th. One station (OBEM 11, red mark in Fig. 9) was released, but never returned to the surface. In a search on June 21st the location of this station was traced by acoustic navigation to a position about 2.5km to the south of the original drop position and on the next day the station was indeed found laying upside down on video footage acquired with the MARTEMIS system. Due to the limited means and equipment, the following rescue attempts did not succeed. A couple of weeks after the cruise we were informed by Icelandic authorities that a fisherman had found the station and in mid August the station was returned to us at GEOMAR.

For experiments like the Coil2Dipole experiment, it is important to know the exact distance between the transmitter antenna and the remote receivers. While the USBL positioning system can provide locations with an accuracy of about $\pm 5\text{m}$ at the given water depth of about 400m (value taken from the calibration measurements), high accuracy is needed in the evaluation of the data, especially for short transmitter receiver offsets. Such improved distance measurements can be achieved with the MARTEMIS on-board ranging system, which is mounted to the upper frame of the MARTEMIS system. Past experiments have shown that measurements with the ranging system are repeatable with ranges varying by at maximum of a few centimeters, even for large offsets, which of course assumes that the TX-RX distance does not vary between measurements. Thus, the accuracy of the ranging system is mainly determined by the knowledge of the sound velocity at the seafloor, which is measured with the external CTD, and we expect it to be better than 1m for the ranges relevant in this experiment ($<300\text{m}$), possibly even better than 10cm.

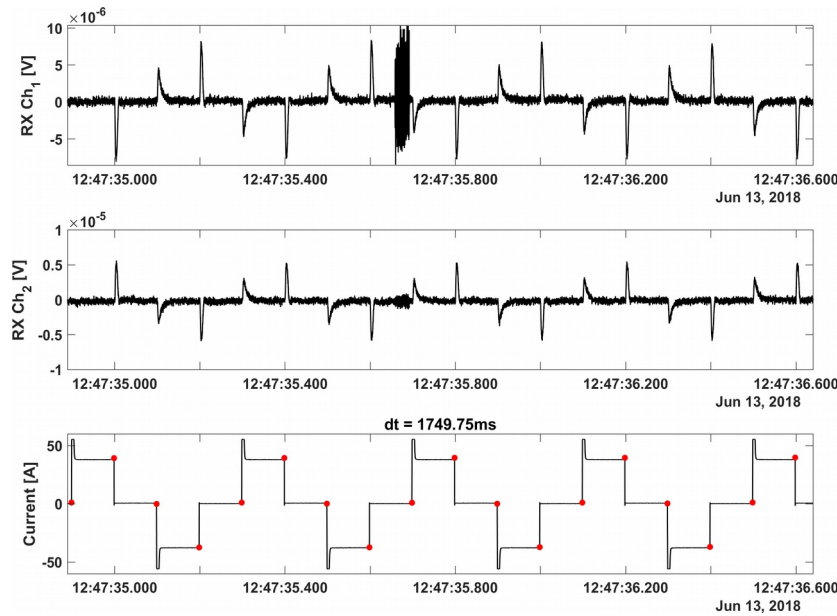


Fig. 18: Data example for Coil2Dipole measurement with signal transmitted at TX station S0570 (bottom) and received signal in the two electrical field channels of RX03 (top & middle).

For the experiment at the GVF we used individual reply frequencies for each OBEM, which allows for a simple and unique identification of OBEMs by the frequencies of received signal. Fig. 16 shows an example from TX station S2345 with the interrogation pulse (11kHz, 0m) sent out from the transducer mounted to the upper frame of the MARTEMIS system (see Fig. 6) and replies of the OBEM stations, the first one from OBEM11 indicating a distance of about 175m. As stated before, the ranging system did not work during the first deployments of the coil system. Thus, for the first experiment (see Fig. 9) the evaluation of the Coil2Dipole data will have to rely on the USBL positions. For the last coil experiment (see Fig. 14, coil stations S1744 – S3123) the ranging system worked properly and evaluation of data will benefit from the increased accuracy of the positioning.

Turning to the data acquired with the OBEM receivers we found that one station (RX06, DEV45) did not record any E-field data, and at one station (RX13, DEV62) one E-field channel was dead. As mentioned above, OBEM station RX11 was displaced by a fisherman, but at the moment we don't know at what time this happened. Thus, 14 of 17 stations recorded useful data during the MARTEMIS experiments and for one the status is currently unknown. The time synchronization between transmitter and receivers has not been verified, yet, and the evaluation of ranging measurements for the last MARTEMIS deployment is also pending. Thus, several steps in the data processing still need to be taken care of before the evaluation of data in terms of an imaging or inversion can be performed.

5.1.3. Dual Polarization CSEM

In addition to the MARTEMIS coil experiment, we performed a novel EM experiment, which we call “Dual Polarization CSEM”. In this experiment, the ropes of the rigging, which connect the lower and the upper frame of the MARTEMIS system, were used to install two perpendicular pairs of transmitter electrodes above the corners of the coil frame (Fig. 19).

This, allows for a CSEM experiment with two independent, horizontal transmitter dipole polarizations, in which the TX dipoles have a length of ~5.4m and should yield an increased depth of investigation down to about 300m.

The Dual Polarization experiment was carried out along a 3.7km long W ↔ E profile crossing the active hydrothermal vent field (Fig. 20).

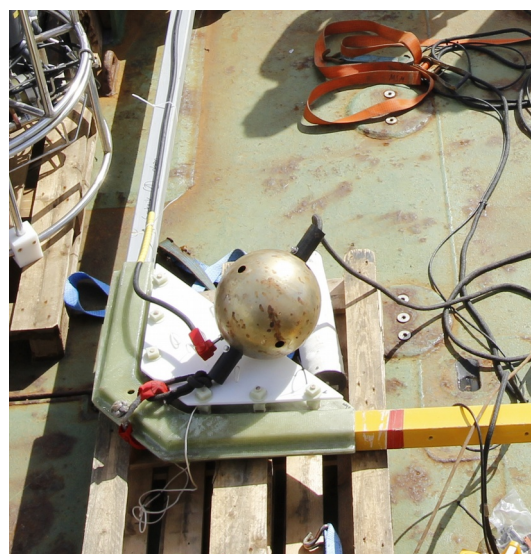


Fig. 19: Transmitter electrode attached to one of the ropes, which connects the upper and lower frame of the MARTEMIS system.

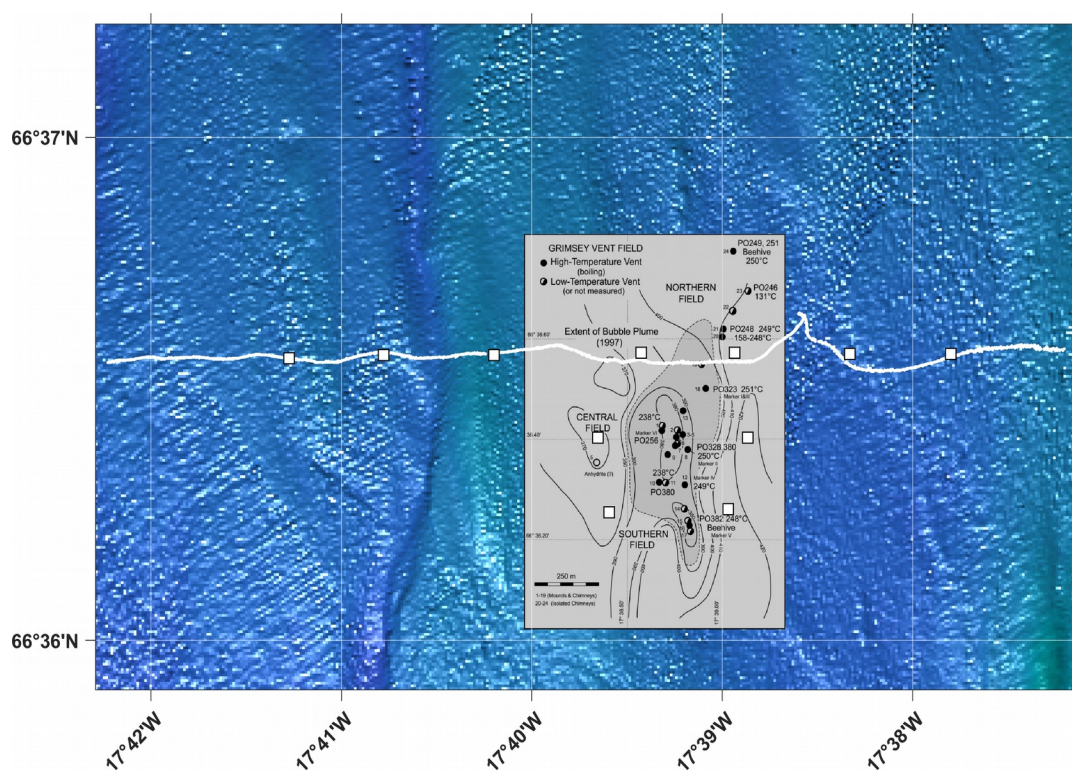


Fig. 20: Station map during Dual Polarization CSEM experiment with the track line of the MARTEMIS system (white line), which carried the two TX dipoles, and the stationary OBEM receiver stations (squares). As reference, the map of Hannington et al. (2001) marks the position of the vent field and locations of previous investigations (compare Fig. 2).

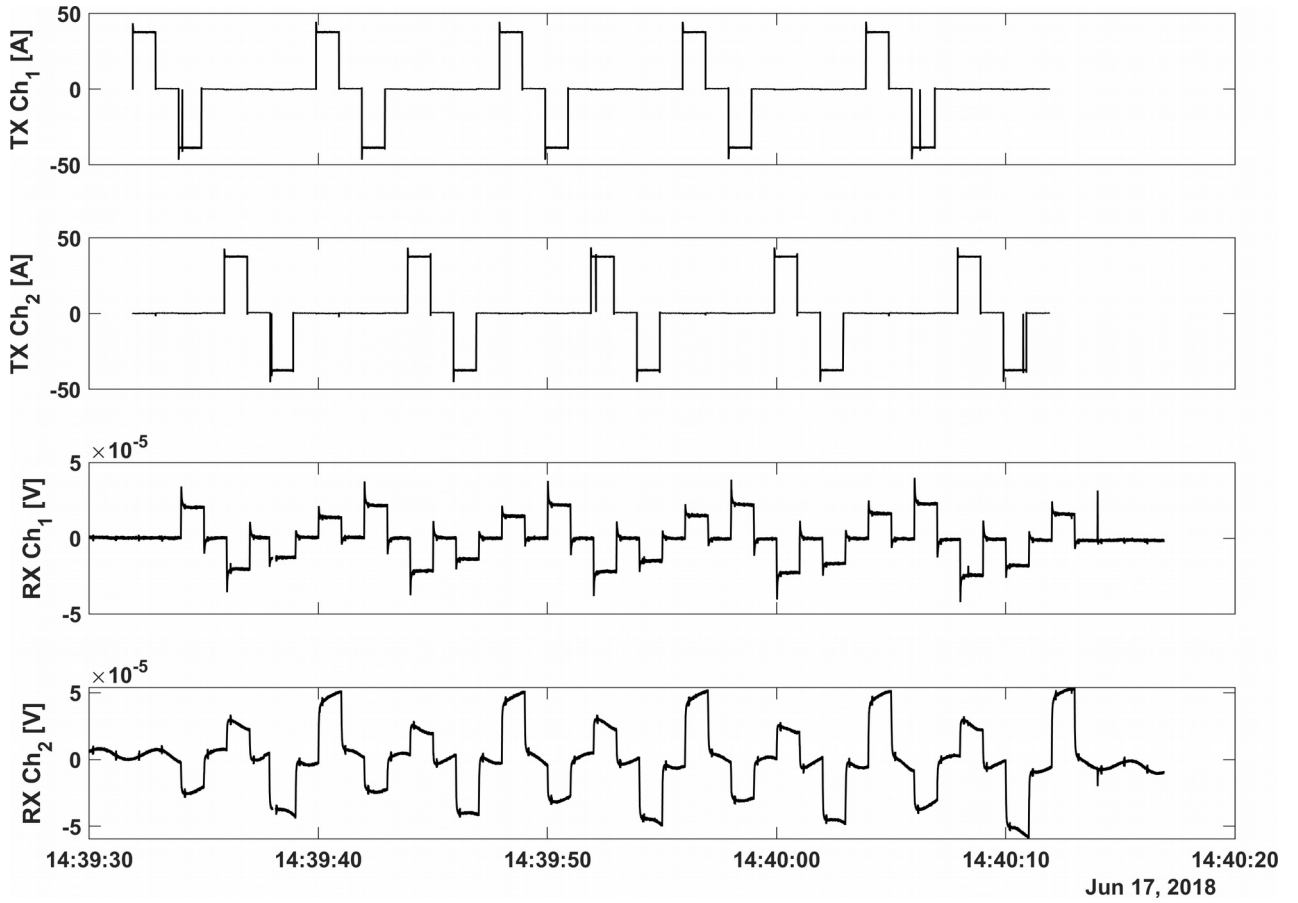


Fig. 21: Data example of Dual Polarization CSEM with the signal in transmitter channels 1 and 2 in the upper pannels and the received signal at RX17 in the lower channels.

Transmitted signals were recorded by seven stationary OBEM receivers along the profile and four additional receivers, which were located to the south of the profile. Fig. 21 shows a data example in which the transmitted signal in the two transmitter polarizations is shown in the upper pannels and the received signal as measured with receiver RX17 is shown in the lower pannels. It can be seen that first one full cycle ($=4s$) is transmitted in the first polarization direction (\rightarrow TX Ch₁) and after that one full cycle is transmitted in the second polarization direction (\rightarrow TX Ch₂). This alternate style of transmitting into the two polarization directions was implemented to facilitate the later data processing in terms of rotational invariants. A look at the lower pannels shows that the time synchronization between transmitter and receiver is not correct at the moment (there seems to be a 1s time difference between the two). This will be checked and corrected in the upcoming data processing.

As this experiment is novel and was conducted for the first time ever, the previously established processing routines for the “regular” CSEM data will need to be changed and extended to handle this new type of data. The established imaging (Swidinsky et al., 2015) and inversion routines (Hölz et al., 2015a) should then be applicable to the processed data without any further changes necessary.

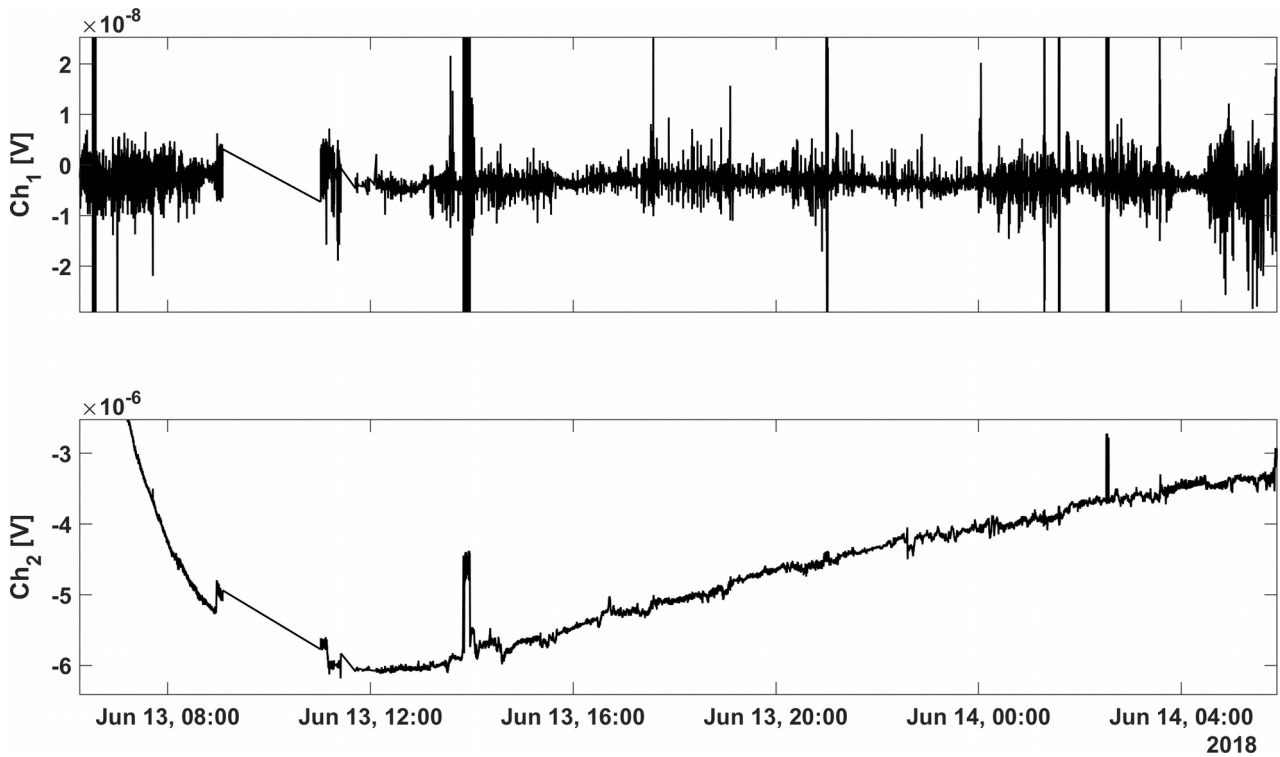


Fig. 22: Measurements of the ambient horizontal electrical field during the second MARTEMIS deployment (see Fig. 9). Times during which the coil transmitter was activated have been removed from the signal.

5.1.4. Selfpotential

With some modifications / additions the system, the MARTEMIS platform was also used for measurements of the self-potential during TEM measurements. Measurements of the self-potential (SP) – which actually measure the ambient horizontal electrical field – were carried out by attaching two pairs of Ag/AgCl-electrodes to the coil frame: the four electrodes were mounted at the centers of the corner connectors of the coil. This allowed for measurements of two perpendicular components of the horizontal electrical field, from which the horizontal component of the ambient electrical field may be constructed. Signals were logged with the same data logger used for the TEM measurements.

SP data were collected during all deployments of the MARTEMIS system. Fig. 22 shows the measured voltages of the horizontal receiver dipoles, which were mounted to the coil frame. Time intervals during which the transmitter coil was active have been removed from the data. However, it seems that some of the visible anomalies are still due to activations of the transmitter, which were not taken care of by the automatic processing script. Also, channel two still shows a significant drift, which will need to be removed before analyzing / searching the data for any anomalies, which are related to hydrothermal activity.

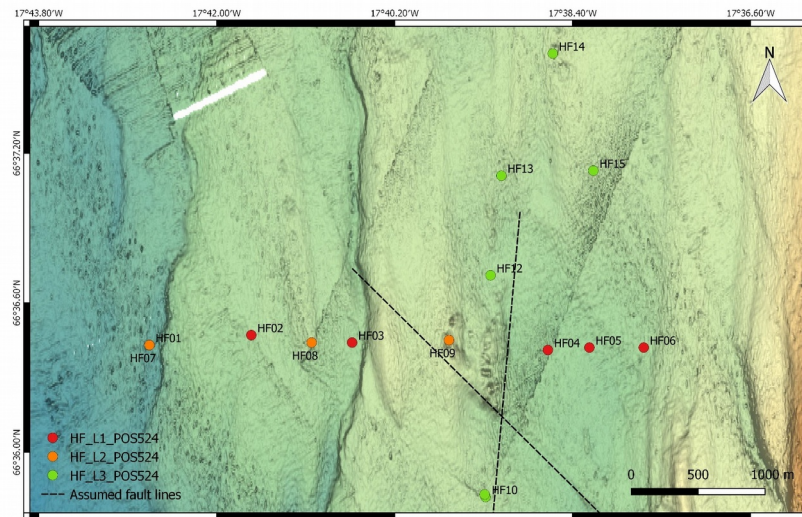


Fig. 23: Heat flow lines measured during cruise POS524, encompassing measurements at 15 locations.

5.2. Heatflow

Sofia Martins and Patrick Schröder

All the recorded temperatures within the GVF were either performed by direct sampling with JAGO or with on-deck measurements on gravity cores (Stoffers et al., 1997; Scholten et al., 2000; Devey et al., 2002). Thus, in-situ measurements at depth within the sediment coverage using heat probes have not been performed so far.

During this cruise, heat flow measurements were performed using GEOMAR's short violin-bow type heat flow probe (Model FIELAX GmbH, Bremerhaven) which allows for data acquisition in seafloor sediments down to a penetration depth of 3m (Hyndman et al., 1979, Lister, 1979). The stainless-steel probe contains 22 thermistors (NTC1 – NTC22) in the sensor string with a temperature resolution of $< 0.01^{\circ}\text{C}$. The sensor string also contains a heating wire from which a heat pulse is released into the sediment.

The probe was deployed on the port-side of the ship and lowered to the seafloor at 1.0m/s winch speed. Upon arrival to the station site, the probe was stabilized for 5 minutes, after which it was “dropped” at a speed of 1.2 – 1.4m/s. Considering the time of temperature measurement, heat pulse duration and measurement of the heat pulse decay, the entire sampling event at each heat flow station, lasted approximately 15 minutes. Due to the distance between stations (up to 1.6km) the heat flow probe was heaved to 200m above seafloor in transit between stations to prevent the rise of the stabilization time upon arrival to the next measuring point.

15 measurements were performed in total with the heat flow probe: Heat flow line 1 (6 points; HF01 – HF06), Heat flow line 2 (3 points, HF07 – HF09) and Heat flow line 3 (6 points, HF10 – HF15) (see Fig. 23 & Appendix 9.2). The probe was operated in an autonomous mode, in which the acquired data was saved to the data logger and retrieved after recovery onboard. The operation in real-time mode was not possible, since a winch wire without cables for communication was used.

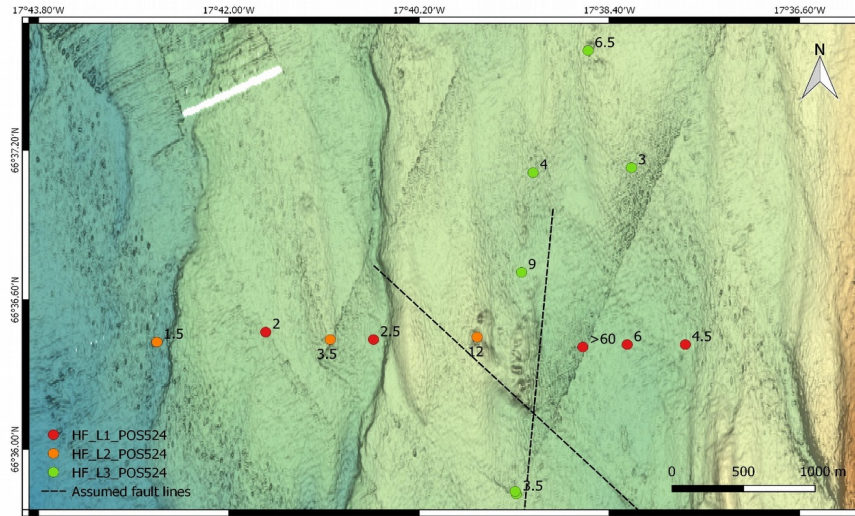


Fig. 24: Maximum temperatures obtained by the heatflow probe during cruise POS524.

Generally, the in-situ thermal conductivity is calculated using the heat pulse method (Lister, 1979). For measurements during this cruise, the first 7min after sediment penetration were used to record the temperature of the sediments. This leaves enough time to dissipate frictional heat to estimate the steady state temperature. After a 10s long calibrated heat pulse of 1kJm^{-1} , the temperature decay was measured for another 7min to estimate the in-situ thermal conductivity. Due to the expected high temperature of the sediment around the GVF, the probe used the calibration file Mem21260.prb. See Villinger and Davis (1987) for a detailed description about the data processing leading to the in-situ temperatures and thermal conductivity values. Due to a technical problem, no heat pulse was generated in the first heat flow deployment along Line 1.

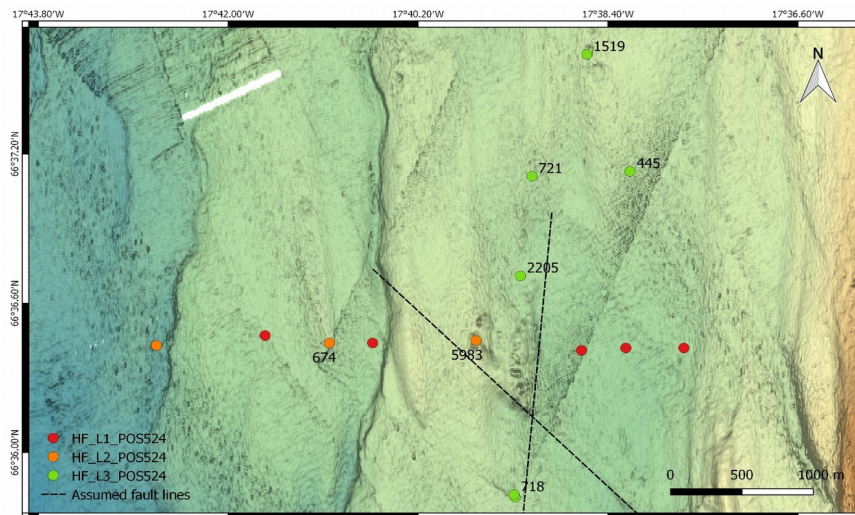


Fig. 25: Thermal conductivity (mW/m^2) obtained around the GVF.

5.3. Gravity Coring

Sofia Martins & Anna Jegen

The objective of the POS524 sampling was to extend the area of observations covered during previous cruises to more distal areas to assess the extent of the hydrothermal influence and complement the existing sampling concerning sediment samples and pore water. The recent seismic activity (see Fig. 4) was taken in consideration when choosing the sampling sites. GEOMAR's short gravity corer (3m, 125mm diameter, 900kg weight) was used at a total of eight stations from which a total of about 20m of sediment cores were collected (Fig. 4). Details can be found in the table below and in the appendix (core descriptions: pp. 48, pore fluid samples: pp. 69).

Station	Latitude Longitude	Water depth	Recovery	Description
POS524/01GC	66°36.413' N 17°39.254' W	390 m	302cm	Coarse grained anhydrite detritus atop a heterogeneous blueish altered sediment layer and indurated dark brownish clay layer, all with abundant disseminated sulphides. T _{max} : 84°C
POS524/02GC	66°36.950' N 17°39.233' W	403 m	290cm	Background sediment composed of homogeneous non-indurated greenish grey clay with a strong H ₂ S smell. T _{max} : 12.5°C
POS524/03GC	66°36.449' N 17°39.664' W	377 m	95cm	Homogeneous dark greenish silt/clay with intercalation of sand size anhydrite. Dehydrated very hard dark brown clay layer. T _{max} : 10.7°C
POS524/04GC	66°36.440' N 17°40.631' W	413 m	290cm	Background sediment composed of homogeneous non-indurated greenish grey clay with a strong H ₂ S smell. T _{max} : 6.3°C
POS524/05GC	66°37.631' N 17°38.582' W	393 m	290cm	Background sediment composed of homogeneous non-indurated greenish grey clay with a strong H ₂ S smell. T _{max} : 7.8°C
POS524/06GC	66°36.400' N 17°38.672' W	419 m	288cm	Background sediment composed of homogeneous non-indurated greenish grey clay with a strong H ₂ S smell. T _{max} : 31.5°C
POS524/07GC	66°36.184' N 17°39.178' W	396 m	150cm	Greenish grey clay with sand size anhydrite/talc grains interlaid with coarser anhydrite sand layers. T _{max} : 66°C
POS524/08GC	66°36.310' N 17°39.285' W	390 m	291cm	Homogeneous dark olive-green clay interlaid with rhythmic lens/layers of coarse anhydrite/talc fragments. T _{max} : 45°C

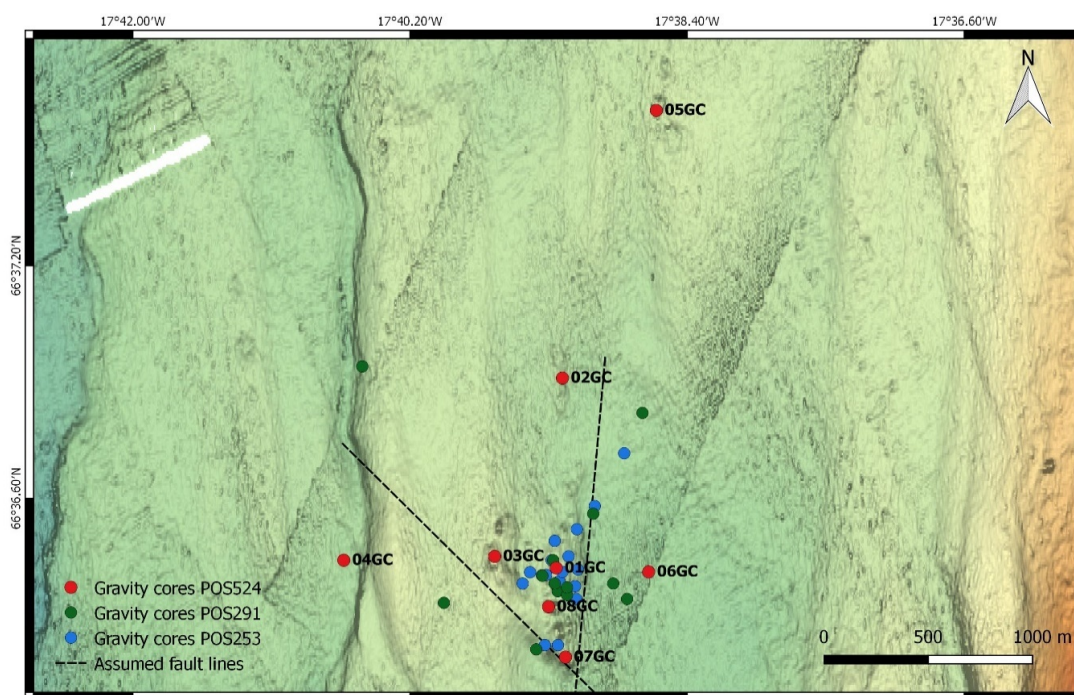


Fig. 26: Location of sediment cores collected during POS524 (red markers). The assumed fault lines were derived by seismic interpretation (see Devey et al., 2002). In addition, locations of sediment cores collected during previous RV Poseidon cruises POS291 (2001) and POS253 (1999) are also indicated by green and blue markers, respectively.

Core handling and sampling

Upon recovery on deck, several parameters (pH, Eh, conductivity and temperature) were immediately measured in the material caught in the core catcher using two separate probes (Hach Multimeter MM110DL & Hach Multimeter MM150DL). Core catcher and core liner were then removed. The liner was then cut into 3 x 1m long sections and measurements with the probes were being repeated on the bottom of each core section and on the top of the shallowest one.

After labeling of the core sections, ends were sealed with caps, after which the sections were moved from the deck to the wet lab for further handling. Afterwards the core sections were split lengthwise into working and archive halves using a power disc-saw (Fein-Multimaster) with special attention being paid to not disturb the sediment inside. Both halves were then photographed, described and the color of sediment was retrieved by visual comparison with color charts of the Munsell color system (HVC) (see core description in Appendix 9.3). Work was continued by taking sub-samples of sediments and pore water from the working halves. Finally, both working and archive halves were stored in plastic sleeves within labeled D-tubes. The sections will be deposited at the core repository at GEOMAR.

Sediment Sampling

Several cm³ of sediment were recovered, for geochemical studies, in the center of the working half using a cut-off, tip-less syringe (20ml). Whenever possible, sediment and pore water were recovered within the same depth interval. The sediment samples were then transferred to properly labeled zip-lock plastic bags.

The sampling spots were also analyzed for pH, Eh, temperature and conductivity (Hach Multimeter MM110DL & Hach Multimeter MM150DL). In total 69 samples were retrieved for subsequent analysis.

Porefluid Sampling

After the cores were split, pore fluids were collected on the working half using Rhizon CSS (Core Solution Samplers) (Fig. 27). These rhizons consists of a 4cm porous polymer tube (0.15 μm) with a flat tip and a diameter of 2.5 mm, supported by a glass fiber strengthener and connected with a PEC/PVC tubing of 12cm and female luer lock. The syringes (20 ml) were screwed directly on the luer and the piston was kept in place with a retainer (wooden piece) that enabled vacuum to be created (Rhizosphere Research Products, 2018). Before usage, all the Rhizons CSS were soaked, for at least 24 hours, in artificial seawater of approximately Atlantic salinity.

The pore fluids were stored in 20 ml, acid-cleaned, HDPE mini vials. For ICP analyses preparation, 3ml of each of the collected pore fluid was transferred into an acid-cleaned 3 ml HDPE mini vial and acidified by adding 30 μl of ultra pure HNO_3 . A total of 68 pore fluid samples were collected, including method blanks (every 8th sample, see Appendix 9.4, pp. 69).



Fig. 27: Pore fluid sampling in POS524/01GC using Rhizons CSS with 4cm porous polymer tubes (photo by Shuangmin Duan)

Sediment description

From the eight gravity cores collected, four were in or in close proximity to the main hydrothermal mound (01GC, 03GC, 07GC, 08GC). Cores 01GC and 08GC were retrieved from the central hydrothermal field, 07GC from the southern field and 03GC west of the central mound (350m). The highest temperatures were recorded on 01GC, 07GC and 08GC, reaching 84°C (see Fig. 26 & Appendix 9.3). Even though these cores are heterogeneous concerning the type of recovered sediment, all of them show evidence for strong hydrothermal influence such as indurated clay layers, blueish altered sediment, disseminated sulfides and mixtures of clay and anhydrite/talc sand. The remaining four gravity cores were retrieved from peripheral or more distal areas (02GC, 04GC, 05GC, 06GC) with core catcher temperatures ranging from 6.3 – 31.5°C. These cores are homogeneous in sediment type, consisting of undisturbed dark greenish gray clay with strong H_2S smell (see Appendix 9.3, pp. 48).

The core collected in the central mound (01GC) is the one that shows the most variety in lithology and texture. It is composed of coarse grained anhydrite detritus with disseminated sulfides (probably derived from the collapse of anhydrite chimneys) in the upper 130cm. A heterogeneous blueish altered sediment layer occurs between 130 and 160cm bsf., showing patches of black material in the first 10cm. This layer ends in a channel that penetrates the adjacent layer. This is an indurated dark brownish clay layer with abundant disseminated sulfides. Towards the bottom of the core, the layer becomes drier and flakier, containing abundant small cracks filled with sulfides. The cracks might result from sediment baking by hot hydrothermal fluids and the consequent hardening of the layer and hydro-fracturing (Fig. 28).

Core 03GC had the shortest recovery (95cm) and is mainly composed of homogeneous dark greenish silt/clay with small shell fragments and a 5cm intercalation of sand size anhydrite and dark mottled clasts (red, black, reddish) with probable volcanic origin. The reduced core recovery was due to a very hard dark brown clay layer (baked sediment), sampled

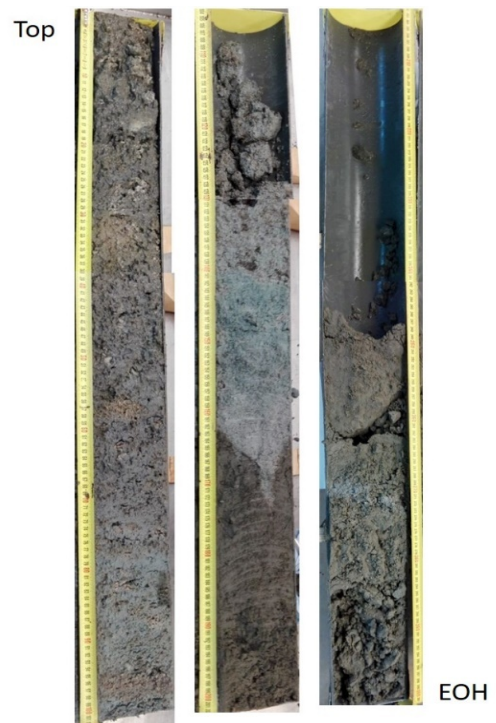


Fig. 28: Sediment core 01GC retrieved in the main central hydrothermal mound with strong evidence for hydrothermal influence.

by the core catcher, that prevented the core penetrating deeper.

Core 07GC was recovered on the southern part of the GVF. The 155cm core is made up of a mixture of greenish gray clay with sand size anhydrite/talc grains and occasional volcanic material. Interlaid are coarser anhydrite sand layers with a brown to whitish color. Between 100 – 120cm bsf the clay/anhydrite mixture is strongly dehydrated with visible cracks.

Recovered at the edge of the central mound, core 08GC is mainly composed of homogeneous dark olive-green clay with scarce shells, anhydrite fragments and occasional black patches. Between 130 and 190cm bsf, the clay is interlaid with rhythmic lens/layers of coarse anhydrite/talc fragments.

The cores collected peripheral or distally of the main hydrothermal mound (02GC, 04GC, 05GC and 06GC) contain a homogeneous, non-indurated, greenish-gray clay with strong H₂S smell and occasional shell fragments and dark patches (Fig. 29).



Fig. 29: Sediment core 04GC, collected 1km west of the main hydrothermal mound. is characterized by homogeneous greenish grey clay with strong smell of H₂S.

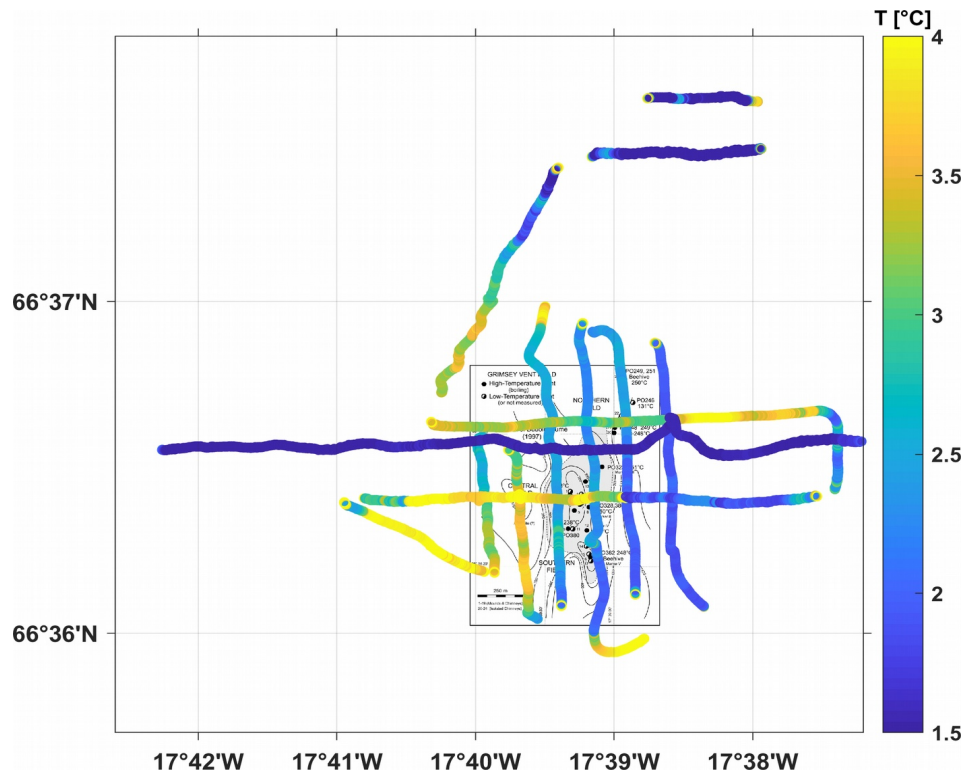


Fig. 30: Map of temperatures measured with CTD probe during deployments of the MARTEMIS system. As reference, the map of Hannington et al. (2001) marks the position of the vent field and locations of previous investigations (compare Fig. 2).

5.4. CTD

CTD measurements were carried out using an autonomous Microcat CTD sensor from Seabird. Measurements were carried out during the initial release test on the 9th of June, which were used for the initial calibration of the Posidonia USBL system, and during all deployments of the MARTEMIS system.

Fig. 30 shows a color coded map of temperatures measured by the CTD probe during experiments with the MARTEMIS system. Since the CTD sensor was mounted to the lower coil frame, most measurements were taken at elevations of less than 10m above the seafloor (see Fig. 8). Quite unexpectedly, there is no anomaly of the temperature which relates to the previously mapped extent of the hydrothermal field and instead elevated temperatures are evident especially to the west of the field. The reason for this finding can be understood when looking at the temperature data recorded at one of the stationary receivers (Fig. 31), which is representative for all stations and demonstrates that there are large and rather quick temporal variations in the temperature. It should be noted that similar variations were measured at all stations, i.e. even at the three

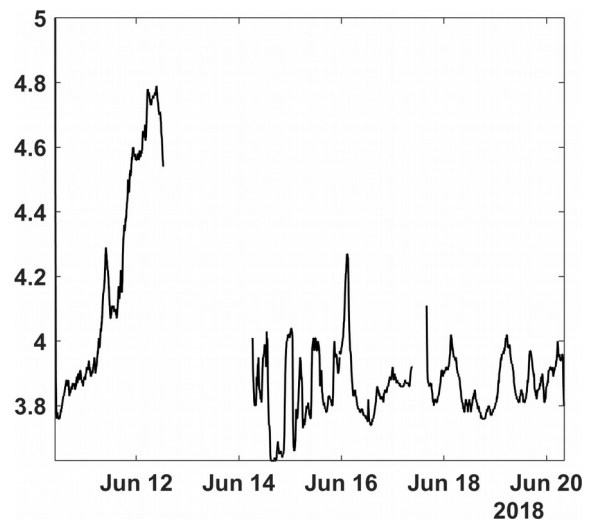


Fig. 31: Temperatures measured at receiver RX05, which is located directly east of the main vent field. Data gaps are due to the fact that temperatures are not logged while the receiver is in CSEM-mode.

remote stations to the north. This seems to indicate that temperature variations are not due to a change in the hydrothermal activity, but rather a reflection of warm water masses passing through the working area. Thus, an unexpected result of CTD measurements is that the temperature data from the mobile CTD probe, even though it was mostly collected close to the seafloor, is not by itself suitable to detect and characterize the hot hydrothermal system. If it is possible to correct the mobile data by means of the temperature data from the stationary OBEM receivers remains to be seen.

6. Data and Sample Storage and Availability

In Kiel a joint data management team of GEOMAR and Kiel University organizes and supervises data storage and publication by marine science projects in a web-based multi-user system. The geophysical data that has been acquired will be for use of GEOMAR scientists and collaborators only for the first phase and can be made available to other researcher by request to Dr. Sebastian Hölz (shoelz@GEOMAR.de) or Dr. Sofia Martins (smartins@geomar.de). All metadata are immediately available publicly via the GEOMAR portal (<https://portal.GEOMAR.de/metadata/leg/show/344880>).

In addition the portal provides a single downloadable KML formatted file (portal.GEOMAR.de/metadata/leg/kmlexport/344880) which retrieves and combines up-to-date cruise related information, links to restricted data and to published data for visualization e.g. in Google Earth.

7. Acknowledgments

We would like to thank the crew of *R/V Poseidon* for their excellent support during cruise POS524, especially Captain M. Günther and the bridge for patient help in all organizational matters and excellent ship handling, Bosun Frank Schrage and his deck crew for helping us to optimize the deployment procedure of the MARTEMIS system and handling of our gear, and finally the crew down in the engine for their support. We would also like thank the directorate of GEOMAR, who granted substantial financial support for the cruise.

We would also like to thank Geir Hagalínsson from NTE for granting us access to the working area, for which NTE hold an exclusive license for the exploration of hydrothermal energy. Bjarne Richter from ISOR is acknowledged for sharing information on marine hydrothermal systems around Iceland, which were really helpful in planing the current cruise as well as applying for future cruises. Also, Pall Bergmann Reynisson provided us with bathymetric data, which are an essential part in the operation of our systems close to the seafloor. The provided ship-based multibeam bathymetry was collected by the Marine Research Institute (MRI) in Reykjavik, now the Marine & Freshwater Research Institute (MFRI) (<https://www.hafogvatn.is/>) and University of Iceland (<https://www.hi.is/>) on board *R/V Árni Friðriksson* during cruises in summer 2002 and 2004 using the onboard Kongsberg EM300 multibeam echosounder.

A special thank goes out to Anett Blischke and other colleagues from ISOR for their support in handling the return of our lost instrument.

8. References

- Ármansson, H., 2016: The fluid geochemistry of Icelandic high temperature geothermal areas. *Applied Geochemistry*, 66, 14 – 64.
- Atkins, D. & Audunsson, H., 2013: Exploration Techniques for Locating Offshore Geothermal Energy Near Iceland. Proceedings of the 38. Workshop on Geothermal Reservoir Engineering, Stanford University, 11-13.2.2013, SGP-TR-198.
- Beltenev, V., V. Ivanov, I. Rozhdestvenskaya, G. Cherkashov, T. Stepanova, V. Shilov, A. Pertsev, M. Davydov, I. Egorov, I. Melekestseva, E. Narkevsky, and V. Ignatov, 2007, A new hydrothermal field at 13_30'N on the Mid-Atlantic Ridge: *InterRidge News*, 16, 9–10.
- Boschen, R.E., Rowden, A.A., Clark, M.R. & Gardner, J.P.A., 2013: Mining of deep-sea seafloor massive sulfides: A review of the deposits, their benthic communities, impacts from mining, regulatory frameworks and management strategies. *Ocean and Coastal Management*, 84, 54–67.
- Botz, R., Winckler, G., Bayer, R., Schmitt, M., Schmidt, M., Garbe-Schönberg, D., Stoffers, P. & Kristjansson, J.K., 1999: Origin of trace gases in submarine hydrothermal vents of the Kolbeinsey Ridge, north Iceland. *EPSL*, 171, 83 – 93.
- Brewitt-Taylor, C., 1975, Self-potential prospecting in the deep oceans: *Geology*, 3, 541–543.
- Cairns, G.W., Evans, R.L. & Edwards, R.N., 1996: A time domain electromagnetic survey of the TAG hydrothermal mound. *Geophysical Research Letters*, 23, 3455–3458.
- Cherkashev, G., V. Ivanov, V. Beltenev, L. Lazareva, I. Rozhdestvenskaya, M. Samovarov, I. Poroshina, M. Sergeev, T. Stepanova, I. Dobretsova, and V. Kuznetsov, 2013, Massive sulfide ores of the northern equatorial Mid-Atlantic Ridge: *Oceanology*, 53, 607–619.
- Cherkashov, G., I. Poroshina, T. Stepanova, V. Ivanov, V. Beltenev, L. Lazareva, I. Rozhdestvenskaya, M. Samovarov, V. Shilov, G. Glasby, Y. Fouquet, and V. Kuznetsov, 2010, Seafloor massive sulfides from the northern equatorial Mid-Atlantic Ridge: New discoveries and perspectives: *Marine Georesources & Geotechnology*, 28, 222–239.
- Corwin, R., 1976, Offshore use of the self-potential method: *Geophysical Prospecting*, 24, 79–90.
- Davis, E.E., Goodfellow, W.D., Bornhold, B.D., Adshead, J., Blaise, B., Villinger, H., Le Cheminant, G.M., 1987: Massive sulfides in a sedimented rift valley, northern Juan de Fuca Ridge. *Earth and Planetary Science Letters*, 82, 49–61.
- Devey, C.W., shipboard scientific party, 2002. Hydrothermal studies of Grimsey Field, volcanic studies of Kolbeinsey Ridge. Cruise Report POS 291 of R/V Poseidon, University of Bremen. 42 pp.
- Evans, R., Webb, S., Jegen, M. & Sananikone K., 1998: Hydrothermal Circulation at the Cleft-Vance Overlapping Spreading Center: Results of a Magnetometric Resistivity Survey. *Journal of Geophysical Research*, B6, 12, 321–12 338.
- Gudmundsdóttir, E.R., Eiríksson, J. & Larsen, G., 2011: Identification and definition of primary and reworked tephra in Late glacial and Holocene marine shelf sediments off North Iceland. *J. Quat. Sci.*, 26, 589–602.
- Hannington, M., Herzig, P., Stoffers, P., Scholten J., Botz, R. Garbe-Schönberg, D., Jonasson, I.R., Roest, W. & Shipboard Scientific Party, 2001: First observations of high-temperature submarine hydrothermal vents and massive anhydrite deposits off the north coast of Iceland. *Marine Geology*, 177, 199 – 220.
- Hannington, M.D., Jamieson, J., Monecke, T. & Petersen, S., 2010: Modern Sea-Floor Massive Sulfides and Base Metal Resources: Toward an Estimate of Global Sea-Floor Massive Sulfide Potential. *Economic Geology Special Publication*, 15, 317–338.
- Hannington M., Jamieson, J., Monecke, T., Petersen, S. & Beaulieu, S., 2011: The abundance of seafloor massive sulfide deposits. *Geology*, 39, 1155–1158.
- Heinson, G., A. White, S. Constable, and K. Key, 1999, Marine self potential exploration: *Exploration Geophysics*, 30, 1–4.
- Heinson, G., A. White, D. Robinson, and N. Fathianpour, 2005, Marine self-potential gradient exploration of the continental margin: *Geophysics*, 70, G109–G118.
- Hölz, S., Swidinsky, A. & Jegen, M., 2013: Investigations on Small Scale Targets with Sputnik, A Two Polarization Transmitter System. Talk with extended abstract during CSEM Workshop (WS09), EAGE, Amsterdam, 16.-19.6.2014.
- Hölz, S., Swidinsky, A., Jegen, M. & Bialas, J., 2015a: The use of rotational invariants for the interpretation of marine CSEM data with a case study from the North Alex mud volcano, West Nile Delta. *Geophysical Journal International*, 1, 224–245.
- Hölz, S., Jegen, M., Petersen, S. & Hannington M., 2015b: How to Find Buried and Inactive Seafloor Massive Sulfides using Transient Electromagnetics - A Case Study from the Palinuro Seamount in the Tyrrhenian Sea. Extended abstract for presentation at the Underwater Mining Conference, Tampa Bay, USA, 1.-6.11.2015.
- Hyndman, R.D., Davis, E.E., and Wright, J.A., 1979. The measurement of marine geothermal heat flow by a multipenetration probe with digital acoustic telemetry and in situ thermal conductivity, *Marine Geophysical Res.*, 4, 181–205.

- IMO (2018a): Icelandic Met Office - 400 earthquakes detected at Grímsey island in last 12 hours. WWW electronic publication, ice-landmonitor.mbl.is/news/nature_and_travel/2018/02/15/400_earthquakes_detected_at_grimsey_island_in_last_, accessed 26.3.18.
- IMO (2018b): Icelandic Met Office - Seismic swarm near Grímsey: update 15:00, 19 February. WWW electronic publication, accessed 26.3.2018, <http://en.vedur.is/about-imo/news/seismic-swarm-near-grimsey-update-15-00-19-february>.
- Iturrino, G.J., Davis, E., Johnson, J., Groeschel-Becker, H., Lewis, T., Chapman, D. & Cermak, V., 2000: Permeability, electrical and thermal properties of sulfide, sedimentary and basaltic units from the Bent Hill area of Middle Valley, Juan de Fuca ridge. *Proceedings of the ODP, Scientific Res.*, Vol. 169.
- Kowalczyk, P., 2008. Geophysical prelude to first exploitation of submarine massive sulphides, *First Break*, 26.
- Lackschewitz, K.S., Botz, R., Garbe-Schönberg, D., Scholten, J. & Stoffers, P., 2006: Mineralogy and geochemistry of clay samples from active hydrothermal vents off the north coast of Iceland. *Marine Geology*, 225, 177 – 190.
- Lister, C.R.B., 1979. The pulse-probe method of conductivity measurement. *Geophys. J. R. Astr. Soc.*, 57, 451–461.
- Magnúsdóttir, S., Brandsdóttir, B. Driscoll, N. & Detrick, R., 2015: Postglacial tectonic activity within the Skjálfandadjúp Basin, Tjörnes Fracture Zone, offshore Northern Iceland, based on high resolution seismic stratigraphy. *Marine Geology*, 367, 159 – 170.
- Monecke, T., Petersen, S., Hannington, M.D., Samson, I. & Grant, H., 2016: Critical element inventory of seafloor massive sulfide deposits. *Reviews in Economic Geology*. In press.
- Palacky, G.V., 1987: Resistivity characteristics of geologic targets, in *Electromagnetic Methods in Applied Geophysics*, Vol. 1, Theory, pp 1351, SEG.
- Quist, A.S. & Marshall, W.L., 1968: Electrical conductances of aqueous sodium chloride solutions from 0–800°C and at pressures to 4000 bars. *Journal of Physical Chemistry*, 72, 684 – 703.
- Riedel, C., Schmidt, M., Botz, R. & Theilen F., 2001: The Grímsey hydrothermal field offshore North Iceland: Crustal structure, faulting and related gas venting. *Earth and Planetary Science Letters*, 193(3-4), 409-421.
- Safipour, R., Hölz, S., Jegen, M., Swidinsky, A. 2017a: On electric fields produced by inductive sources on the seafloor, *Geophysics*, 82, E297-E313.
- Safipour, R., Hölz, S., Halbach, J., Jegen, M., Petersen, S., Swidinsky, A., 2017b: A self-potential investigation of submarine massive sulfides: Palinuro seamount, *Geophysics*, 82, A51-A56.
- Safipour, R., Hölz, S., Jegen, M., Swidinsky, A., 2018: A first application of a marine inductive source EM configuration with remote electric dipole receivers: Palinuro Seamount, Tyrrhenian Sea. *Geophysical Prospecting*, 2018, 66, 1415-1432.
- Scholten, J., Blaschek, H., Becker, K.-P., Hannington, M., Herzig, P., Hißmann, K., Jonasson, I., Krüger, O., Marteinsson, V., Preißler, H., Schauer, J., Schmidt, M., Solveig, P., Theißen, O., 2000. Hydrothermalism at the Kolbeinsey Ridge, Iceland. *Technical Cruise Report PO 253*, University of Kiel, pp. 22–43.
- Shilov, V., V. Beltenev, V. Ivanov, G. Cherkashev, I. Rozhdestvenskaya, I. Gablina, I. Dobretsova, E. Narkevskii, A. Gustaitis, and V. Kuznetsov, 2012, New hydrothermal ore fields in the Mid-Atlantic Ridge: Zenith-Victoria (20°08'N) and Petersburg (19°52'N): *Doklady Earth Sciences*, 442, 63–69.
- Stoffers, P., Shipboard Scientific Party, 1997. *Cruise Report of R/V Poseidon 229* Institute of Geosciences, Departments of Geophysics and Geology–Paleontology, University of Kiel, 58 pp.
- Swidinsky, A., Hölz, S. & Jegen, M.: On mapping seafloor mineral deposits with central loop transient electromagnetics. *Geophysics*, 2012, 77, E171-E184.
- Swidinsky, A., Hölz, S. & Jegen, M., 2015: Rapid resistivity imaging for marine CSEM surveys with two transmitter polarizations: An application to the North Alex mud volcano. *Geophysics*, 80, E97-E110.
- Villinger, H. & Davis, E.E., 1987. A new reduction algorithm for marine heat-flow measurements. *Journal of Geophysical Research*, 92(B12), 12846-12856.
- Von Herzen, R., J. Kirklin, and K. Becker, 1996, Geoelectrical measurements at the TAG hydrothermal mound: *Geophysical Research Letters*, 23, 3451–3454.

9. Appendix

9.1. Station Log

Activity Device Oper- ation	Timestamp	Device	Action	Latitude	Longitude	Depth (m)	Speed (kn)	Course	Wind Dir	Wind Velocity	Comment
POS524_1-1	2018-06-08 22:46:35	Releaser Test	in the water	66° 37,007' N	017° 41,414' W	402.1	0.0	63.0	247.0	4.6	Commence of research operations POS 524
POS524_1-1	2018-06-08 22:58:15	Releaser Test	max depth/on ground	66° 37,029' N	017° 41,424' W	411.2	0.0	267.0	261.0	3.7	370 m max
POS524_1-1	2018-06-08 23:51:07	Releaser Test	on deck	66° 37,037' N	017° 41,509' W	402.5	0.0	174.0	269.0	3.3	
POS524_1-2	2018-06-09 08:23:35	USBL	in the water	66° 36,981' N	017° 41,490' W	404.3	0.0	10.0	118.0	2.0	Transponder in the water
POS524_1-2	2018-06-09 08:28:20	USBL	information	66° 36,995' N	017° 41,465' W	403.4	0.0	50.0	122.0	2.3	Deployed
POS524_1-2	2018-06-09 09:14:13	USBL	profile start	66° 36,974' N	017° 41,501' W	404.0	0.0	172.0	133.0	2.4	Commence calibration
POS524_1-2	2018-06-09 15:05:32	USBL	profile end	66° 37,061' N	017° 41,596' W	404.6	1.0	111.0	57.0	5.2	Calibration completed
POS524_1-2	2018-06-09 15:22:03	USBL	information	66° 36,906' N	017° 41,683' W	405.3	0.0	282.0	64.0	5.0	Transponder released
POS524_1-2	2018-06-09 15:25:25	USBL	information	66° 36,899' N	017° 41,683' W	406.8	0.0	216.0	66.0	5.2	Transponder at surface
POS524_1-2	2018-06-09 15:34:48	USBL	on deck	66° 36,938' N	017° 41,541' W	403.4	0.0	14.0	65.0	5.3	Transponder on deck
POS524_2-1	2018-06-09 16:20:51	OBEM receiver	in the water	66° 36,249' N	017° 39,593' W	382.1	0.0	26.0	52.0	5.7	
POS524_2-1	2018-06-09 16:39:50	OBEM receiver	deployed	66° 36,249' N	017° 39,600' W	381.8	0.0	338.0	59.0	5.7	SL max = 360m
POS524_2-1	2018-06-09 16:48:56	OBEM receiver	information	66° 36,237' N	017° 39,561' W	385.3	0.0	145.0	60.0	5.8	releaser on deck
POS524_3-1	2018-06-09 17:03:35	OBEM receiver	in the water	66° 36,154' N	017° 39,328' W	402.8	0.0	74.0	63.0	6.2	
POS524_3-1	2018-06-09 17:21:50	OBEM receiver	deployed	66° 36,164' N	017° 39,324' W	402.1	0.0	323.0	65.0	5.9	SL max = 380m
POS524_3-1	2018-06-09 17:29:15	OBEM receiver	information	66° 36,156' N	017° 39,333' W	402.1	0.0	202.0	63.0	6.2	releaser on deck
POS524_4-1	2018-06-10 08:20:00	OBEM receiver	in the water	66° 36,257' N	017° 38,979' W	419.3	0.0	20.0	84.0	9.6	
POS524_4-1	2018-06-10 08:40:19	OBEM receiver	information	66° 36,245' N	017° 38,963' W	418.9	0.0	120.0	86.0	9.7	Released and deployed
POS524_4-1	2018-06-10 08:48:17	OBEM receiver	on deck	66° 36,245' N	017° 38,947' W	414.3	0.0	159.0	85.0	9.3	Releaser on deck
POS524_5-1	2018-06-10 09:09:07	OBEM receiver	in the water	66° 36,403' N	017° 39,635' W	375.3	0.0	143.0	84.0	9.6	
POS524_5-1	2018-06-10 09:21:58	OBEM receiver	information	66° 36,391' N	017° 39,664' W	374.7	0.0	14.0	86.0	9.6	Released and deployed
POS524_5-1	2018-06-10 09:28:19	OBEM receiver	on deck	66° 36,387' N	017° 39,655' W	375.1	0.0	106.0	88.0	9.6	Releaser on deck
POS524_6-1	2018-06-10 09:40:40	OBEM receiver	in the water	66° 36,410' N	017° 38,880' W	418.9	0.0	118.0	88.0	10.1	
POS524_6-1	2018-06-10 09:55:23	OBEM receiver	information	66° 36,417' N	017° 38,884' W	416.0	0.0	10.0	88.0	9.5	Released and deployed

POS524_6-1	2018-06-10 10:02:14	OBEM receiver	on deck	66° 36,413' N	017° 38,905' W	417.1	0.0	258.0	90.0	10.4	Releaser on deck
POS524_7-1	2018-06-10 10:22:12	OBEM receiver	in the water	66° 36,576' N	017° 39,445' W	398.3	0.0	189.0	93.0	10.3	
POS524_7-1	2018-06-10 10:37:32	OBEM receiver	information	66° 36,562' N	017° 39,442' W	399.1	0.0	51.0	87.0	11.0	Released and deployed
POS524_7-1	2018-06-10 10:44:10	OBEM receiver	on deck	66° 36,573' N	017° 39,416' W	403.9	0.0	9.0	86.0	9.5	Releaser on deck
POS524_8-1	2018-06-10 10:54:50	OBEM receiver	in the water	66° 36,571' N	017° 38,939' W	413.8	0.0	290.0	90.0	10.5	
POS524_8-1	2018-06-10 11:09:47	OBEM receiver	information	66° 36,567' N	017° 38,937' W	414.6	0.0	134.0	85.0	11.7	Released and deployed
POS524_8-1	2018-06-10 11:16:36	OBEM receiver	on deck	66° 36,571' N	017° 38,936' W	414.8	0.0	308.0	87.0	11.1	Releaser on deck
POS524_9-1	2018-06-10 11:59:09	OBEM receiver	in the water	66° 36,756' N	017° 39,203' W	415.1	0.0	159.0	88.0	9.6	
POS524_9-1	2018-06-10 12:16:09	OBEM receiver	information	66° 36,774' N	017° 39,204' W	413.0	0.0	63.0	87.0	10.0	Released and deployed
POS524_9-1	2018-06-10 12:23:23	OBEM receiver	on deck	66° 36,772' N	017° 39,203' W	415.1	0.0	302.0	87.0	10.5	releaser on Deck
POS524_10-1	2018-06-10 12:33:25	OBEM receiver	in the water	66° 36,786' N	017° 38,703' W	409.8	0.0	108.0	87.0	10.7	
POS524_10-1	2018-06-10 12:49:39	OBEM receiver	information	66° 36,786' N	017° 38,676' W	410.0	0.0	31.0	85.0	12.2	released and deployed
POS524_10-1	2018-06-10 12:55:47	OBEM receiver	on deck	66° 36,771' N	017° 38,705' W	414.4	0.0	208.0	87.0	11.3	Releaser on Deck
POS524_11-1	2018-06-10 13:35:08	OBEM receiver	in the water	66° 37,554' N	017° 38,857' W	393.8	0.0	177.0	84.0	11.7	
POS524_11-1	2018-06-10 13:47:43	OBEM receiver	information	66° 37,534' N	017° 38,897' W	389.0	0.0	266.0	85.0	11.3	released and deployed
POS524_11-1	2018-06-10 13:53:43	OBEM receiver	on deck	66° 37,531' N	017° 38,930' W	387.9	1.0	76.0	84.0	11.7	Releaser on Deck
POS524_12-1	2018-06-10 14:02:39	OBEM receiver	in the water	66° 37,519' N	017° 38,385' W	394.6	0.0	83.0	84.0	10.4	
POS524_12-1	2018-06-10 14:15:37	OBEM receiver	information	66° 37,527' N	017° 38,405' W	385.1	0.0	251.0	85.0	10.8	Released and deployed
POS524_12-1	2018-06-10 14:23:35	OBEM receiver	on deck	66° 37,526' N	017° 38,446' W	391.8	0.0	261.0	87.0	10.3	Releaser on Deck
POS524_13-1	2018-06-10 14:40:32	OBEM receiver	in the water	66° 37,658' N	017° 38,701' W	391.2	1.0	105.0	90.0	11.0	
POS524_13-1	2018-06-10 15:39:10	OBEM receiver	information	66° 37,659' N	017° 38,617' W	355.6	0.0	225.0	85.0	11.4	released and deployed
POS524_13-1	2018-06-10 15:39:46	OBEM receiver	on deck	66° 37,658' N	017° 38,625' W	391.2	0.0	256.0	86.0	11.8	releaser on deck
POS524_14-1	2018-06-10 16:25:06	Gravity corer	in the water	66° 36,410' N	017° 39,281' W	392.5	0.0	158.0	85.0	11.6	
POS524_14-1	2018-06-10 16:32:04	Gravity corer	max depth/on ground	66° 36,413' N	017° 39,256' W	1.0	0.0	133.0	85.0	12.2	SL max = 379m
POS524_14-1	2018-06-10 16:40:21	Gravity corer	on deck	66° 36,413' N	017° 39,238' W	389.5	0.0	138.0	86.0	12.4	
POS524_15-1	2018-06-11 08:01:40	Gravity corer	in the water	66° 36,910' N	017° 39,228' W	406.2	0.0	311.0	88.0	10.0	
POS524_15-1	2018-06-11 08:09:21	Gravity corer	max depth/on ground	66° 36,915' N	017° 39,234' W	405.4	0.0	129.0	83.0	10.8	392 m max
POS524_15-1	2018-06-11 08:19:12	Gravity corer	on deck	66° 36,913' N	017° 39,192' W	403.8	0.0	80.0	85.0	10.1	
POS524_16-1	2018-06-11 10:21:42	Heat Flow Probe	in the water	66° 36,432' N	017° 42,724' W	448.0	0.0	157.0	81.0	9.2	
POS524_16-1	2018-06-11 10:36:55	Heat Flow Probe	max depth/on ground	66° 36,435' N	017° 42,716' W	446.3	0.0	146.0	86.0	9.2	433 m max
POS524_16-1	2018-06-11 10:50:41	Heat Flow Probe	hoisting	66° 36,427' N	017° 42,702' W	446.9	0.0	98.0	81.0	9.3	

POS524_16-1	2018-06-11 11:21:17	Heat Flow Probe	max depth/on ground	66° 36,454' N	017° 41,642' W	411.8	0.0	96.0	74.0	9.4	401 m max
POS524_16-1	2018-06-11 11:36:15	Heat Flow Probe	hoisting	66° 36,455' N	017° 41,641' W	414.6	0.0	317.0	73.0	8.1	
POS524_16-1	2018-06-11 12:09:07	Heat Flow Probe	max depth/on ground	66° 36,435' N	017° 40,585' W	413.7	0.0	73.0	74.0	9.4	SL max = 402 m
POS524_16-1	2018-06-11 12:23:28	Heat Flow Probe	hoisting	66° 36,428' N	017° 40,586' W	415.7	0.0	121.0	73.0	9.5	
POS524_16-1	2018-06-11 13:09:15	Heat Flow Probe	max depth/on ground	66° 36,412' N	017° 38,657' W	419.7	0.0	118.0	73.0	8.9	SL max = 410 m
POS524_16-1	2018-06-11 13:23:56	Heat Flow Probe	hoisting	66° 36,398' N	017° 38,668' W	417.5	0.0	196.0	72.0	8.4	
POS524_16-1	2018-06-11 13:47:45	Heat Flow Probe	max depth/on ground	66° 36,418' N	017° 38,244' W	419.3	0.0	10.0	77.0	9.0	SLmax = 414 m
POS524_16-1	2018-06-11 14:02:15	Heat Flow Probe	hoisting	66° 36,426' N	017° 38,201' W	420.8	0.0	125.0	72.0	8.8	
POS524_16-1	2018-06-11 14:25:19	Heat Flow Probe	max depth/on ground	66° 36,408' N	017° 37,646' W	406.6	0.0	128.0	72.0	8.2	SL max = 407 m
POS524_16-1	2018-06-11 14:40:28	Heat Flow Probe	hoisting	66° 36,404' N	017° 37,625' W	404.6	0.0	312.0	70.0	8.5	
POS524_16-1	2018-06-11 14:55:15	Heat Flow Probe	on deck	66° 36,387' N	017° 37,562' W	401.1	0.0	105.0	71.0	8.7	
POS524_17-1	2018-06-11 16:01:19	Martemis	in the water	66° 36,314' N	017° 36,773' W	391.8	0.0	196.0	78.0	8.5	Test
POS524_17-1	2018-06-11 16:48:20	Martemis	on deck	66° 36,270' N	017° 36,371' W	346.6	0.0	217.0	75.0	9.1	
POS524_18-1	2018-06-12 09:18:43	Gravity corer	in the water	66° 36,462' N	017° 39,619' W	383.2	0.0	230.0	93.0	9.3	
POS524_18-1	2018-06-12 09:25:51	Gravity corer	max depth/on ground	66° 36,449' N	017° 39,664' W	386.4	0.0	349.0	87.0	9.1	367 m max
POS524_18-1	2018-06-12 09:35:05	Gravity corer	on deck	66° 36,447' N	017° 39,639' W	382.9	0.0	106.0	87.0	9.0	
POS524_19-1	2018-06-12 10:11:47	Gravity corer	in the water	66° 36,446' N	017° 40,662' W	413.7	0.0	108.0	95.0	9.0	
POS524_19-1	2018-06-12 10:18:48	Gravity corer	max depth/on ground	66° 36,441' N	017° 40,630' W	414.2	0.0	181.0	95.0	8.0	403 m max
POS524_19-1	2018-06-12 10:28:09	Gravity corer	on deck	66° 36,434' N	017° 40,597' W	415.3	0.0	110.0	91.0	8.9	
POS524_20-1	2018-06-12 12:21:52	Gravity corer	in the water	66° 37,624' N	017° 38,615' W	392.8	0.0	85.0	92.0	9.9	
POS524_20-1	2018-06-12 12:28:27	Gravity corer	max depth/on ground	66° 37,631' N	017° 38,581' W	391.7	0.0	248.0	83.0	9.4	SL max = 379 m
POS524_20-1	2018-06-12 12:37:33	Gravity corer	on deck	66° 37,625' N	017° 38,392' W	394.2	0.0	254.0	87.0	9.4	
POS524_21-1	2018-06-12 15:05:29	Martemis	in the water	66° 36,108' N	017° 40,733' W	411.3	0.0	222.0	83.0	9.6	
POS524_21-1	2018-06-12 15:51:36	Martemis	max depth/on ground	66° 36,139' N	017° 39,832' W	388.9	0.0	21.0	86.0	10.4	SL mx = 370 m
POS524_21-1	2018-06-12 15:54:07	Martemis	profile start	66° 36,144' N	017° 39,812' W	388.6	0.0	72.0	88.0	10.5	
POS524_21-1	2018-06-12 17:00:13	Martemis	profile end	66° 36,561' N	017° 39,715' W	383.2	0.0	108.0	83.0	10.3	
POS524_21-1	2018-06-12 17:16:43	Martemis	on deck	66° 36,553' N	017° 39,683' W	381.9	0.0	68.0	84.0	11.5	
POS524_22-1	2018-06-13 06:00:54	Martemis	in the water	66° 36,089' N	017° 37,991' W	423.1	0.0	237.0	306.0	2.7	
POS524_22-1	2018-06-13 06:30:10	Martemis	max depth/on ground	66° 36,146' N	017° 38,488' W	425.1	0.0	329.0	327.0	3.8	SL max = 396m
POS524_22-1	2018-06-13 06:45:09	Martemis	profile start	66° 36,255' N	017° 38,565' W	422.2	0.0	350.0	317.0	3.0	
POS524_22-1	2018-06-13 08:33:24	Martemis	information	66° 36,967' N	017° 39,055' W	420.1	0.0	288.0	316.0	2.4	Profile ceased, winch trouble

POS524_22-1	2018-06-13 11:25:54	Martemis	information	66° 36,908' N	017° 39,093' W	410.0	0.0	58.0	76.0	0.9	Profile resumed
POS524_22-1	2018-06-14 05:39:13	Martemis	profile end	66° 37,611' N	017° 38,798' W	390.7	0.0	256.0	58.0	12.3	
POS524_22-1	2018-06-14 06:00:11	Martemis	on deck	66° 37,624' N	017° 38,851' W	396.1	0.0	185.0	58.0	12.2	Cease of research due to weather forecast
POS524_23-1	2018-06-16 10:09:08	Heat Flow Probe	in the water	66° 36,417' N	017° 42,653' W	353.9	0.0	17.0	46.0	5.8	
POS524_23-1	2018-06-16 10:25:46	Heat Flow Probe	max depth/on ground	66° 36,416' N	017° 42,691' W	1.1	0.0	149.0	43.0	6.1	436 m max
POS524_23-1	2018-06-16 10:40:20	Heat Flow Probe	hoisting	66° 36,418' N	017° 42,665' W	1.5	0.0	327.0	38.0	7.3	
POS524_23-1	2018-06-16 11:52:16	Heat Flow Probe	max depth/on ground	66° 36,436' N	017° 41,060' W	1.0	0.0	144.0	48.0	5.8	396 m max
POS524_23-1	2018-06-16 12:07:19	Heat Flow Probe	hoisting	66° 36,425' N	017° 41,087' W	3.8	0.0	303.0	53.0	6.1	
POS524_23-1	2018-06-16 13:32:46	Heat Flow Probe	max depth/on ground	66° 36,453' N	017° 39,630' W	1.0	0.0	336.0	64.0	5.3	SL max = 370 m
POS524_23-1	2018-06-16 13:55:13	Heat Flow Probe	hoisting	66° 36,448' N	017° 39,446' W	396.7	0.0	78.0	57.0	5.8	
POS524_23-1	2018-06-16 13:59:41	Heat Flow Probe	on deck	66° 36,478' N	017° 39,297' W	401.0	0.0	77.0	60.0	5.7	
POS524_24-1	2018-06-16 14:32:06	OBEM receiver	information	66° 36,001' N	017° 39,566' W	395.6	0.0	74.0	54.0	5.6	Released
POS524_24-1	2018-06-16 14:39:24	OBEM receiver	at surface	66° 36,055' N	017° 39,430' W	393.3	2.0	54.0	49.0	5.9	
POS524_24-1	2018-06-16 14:55:13	OBEM receiver	on deck	66° 36,159' N	017° 39,351' W	393.3	0.0	77.0	43.0	5.7	
POS524_25-1	2018-06-16 15:15:55	OBEM receiver	information	66° 36,660' N	017° 39,396' W	393.3	1.0	63.0	58.0	5.8	Released
POS524_25-1	2018-06-16 15:23:33	OBEM receiver	at surface	66° 36,631' N	017° 39,415' W	393.3	0.0	231.0	60.0	5.7	
POS524_25-1	2018-06-16 15:32:35	OBEM receiver	on deck	66° 36,826' N	017° 39,210' W	393.3	0.0	68.0	57.0	5.6	
POS524_26-1	2018-06-16 15:54:17	OBEM receiver	information	66° 36,654' N	017° 38,762' W	393.3	0.0	132.0	60.0	6.0	released
POS524_26-1	2018-06-16 16:01:38	OBEM receiver	at surface	66° 36,654' N	017° 38,731' W	393.3	0.0	126.0	62.0	5.5	
POS524_26-1	2018-06-16 16:09:03	OBEM receiver	on deck	66° 36,751' N	017° 38,602' W	393.3	0.0	106.0	71.0	6.4	
POS524_27-1	2018-06-16 16:43:09	OBEM receiver	deployed	66° 36,561' N	017° 41,275' W	393.3	0.0	93.0	65.0	6.0	
POS524_28-1	2018-06-16 17:02:14	OBEM receiver	deployed	66° 36,567' N	017° 40,780' W	393.3	0.0	13.0	68.0	5.6	
POS524_29-1	2018-06-16 17:18:03	OBEM receiver	deployed	66° 36,567' N	017° 40,193' W	393.3	0.0	60.0	64.0	6.6	
POS524_30-1	2018-06-17 06:04:19	OBEM receiver	information	66° 37,430' N	017° 39,845' W	390.6	0.0	165.0	98.0	6.3	released
POS524_30-1	2018-06-17 06:18:28	OBEM receiver	at surface	66° 37,451' N	017° 39,669' W	399.0	0.0	72.0	107.0	8.7	
POS524_30-1	2018-06-17 06:27:21	OBEM receiver	on deck	66° 37,430' N	017° 39,197' W	397.4	0.0	192.0	106.0	8.2	
POS524_31-1	2018-06-17 06:33:00	OBEM receiver	information	66° 37,431' N	017° 39,175' W	392.6	0.0	57.0	102.0	8.0	released
POS524_31-1	2018-06-17 07:00:46	OBEM receiver	information	66° 37,464' N	017° 38,987' W	392.6	0.0	44.0	110.0	7.7	stays at bottom, no surface movements detectable
POS524_32-1	2018-06-17 07:10:14	OBEM receiver	information	66° 37,484' N	017° 38,950' W	392.6	0.0	352.0	109.0	7.6	released
POS524_32-1	2018-06-17 07:20:05	OBEM receiver	at surface	66° 37,619' N	017° 38,818' W	392.6	2.0	15.0	107.0	7.3	
POS524_32-1	2018-06-17 07:26:26	OBEM receiver	on deck	66° 37,703' N	017° 38,750' W	392.6	0.0	14.0	108.0	6.9	

POS524_33-1	2018-06-17 08:23:07	OBEM receiver	deployed	66° 36,563' N	017° 38,346' W	392.6	0.0	354.0	108.0	6.2	
POS524_34-1	2018-06-17 08:34:17	OBEM receiver	deployed	66° 36,564' N	017° 37,786' W	392.6	0.0	189.0	107.0	5.3	
POS524_35-1	2018-06-17 09:00:34	Gravity corer	in the water	66° 36,394' N	017° 38,702' W	418.4	0.0	337.0	104.0	5.3	
POS524_35-1	2018-06-17 09:05:47	Gravity corer	max depth/on ground	66° 36,396' N	017° 38,666' W	419.2	0.0	339.0	104.0	5.2	406 m max
POS524_35-1	2018-06-17 09:15:23	Gravity corer	on deck	66° 36,414' N	017° 38,694' W	415.4	0.0	339.0	100.0	5.2	
POS524_36-1	2018-06-17 10:10:31	Martemis	in the water	66° 36,526' N	017° 42,906' W	416.3	0.0	134.0	86.0	5.0	
POS524_36-1	2018-06-17 11:01:38	Martemis	profile start	66° 36,570' N	017° 41,796' W	414.4	0.0	71.0	86.0	6.8	
POS524_36-1	2018-06-17 15:12:50	Martemis	profile end	66° 36,572' N	017° 37,158' W	384.4	0.0	78.0	91.0	12.2	
POS524_36-1	2018-06-17 15:35:14	Martemis	on deck	66° 36,629' N	017° 36,649' W	377.4	0.0	76.0	96.0	12.1	Cease research operations due to weather situation
POS524_37-1	2018-06-19 12:37:45	Heat Flow Probe	in the water	66° 35,814' N	017° 39,177' W	400.5	0.0	272.0	300.0	7.4	Resume of research operations
POS524_37-1	2018-06-19 12:45:20	Heat Flow Probe	max depth/on ground	66° 35,826' N	017° 39,194' W	408.7	0.0	19.0	313.0	7.8	SL max = 398 m
POS524_37-1	2018-06-19 13:00:18	Heat Flow Probe	hoisting	66° 35,854' N	017° 39,177' W	403.3	0.0	116.0	316.0	7.5	
POS524_37-1	2018-06-19 13:09:06	Heat Flow Probe	max depth/on ground	66° 35,855' N	017° 39,140' W	405.2	0.0	100.0	315.0	7.0	SL max = 401 m
POS524_37-1	2018-06-19 13:23:22	Heat Flow Probe	hoisting	66° 35,859' N	017° 39,157' W	403.1	0.0	190.0	311.0	7.7	
POS524_37-1	2018-06-19 14:24:01	Heat Flow Probe	max depth/on ground	66° 36,723' N	017° 39,167' W	411.2	0.0	267.0	316.0	5.5	SL max = 407 m
POS524_37-1	2018-06-19 14:37:39	Heat Flow Probe	hoisting	66° 36,715' N	017° 39,117' W	413.4	0.0	159.0	310.0	5.8	
POS524_37-1	2018-06-19 15:16:05	Heat Flow Probe	max depth/on ground	66° 37,105' N	017° 39,096' W	403.7	0.0	296.0	312.0	6.2	SL max = 398 m
POS524_37-1	2018-06-19 15:30:49	Heat Flow Probe	hoisting	66° 37,119' N	017° 39,075' W	399.7	0.0	139.0	316.0	6.2	
POS524_37-1	2018-06-19 16:02:04	Heat Flow Probe	max depth/on ground	66° 37,597' N	017° 38,557' W	393.4	0.0	122.0	311.0	6.1	SL max = 382m
POS524_37-1	2018-06-19 16:16:20	Heat Flow Probe	hoisting	66° 37,595' N	017° 38,530' W	393.4	0.0	340.0	303.0	6.0	
POS524_37-1	2018-06-19 17:03:45	Heat Flow Probe	max depth/on ground	66° 37,134' N	017° 38,167' W	393.0	0.0	117.0	318.0	6.0	SL max = 389m
POS524_37-1	2018-06-19 17:18:17	Heat Flow Probe	hoisting	66° 37,134' N	017° 38,146' W	393.7	0.0	95.0	310.0	5.9	
POS524_37-1	2018-06-19 17:41:51	Heat Flow Probe	on deck	66° 37,149' N	017° 38,042' W	395.1	0.0	113.0	314.0	5.9	
POS524_38-1	2018-06-20 08:02:00	Gravity corer	in the water	66° 36,181' N	017° 39,166' W	396.7	0.0	238.0	288.0	6.9	
POS524_38-1	2018-06-20 08:08:17	Gravity corer	max depth/on ground	66° 36,183' N	017° 39,177' W	393.6	0.0	186.0	284.0	6.5	388 m max
POS524_38-1	2018-06-20 08:18:40	Gravity corer	on deck	66° 36,189' N	017° 39,149' W	393.0	0.0	259.0	291.0	6.5	
POS524_39-1	2018-06-20 08:42:18	Gravity corer	in the water	66° 36,316' N	017° 39,311' W	391.2	0.0	186.0	292.0	6.9	
POS524_39-1	2018-06-20 08:48:21	Gravity corer	max depth/on ground	66° 36,310' N	017° 39,293' W	390.8	0.0	101.0	291.0	7.1	384 m max
POS524_39-1	2018-06-20 08:56:35	Gravity corer	on deck	66° 36,314' N	017° 39,300' W	394.8	0.0	310.0	291.0	6.9	
POS524_40-1	2018-06-20 09:29:33	Martemis	in the water	66° 35,745' N	017° 40,053' W	406.5	0.0	286.0	296.0	7.4	
POS524_40-1	2018-06-20 10:22:27	Martemis	profile start	66° 35,990' N	017° 40,949' W	428.4	0.0	2.3	284.0	7.7	

POS524_40-1	2018-06-21 05:54:02	Martemis	profile end	66° 36,708' N	017° 37,470' W	396.6	0.0	94.0	192.0	5.3	
POS524_40-1	2018-06-21 06:13:40	Martemis	on deck	66° 36,604' N	017° 37,428' W	395.0	0.0	200.0	198.0	4.7	
POS524_41-1	2018-06-21 06:46:27	OBEM receiver	information	66° 36,328' N	017° 37,575' W	401.1	0.0	211.0	207.0	4.1	released
POS524_41-1	2018-06-21 06:53:20	OBEM receiver	at surface	66° 36,395' N	017° 37,628' W	407.4	1.0	21.0	204.0	3.9	
POS524_41-1	2018-06-21 07:06:38	OBEM receiver	on deck	66° 36,631' N	017° 37,693' W	409.7	0.0	86.0	201.0	4.4	
POS524_42-1	2018-06-21 07:54:59	OBEM receiver	information	66° 36,728' N	017° 37,937' W	411.5	0.0	350.0	176.0	3.3	released
POS524_42-1	2018-06-21 08:01:15	OBEM receiver	at surface	66° 36,759' N	017° 37,922' W	413.6	0.0	350.0	182.0	2.8	
POS524_42-1	2018-06-21 08:11:01	OBEM receiver	on deck	66° 36,605' N	017° 38,415' W	415.9	0.0	271.0	187.0	3.1	
POS524_43-1	2018-06-21 08:27:15	OBEM receiver	information	66° 36,616' N	017° 40,017' W	388.2	0.0	75.0	232.0	2.4	Released
POS524_43-1	2018-06-21 08:33:45	OBEM receiver	at surface	66° 36,617' N	017° 39,940' W	392.0	0.0	89.0	231.0	2.6	
POS524_43-1	2018-06-21 08:40:35	OBEM receiver	on deck	66° 36,575' N	017° 40,255' W	375.1	0.0	269.0	209.0	3.1	
POS524_44-1	2018-06-21 08:59:57	OBEM receiver	information	66° 36,620' N	017° 40,213' W	380.3	0.0	73.0	220.0	2.8	Released
POS524_44-1	2018-06-21 09:05:56	OBEM receiver	at surface	66° 36,656' N	017° 40,409' W	384.0	1.0	271.0	229.0	2.6	
POS524_44-1	2018-06-21 09:11:36	OBEM receiver	on deck	66° 36,637' N	017° 40,889' W	406.4	0.0	279.0	222.0	2.3	
POS524_45-1	2018-06-21 09:23:26	OBEM receiver	information	66° 36,661' N	017° 40,986' W	408.0	0.0	148.0	218.0	1.9	Released
POS524_45-1	2018-06-21 09:29:25	OBEM receiver	at surface	66° 36,651' N	017° 40,944' W	408.0	0.0	149.0	220.0	2.3	
POS524_45-1	2018-06-21 09:37:04	OBEM receiver	on deck	66° 36,546' N	017° 41,530' W	408.0	0.0	237.0	206.0	2.4	
POS524_46-1	2018-06-21 09:56:36	OBEM receiver	information	66° 36,628' N	017° 39,659' W	408.0	0.0	40.0	166.0	1.6	Released
POS524_46-1	2018-06-21 10:08:44	OBEM receiver	on deck	66° 36,534' N	017° 39,471' W	408.0	0.0	117.0	162.0	0.9	
POS524_47-1	2018-06-21 10:18:02	OBEM receiver	information	66° 36,500' N	017° 39,368' W	408.0	0.0	89.0	118.0	0.6	Released
POS524_47-1	2018-06-21 10:24:32	OBEM receiver	at surface	66° 36,500' N	017° 39,289' W	408.0	0.0	73.0	119.0	0.7	
POS524_47-1	2018-06-21 10:32:31	OBEM receiver	on deck	66° 36,606' N	017° 38,900' W	408.0	0.0	107.0	130.0	0.6	
POS524_48-1	2018-06-21 10:38:19	OBEM receiver	information	66° 36,586' N	017° 38,853' W	408.0	0.0	170.0	91.0	0.4	Released
POS524_48-1	2018-06-21 10:44:40	OBEM receiver	at surface	66° 36,548' N	017° 38,855' W	408.0	0.0	188.0	103.0	1.2	
POS524_48-1	2018-06-21 10:51:10	OBEM receiver	on deck	66° 36,431' N	017° 38,891' W	408.0	0.0	186.0	92.0	0.7	
POS524_49-1	2018-06-21 10:58:21	OBEM receiver	information	66° 36,386' N	017° 38,941' W	408.0	0.0	219.0	88.0	1.1	Released
POS524_49-1	2018-06-21 11:04:11	OBEM receiver	at surface	66° 36,394' N	017° 39,211' W	408.0	0.0	289.0	66.0	1.4	
POS524_49-1	2018-06-21 11:10:51	OBEM receiver	on deck	66° 36,350' N	017° 39,593' W	408.0	0.0	220.0	47.0	1.2	
POS524_50-1	2018-06-21 11:58:33	OBEM receiver	information	66° 36,363' N	017° 39,774' W	408.0	0.0	213.0	49.0	1.7	Released
POS524_50-1	2018-06-21 12:03:31	OBEM receiver	at surface	66° 36,340' N	017° 39,778' W	408.0	0.0	193.0	33.0	1.6	
POS524_50-1	2018-06-21 12:13:08	OBEM receiver	on deck	66° 36,119' N	017° 39,594' W	408.0	0.0	167.0	33.0	2.2	

POS524_51-1	2018-06-21 12:26:37	OBEM receiver	information	66° 36,161' N	017° 39,299' W	408.0	0.0	8.4	11.0	3.1	released
POS524_51-1	2018-06-21 12:32:40	OBEM receiver	at surface	66° 36,183' N	017° 39,261' W	408.0	0.0	98.0	15.0	3.1	
POS524_51-1	2018-06-21 12:50:19	OBEM receiver	on deck	66° 36,209' N	017° 38,641' W	408.0	0.0	108.0	22.0	2.5	
POS524_52-1	2018-06-21 14:02:34	OBEM receiver	information	66° 37,522' N	017° 38,487' W	408.0	2.0	341.0	53.0	3.0	Start dredging attempt
POS524_52-1	2018-06-21 14:26:38	OBEM receiver	in the water	66° 37,506' N	017° 38,379' W	396.8	0.0	125.0	40.0	2.7	Camera and dredging device to water
POS524_52-1	2018-06-21 14:38:41	OBEM receiver	max depth/on ground	66° 37,515' N	017° 38,398' W	388.6	0.0	191.0	46.0	2.9	At bottom, 373 m max
POS524_52-1	2018-06-21 15:33:33	OBEM receiver	on deck	66° 37,580' N	017° 38,249' W	386.3	0.0	33.0	46.0	4.0	No success
POS524_52-1	2018-06-21 23:41:55	OBEM receiver	information	66° 37,474' N	017° 38,021' W	384.8	0.0	140.0	184.0	7.6	
POS524_53-1	2018-06-22 06:00:03	OBEM receiver	information	66° 37,043' N	017° 38,024' W	403.8	0.0	191.0	283.0	3.2	Start dredging attempt
POS524_53-1	2018-06-22 06:00:47	OBEM receiver	information	66° 37,039' N	017° 38,026' W	403.5	0.0	189.0	282.0	3.1	camera and dredging device to water
POS524_53-1	2018-06-22 06:14:42	OBEM receiver	max depth/on ground	66° 36,999' N	017° 38,037' W	403.9	0.0	237.0	281.0	2.7	SL max = 392m
POS524_53-1	2018-06-22 10:55:52	OBEM receiver	on deck	66° 37,025' N	017° 38,232' W	403.7	0.0	32.0	270.0	13.8	No success. Completion of research POS 524

9.2. Station Protocol Heatflow

HF	Date	Time	Position		Depth [m]	Penetration [cm]	Heat Pulse	Max. tension [kN]	T _{max} [°C]	dT/dz [K / m]
			Latitude	Longitude						
01	11.06	10:36 - 10:43	66°36.43	-17°42.68	443	210	No	36	1.5	0.24
02		11:21 - 11:36	66°36.47	-17°41.65	420	180	No	29	2.0	0.34
03		12:08 - 12:24	66°36.44	-17°40.63	412	180	No	32	2.5	0.46
04		13:09 - 13:24	66°36.41	-17°38.65	420	-	No	39	> 60.0	>30
05		13:47 - 14:02	66°36.42	-17°38.23	424	210	No	33	6.0	2.03
06		14:25 - 14:40	66°36.42	-17°37.68	409	170	No	33	4.5	1.45
07	16.06	10:25 - 10:40	66°36.43	-17°42.68	440	210	Yes	32	-	-
08		11:52 - 12:07	66°36.44	-17°41.04	407	150	Yes	32	3.5	0.8
09		13:32 - 13:48	66°36.45	-17°39.65	385	120	Yes	21	12.0	6.24
10	19.6	12:45 - 13:00	66°35.82	-17°39.28	402	170	Yes	33	3.5	0.73
11		13:08 - 13:23	66°35.83	-17°39.29	402	160	Yes	36	3.5	0.82
12		14:23 - 14:37	66°36.71	-17°39.23	411	170	Yes	27	9.0	2.93
13		15:15 - 15:30	66°37.11	-17°39.12	401	150	Yes	25	4.0	0.64
14		16:01 - 16:16	66°37.60	-17°38.60	393	190	Yes	27	6.5	2.02
15		17:03 - 17:18	66°37.13	-17°38.19	396	90	Yes	28	3.0	-

- After ground contact (“BoKo”) an extra 5m of winch cable was given as slack.
- There was no change in tension during the bottom time for any measurement with penetration.
- USBL transponder 30m above the probe.

9.3. Core Descriptions

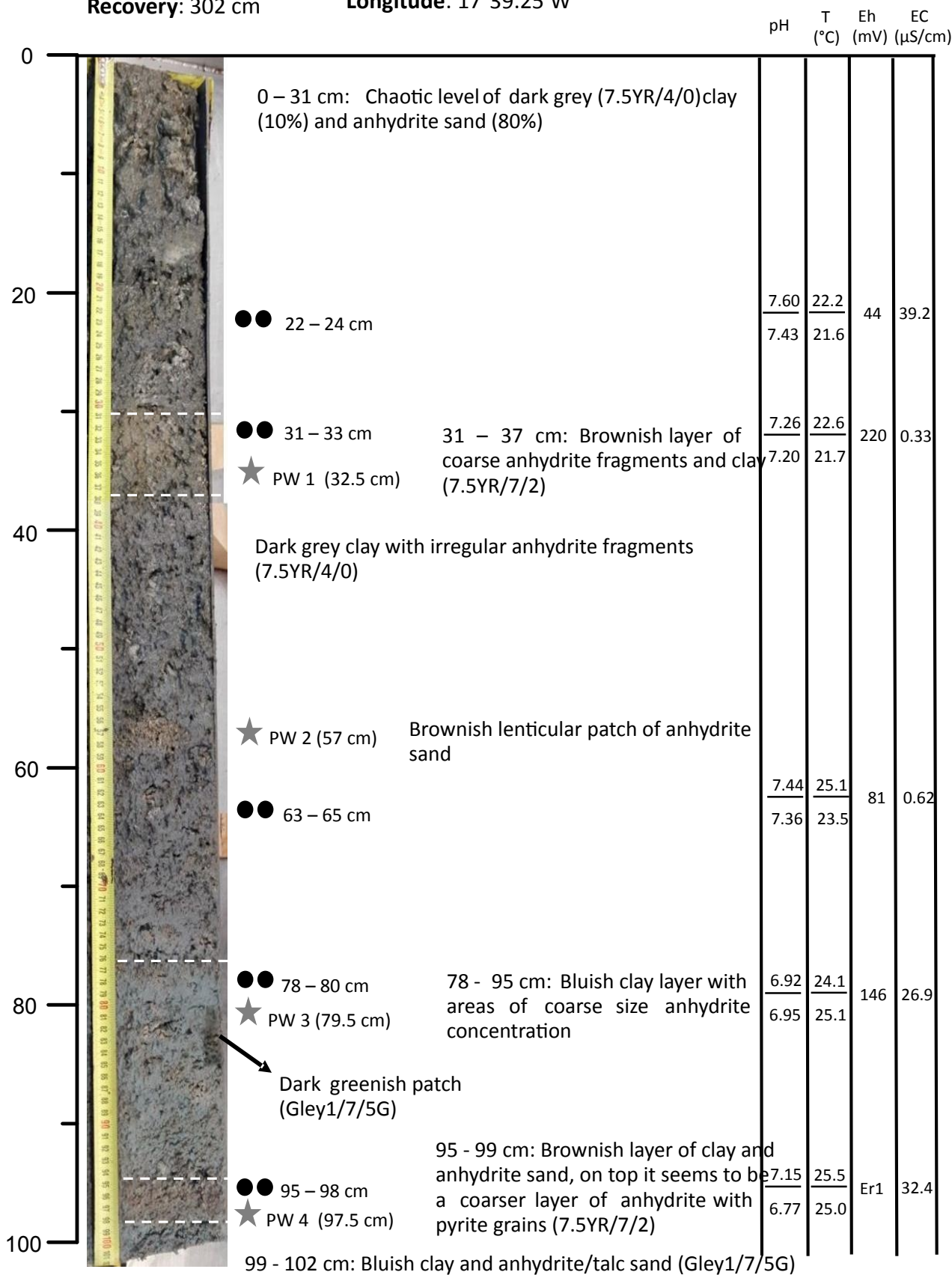
Core: POS524/01GC

Core section: C (1 of 3)

Latitude: 66°36.42'N

Recovery: 302 cm

Longitude: 17°39.25'W




Core: POS524/01GC

Core section: B (2 of 3)

Latitude: 66°36.42'N

Recovery: 302 cm

Longitude: 17°39.25'W

			pH	T (°C)	Eh (mV)	EC (μS/cm)
102	 <p>Faint smell of H_2S when opening the core</p> <p>Disturbed section</p> <p>127 - 140 cm: Silt/clay bluish grey layer with darker spots (dark brown). Mottled appearance. Disseminated sulfides. Gley18/5G</p> <p>★ PW 5 (134.5 cm)</p> <p>●● 136 – 138 cm</p> <p>★ PW 6 (144 cm)</p> <p>●● 146 – 148 cm</p> <p>140 - 164 cm: Homogenous silt/clay layer with a bluish grey colour that ends in a channel shaped area Gley17/5GY</p> <p>●● 160 – 162 cm Change in colour to lighter shade of blue/grey. Gley17/5G</p> <p>★ PW 7 (164 cm)</p> <p>164 – 202 cm: Dark brownish homogenous clay layer, very compact with frequent disseminated sulfides</p> <p>●● 178 – 180 cm</p>					
			7.13	16.9	137	39.6
			7.28	17.4		
122						
			7.36	17.6	166	Er1
			7.15	16.9		
142						
			7.36	17.2	147	27.9
			7.18	16.9		
162						
			7.25	17.4	177	25.8
			7.12	17.3		
182						
202						


Core: POS524/01GC

Core section: A (3 of 3)

Latitude: 66°36.42'N

Recovery: 302 cm

Longitude: 17°39.25'W

			pH	T (°C)	Eh (mV)	EC (µS/cm)
202	 <p>Empty section</p> <p>247 – 268 cm: Dark brown homogeneous clay layer with abundant disseminated sulfides. 10YR/6/6</p> <p>●● 263 – 265 cm</p> <p>★ PW 9 (270 cm) 268 – 272 cm: Layer of irregular greyish anhydrite sand</p> <p>272 – 302 cm: Homogeneous brown clay layer with disseminated sulfides and anhydrite flakes</p> <p>●● 281 – 283 cm</p> <p>Towards the bottom the layer becomes more flaky and broken into pieces. The sulfides are no longer disseminated, they occur concentrated in small channels (linear structures)</p>					
222						
242						
262			6.95 6.54	17.2 16.8	212	31.5
282			7.05 6.89	17.9 17.3	191	Er1
302			7.37 7.16	18.0 17.3	175	20.0

●● POS524/01GC/CC

Core: POS524/02GC

Core section: C (1 of 3)

Latitude: 66°36.91'N

Recovery: 290 cm

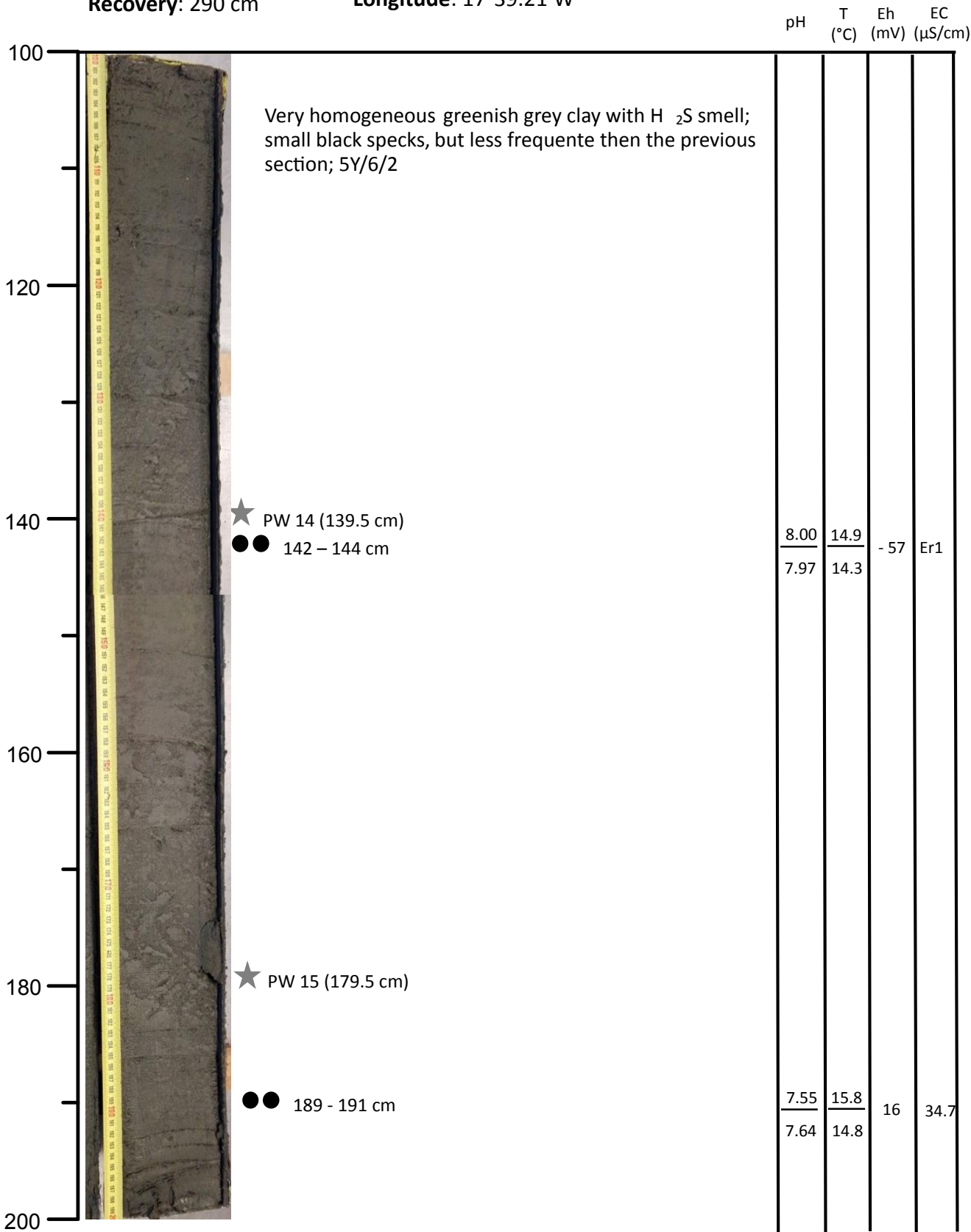
Longitude: 17°39.21'W

		pH	T (°C)	Eh (mV)	EC (μS/cm)
0					
	●● 10 – 12 cm	7.80	15.3	- 148	26.8
	14 cm: small shell fragment (<0.5 cm)	7.71	14.2		
20	Greenish grey clay with H ₂ S smell; very homogeneous; 5Y/6/2 Dispersed in the sediment are black patches (lines and points)				
	★ PW 10 (34 cm)				
40					
	●● 53 – 55 cm	7.77	15.2	- 32	20.5
	★ PW 11 (54.5 cm)	7.99	14.2		
60	50 – 57 cm: Black patches within the clay				
	★ PW 12 (72 cm)				
80					
	●● 92 - 94 cm	7.90	15.8	- 35	21.5
	★ PW 13 (96 cm)	7.75	14.6		
100					

Core: POS524/02GC

Core section: B (2 of 3)
Recovery: 290 cm

Latitude: 66°36.91'N
Longitude: 17°39.21'W



Core: POS524/02GC

Core section: A (3 of 3)
Recovery: 290 cm

Latitude: 66°36.91'N
Longitude: 17°39.21'W

		pH	T (°C)	Eh (mV)	EC (µS/cm)
200	Very homogeneous greenish grey clay with H ₂ S smell; 5Y/6/2				
	Shell (intact valve)				
220	★ PW 17 (219.5 cm)				
	●● 229 – 231 cm	7.76 7.47	15.6 14.6	- 78	28.2
240					
	★ PW 18 (250 cm)				
260					
	●● 269 - 271 cm	7.7 7.49	15.9 14.8	- 5	23.0
280	★ PW 19 (280 cm)				
300	●● POS524/02GC/CC				

Core: POS524/03GC

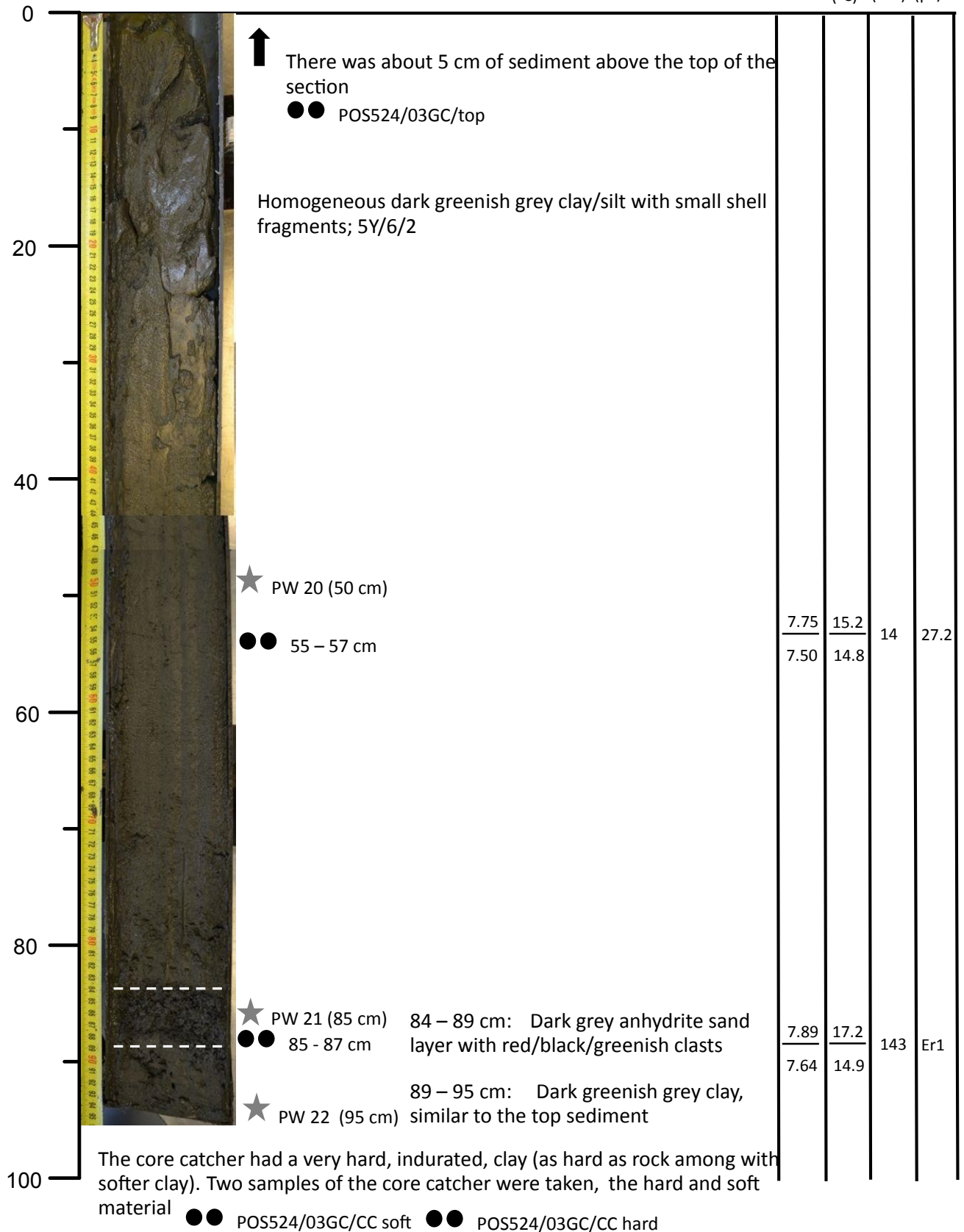
Core section: 1 of 1

Latitude: 66°36.45'N

Recovery: 95 cm

Longitude: 17°39.65'W

pH T (°C) Eh (mV) EC (μS/cm)



Core: POS524/04GC

Core section: C (1 of 3)

Latitude: 66°36.44'N

Recovery: 290 cm

Longitude: 17°40.63'W

		pH	T (°C)	Eh (mV)	EC (μS/cm)
0	Homogeneous dark greenish grey clay/silt; smell of H ₂ S; ocasional small shell fragments; 5Y/6/2				
●● 14 – 16 cm		7.92 7.90	14.5 13.2	58	31.8
★ PW 23 (30 cm)		7.93	13.8		
●● 32 – 34 cm		7.94	14.1	64	21.8
		7.75 7.50	15.2 14.8	14	27.2
★ PW 25 (70 cm)					
Shell fragments					
●● 80 – 82 cm		7.98 Er1	14.8 13.7	37	23.4
100					

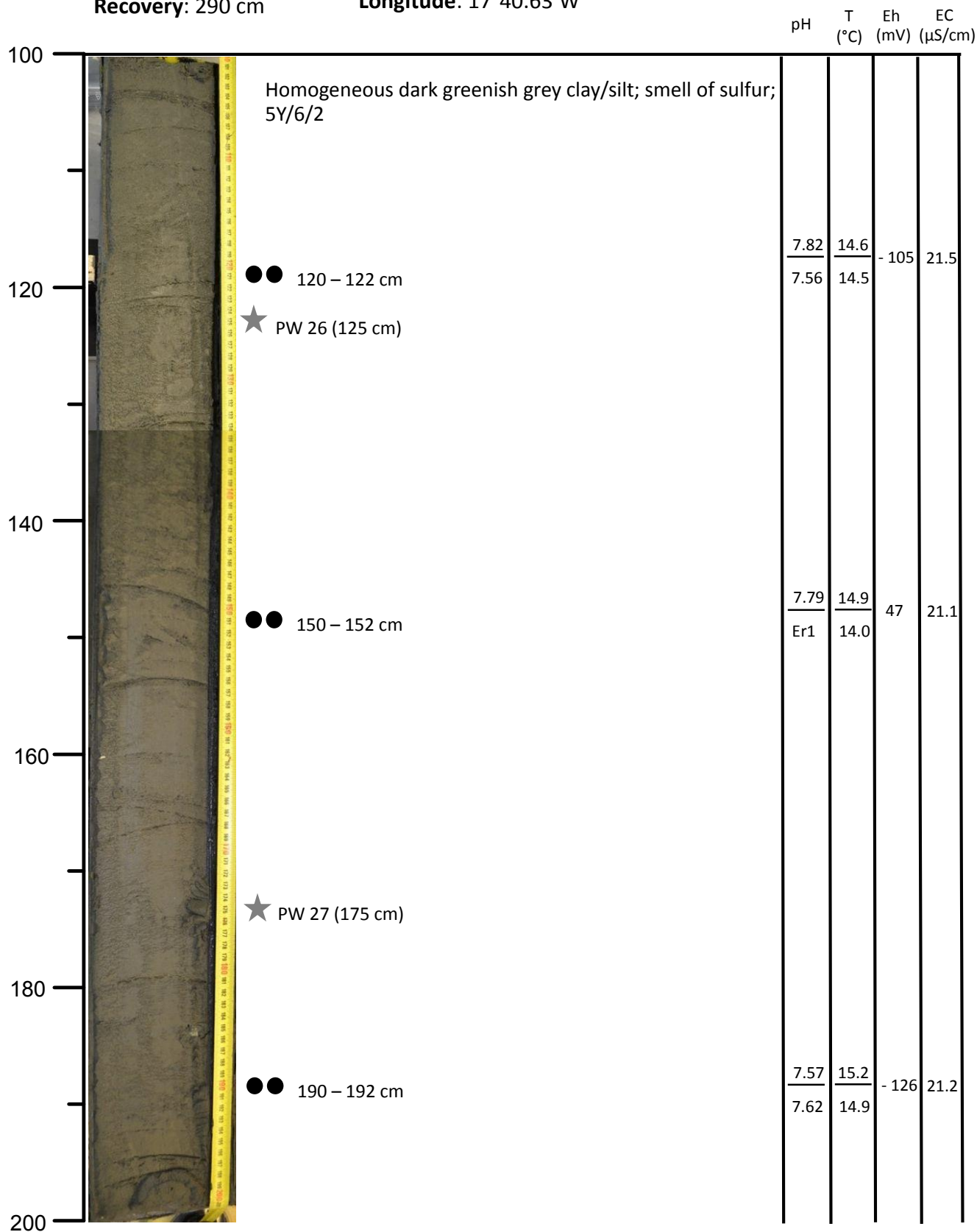
Core: POS524/04GC

Core section: B (2 of 3)

Latitude: 66°36.44'N

Recovery: 290 cm

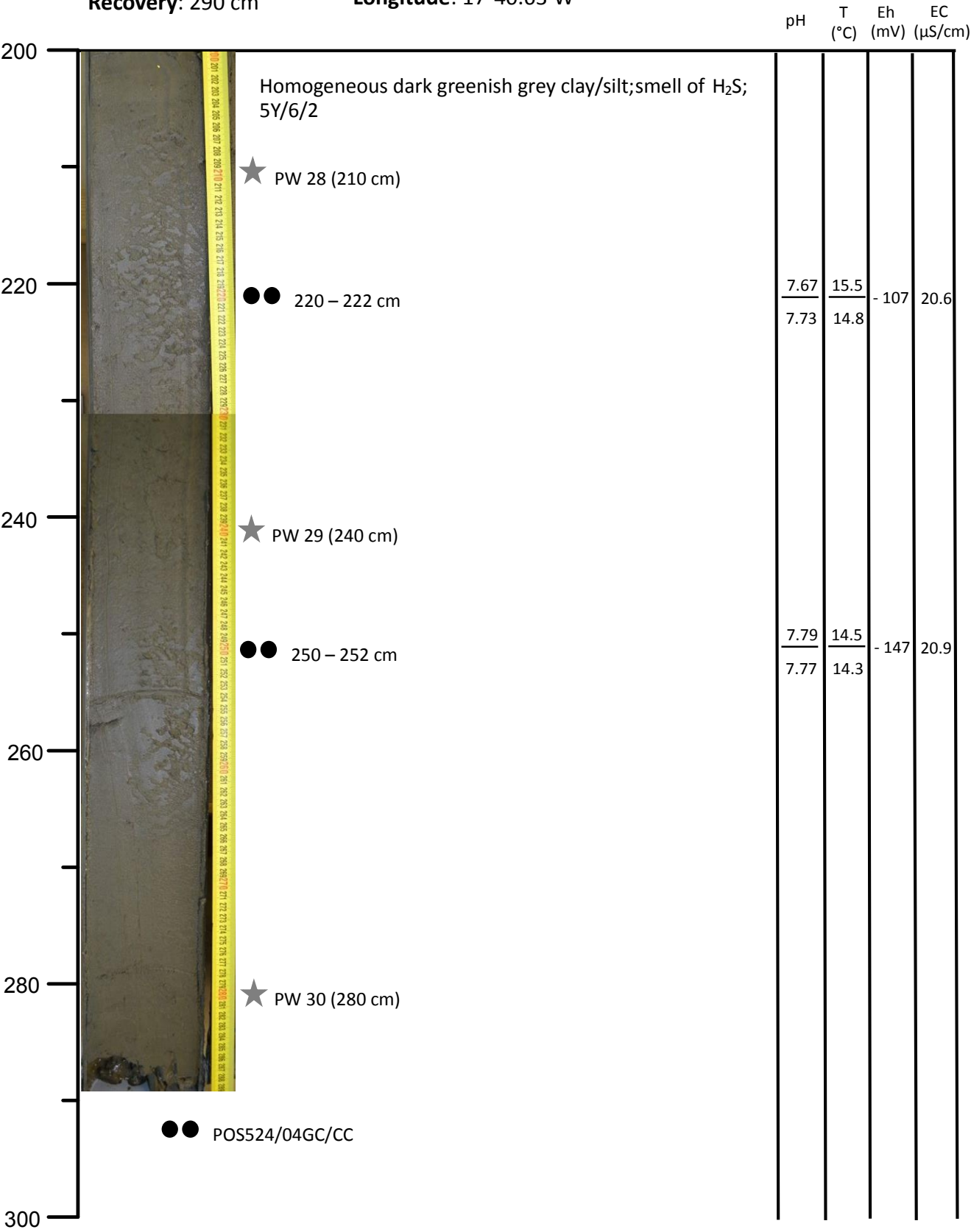
Longitude: 17°40.63'W



Core: POS524/04GC

Core section: A (3 of 3)
Recovery: 290 cm

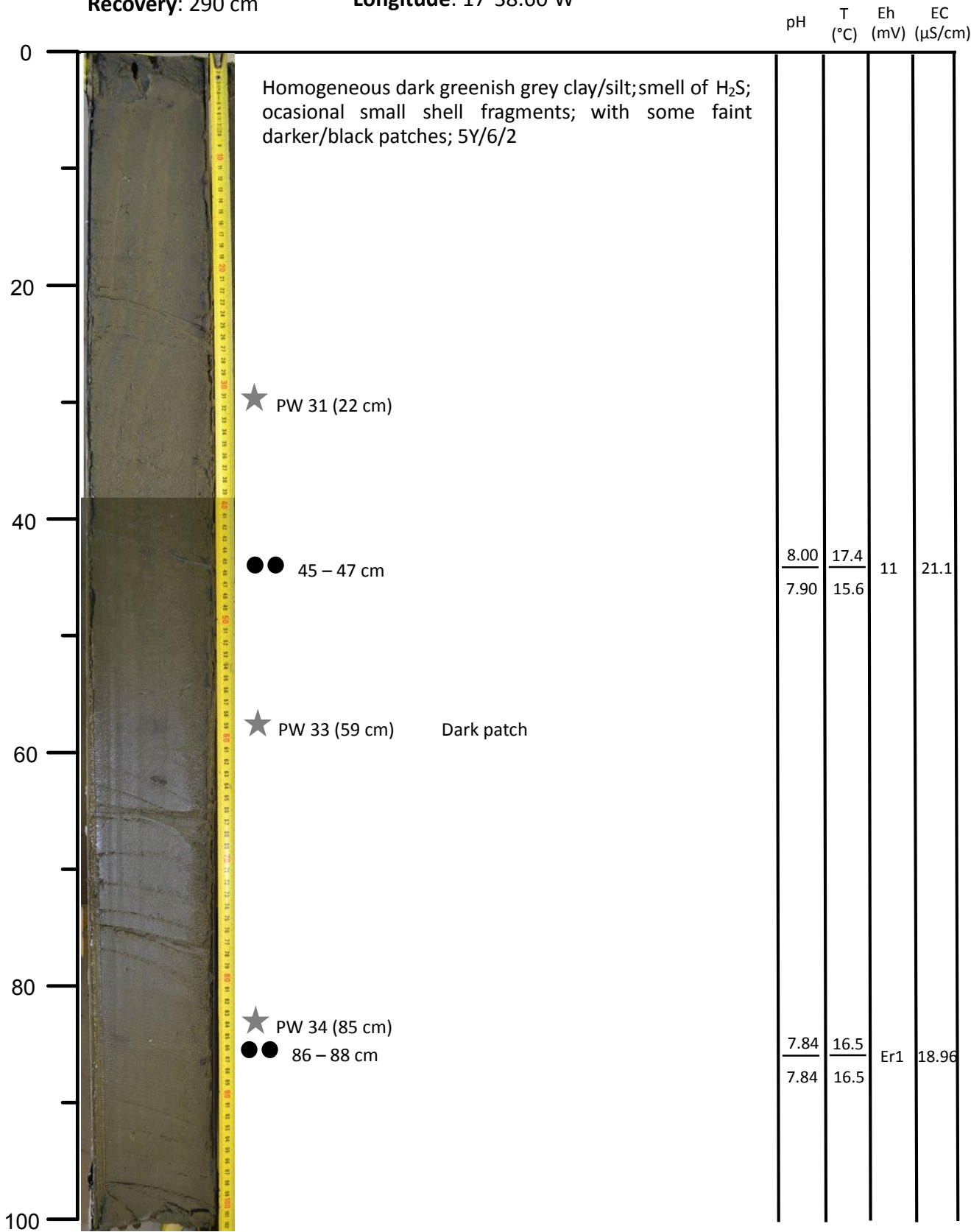
Latitude: 66°36.44'N
Longitude: 17°40.63'W



Core: POS524/05GC

Core section: C (1 of 3)
Recovery: 290 cm

Latitude: 66°37.60'N
Longitude: 17°38.60'W



Core: POS524/05GC


Core section: B (2 of 3)

Latitude: 66°37.60'N

Recovery: 290 cm

Longitude: 17°38.60'W

pH T Eh EC
(°C) (mV) (μS/cm)

101	 <p>Homogeneous dark greenish grey clay/silt; smell of H₂S; occasional small shell fragments; with some faint darker/black patches; 5Y/6/2</p> <p>★ PW 35 (130 cm)</p> <p>● ● 135 – 137 cm</p> <p>★ PW 36 (187 cm)</p> <p>● ● 189 – 191 cm</p>				
121					
141		7.95	16.2	- 4	22.8
		7.83	16.0		
161					
181		7.85	16.8	- 137	18.79
		7.72	16.2		
201					

Core: POS524/05GC

Core section: A (3 of 3)
Recovery: 290 cm

Latitude: 66°37.60'N
Longitude: 17°38.60'W

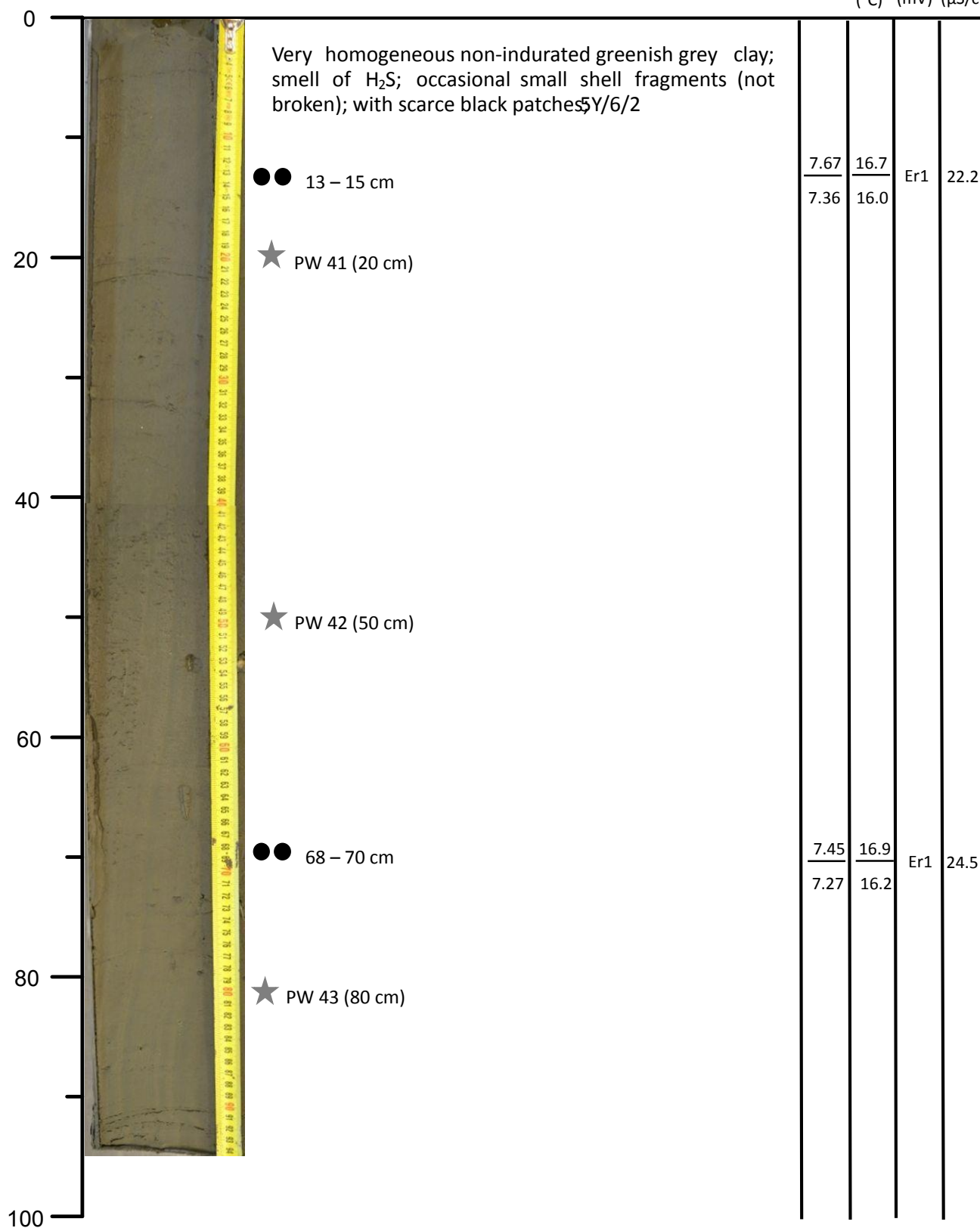
			pH	T (°C)	Eh (mV)	EC (µS/cm)
201		Homogeneous dark greenish grey clay/silt; smell of H ₂ S; occasional small shell fragments; with some faint darker/black patches; 5Y/6/2				
221						
		●● 228 – 230 cm ★ PW 37 (230 cm) Anhydrite fragments ??	7.77 7.64	16.9 16.1	- 239	23.4
241						
		●● 245 – 247 cm ★ PW 38 (248 cm)	7.83 7.85	16.7 16.4	- 11	16.91
261						
281		★ PW 39 (283 cm)				
		●● POS524/05GC/CC				
301						

GEOMAR
Helmholtz Centre for Ocean Research Kiel

Latitude: 66°36.41'N

Longitude: 17°38.65'W

pH	T (°C)	Eh (mV)	EC (μS/cm)
----	-----------	------------	---------------



Core: POS524/06GC

Core section: B (2 of 3)

Latitude: 66°36.41'N

Recovery: 288 cm

Longitude: 17°38.65'W

			pH	T (°C)	Eh (mV)	EC (µS/cm)
95	Very homogeneous non-indurated greenish grey clay; smell of H ₂ S ; with scarce black patches; 5Y/6/2					
115	●● 117 – 119 cm		7.54	17.3	- 273	21.5
	★ PW 44 (120 cm)		7.50	16.3		
135						
155	★ PW 45 (150 cm)		7.60	17.7	- 187	25.4
	●● 151 – 153 cm		7.37	17.2		
175						
	★ PW 46 (181 cm)		7.41	17.7	- 90	22.7
	●● 182 – 184 cm		7.37	17.1		
195						

Core: POS524/06GC

Core section: A (3 of 3)
Recovery: 288 cm

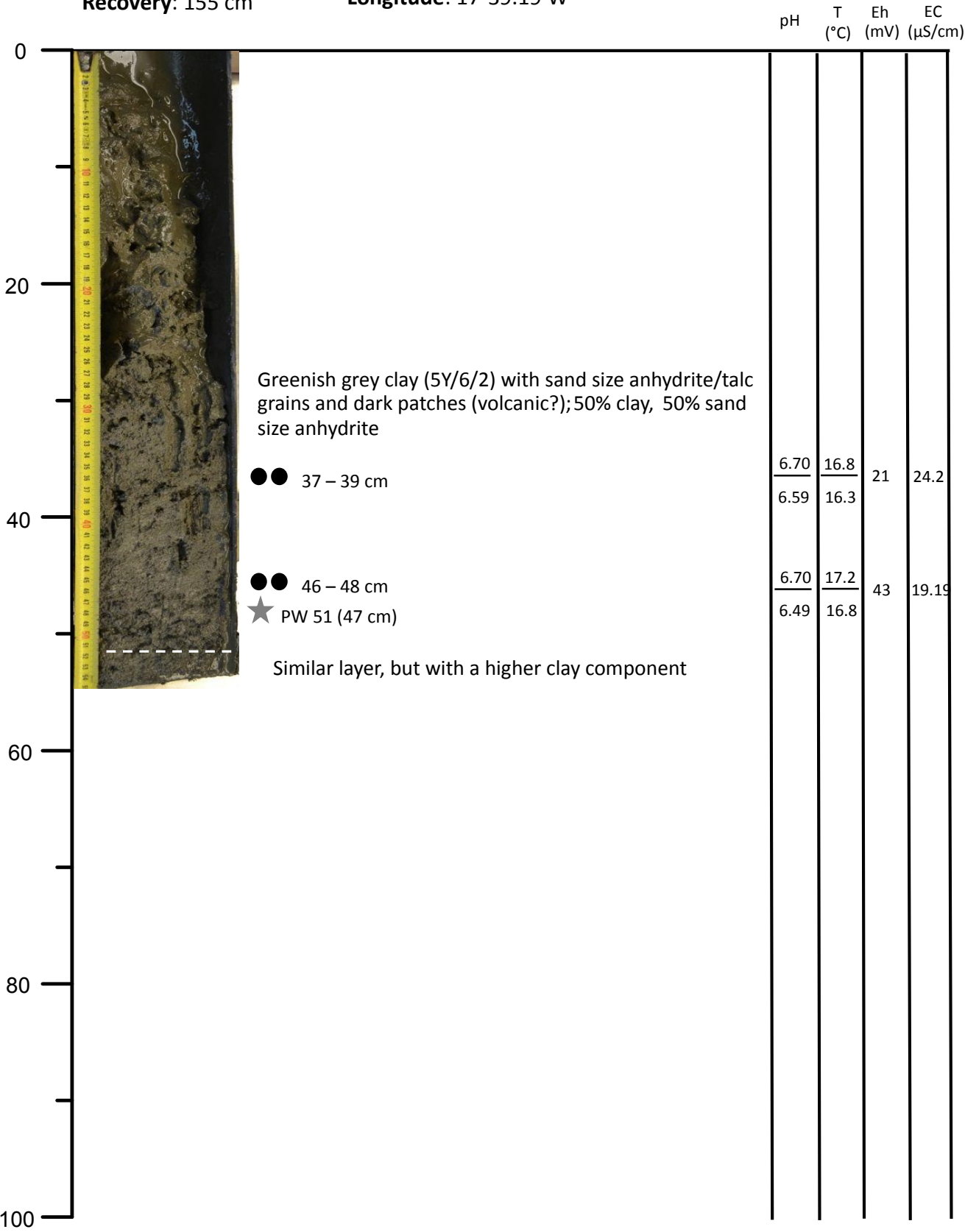
Latitude: 66°36.41'N
Longitude: 17°38.65'W

			pH	T (°C)	Eh (mV)	EC (µS/cm)
195	Very homogeneous non-indurated greenish grey clay; with scarce black patches; smell of H_2S ; 5Y/6/2					
215	★ PW 47 (261.5 cm)					
	●● 218 – 220 cm		7.41	17.5	-196	20.2
			7.22	17.8		
235						
	●● 248 – 250 cm		7.23	19.1	-132	23.2
			7.18	16.5		
255	★ PW 49 (260.5 cm)					
275	★ PW 50 (280 cm)					
	●● POS524/6GC/CC					
295						

Core: POS524/07GC

Core section: B (1 of 2)
Recovery: 155 cm

Latitude: 66°36.19'N
Longitude: 17°39.19'W



Core: POS524/07GC

Core section: A (2 of 2)

Latitude: 66°36.19'N

Recovery: 155 cm

Longitude: 17°39.19'W

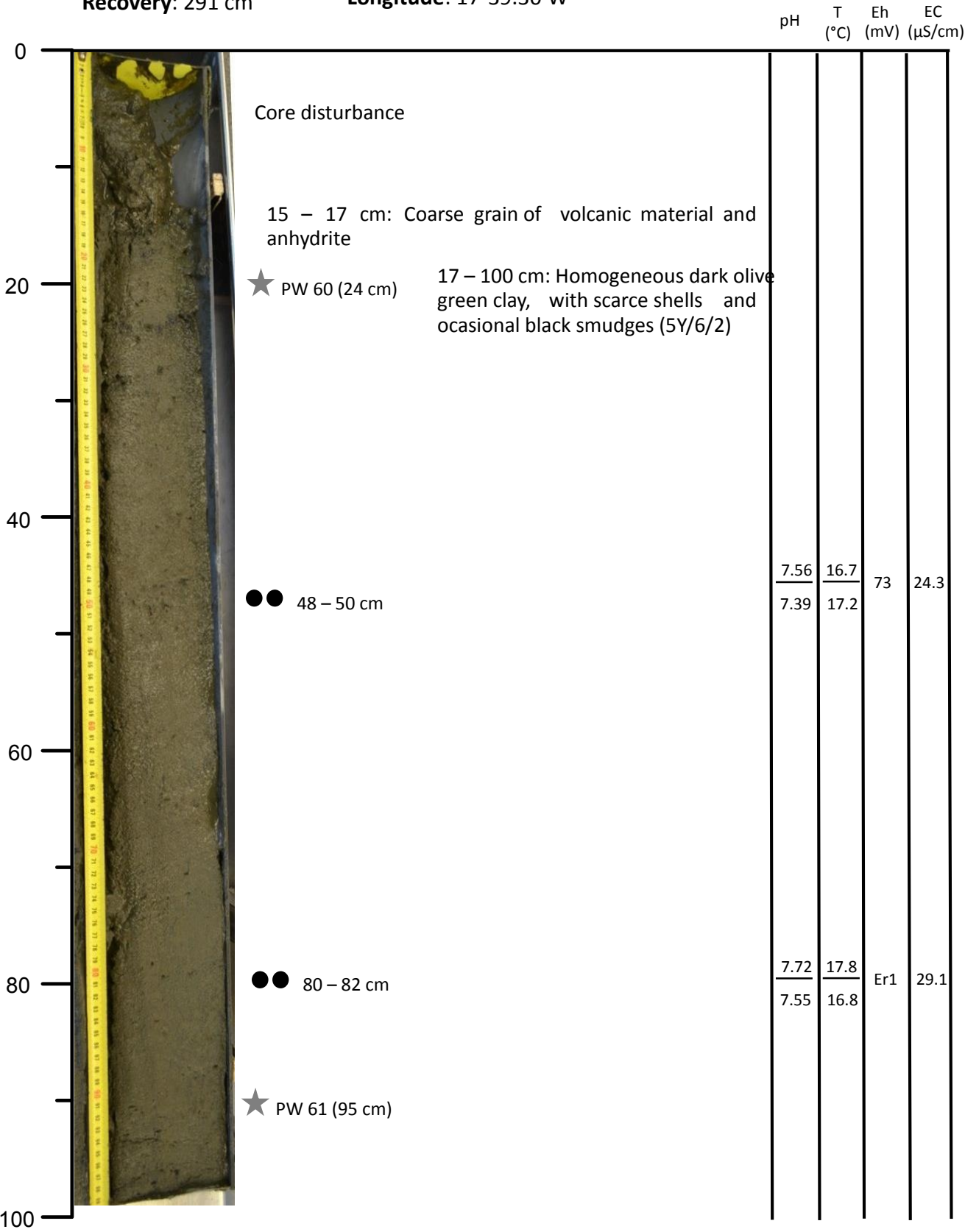
pH T (°C) Eh (mV) EC (μS/cm)

55	Greenish grey clay (5Y/6/2) with sand size anhydrite/talc grains and volcanic fragments; 40% clay, 60% sand size particle				
	★ PW 52 (63 cm) 62 – 66 cm: coarser layer of anhydrite fragments				
75	73.5 – 85 cm: Olive green layer (5Y/6/2) richer in clay	5.84	19.6	162	26.1
	●● 79 – 81 cm	5.50	19.4		
	★ PW 53 (80 cm)				
	●● 87 – 89 cm 85 – 92.5 cm: Coarse brownish layer with sand to coarse anhydrite and talc fragments	5.66	20.2	130	25.6
	★ PW 54 (89 cm)	5.71	20.1		
95	●● 95 – 97 cm 92.5 – 102 cm: Olive green layer (5Y/6/2) with small volcanic and anhydrite fragments; coarse brownish layer with anhydrite fragments at the bottom	5.95	21.2	213	17.97
	★ PW 55 (101 cm)	5.71	21.1		
	102 – 120 cm: Indurated green homogeneous clay with anhydrite and volcanic sand size fragments				
	★ PW 57 (110 cm)	5.76	23.1	- 34	20.91
	●● 110 – 112 cm	5.98	22.3		
115	120 – 124 cm: Coarse anhydrite sand layer; brown on top and whiteish on the bottom				
	●● 125 – 127 cm 124 – 138 cm: Grey clay layer with dispersed anhydrite fragments; 2.5YR/6/5; coarser anhydrite sand layer between 129 and 130 cm	5.62	23.6	129	21.9
		5.57	22.7		
	●● 133 – 135 cm	5.99	22.8	165	23.1
		5.96	22.4		
135	138 - 150 cm: Grey clay layer with dispersed anhydrite fragments; 2.5YR/6/5; coarser anhydrite sand layer between 129 and 130 cm				
155	●● POS524/07GC/CC				

Core: POS524/08GC

Core section: C (1 of 3)
Recovery: 291 cm

Latitude: 66°36.32'N
Longitude: 17°39.30'W



Core: POS524/08GC

Core section: B (2 of 3)

Latitude: 66°36.32'N

Recovery: 291 cm

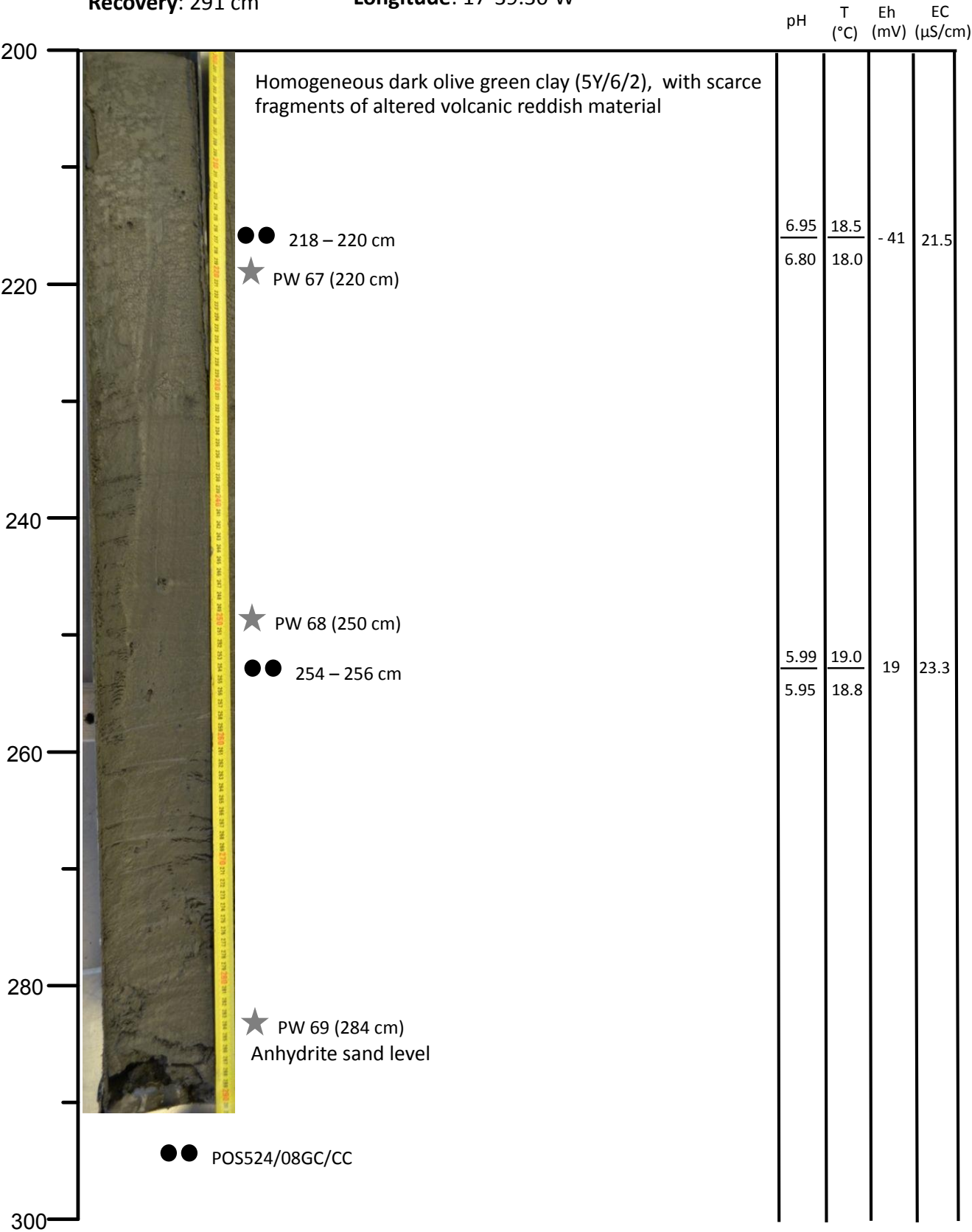
Longitude: 17°39.30'W

		pH	T (°C)	Eh (mV)	EC (μS/cm)
100	100 - 132 cm: Homogeneous dark olive green clay, with scarce anhydrite fragments (5Y/6/2)				
	●● 108 – 110 cm	7.70	17.8	79	23.3
		7.46	16.7		
	★ PW 62 (115 cm)				
120					
	132 – 155 cm: Dark olive green (5Y/6/2) clay with abundant fragments of coarse anhydrite (< 0.5 cm)				
	★ PW 63 (142 cm)				
	●● 147 – 149 cm	7.49	18.6	Er1	20.71
		7.40	17.3		
	●● 155 – 157 cm	7.54	18.1	- 88	20.2
	★ PW 65 (156 cm)	7.53	17.7		
	●● 158.5 – 160.5 cm	7.71	18.2	103	Er1
		7.42	17.7		
	155 - 200 cm: Dark olive green (5Y/6/2) clay, with rhythmic intercalations of coarse anhydrite/talc, not always continuous (also in lens)				
	★ PW 66 (175 cm)				
180					
	●● 190 – 192 cm	7.47	18.6	90	19.5
	To the bottom the clay becomes more compact and with less anhydrite/talc fragments	7.19	18.6		
200					

Core: POS524/08GC

Core section: A (3 of 3)
Recovery: 291 cm

Latitude: 66°36.32'N
Longitude: 17°39.30'W



9.4. Pore Fluid Samples

Sample	Core	Depth	Sample	Core	Depth
POS524_PoreWater_001	01GC/C	32.5	POS524_PoreWater_031	05GC/C	22.0
POS524_PoreWater_002	01GC/C	57.0	POS524_PoreWater_032	blank	blank
POS524_PoreWater_003	01GC/C	79.5	POS524_PoreWater_033	05GC/C	59.0
POS524_PoreWater_004	01GC/C	97.5	POS524_PoreWater_034	05GC/C	85.0
POS524_PoreWater_005	01GC/B	134.5	POS524_PoreWater_035	05GC/B	130.0
POS524_PoreWater_006	01GC/B	144.0	POS524_PoreWater_036	05GC/B	187.0
POS524_PoreWater_007	01GC/B	164.0	POS524_PoreWater_037	05GC/A	230.0
POS524_PoreWater_008	blank	blank	POS524_PoreWater_038	05GC/A	248.0
POS524_PoreWater_009	01GC/A	270.0	POS524_PoreWater_039	05GC/A	283.0
POS524_PoreWater_010	02GC/C	34.0	POS524_PoreWater_040	blank	blank
POS524_PoreWater_011	02GC/C	54.5	POS524_PoreWater_041	06GC/C	20.0
POS524_PoreWater_012	02GC/C	72.0	POS524_PoreWater_042	06GC/C	50.0
POS524_PoreWater_013	02GC/C	96.0	POS524_PoreWater_043	06GC/C	80.0
POS524_PoreWater_014	02GC/B	139.5	POS524_PoreWater_044	06GC/B	120.0
POS524_PoreWater_015	02GC/B	179.5	POS524_PoreWater_045	06GC/B	150.0
POS524_PoreWater_016	blank	blank	POS524_PoreWater_046	06GC/B	181.0
POS524_PoreWater_017	02GC/A	219.0	POS524_PoreWater_047	06GC/A	216.5
POS524_PoreWater_018	02GC/A	250.0	POS524_PoreWater_048	blank	blank
POS524_PoreWater_019	02GC/A	280.0	POS524_PoreWater_049	06GC/A	260.5
POS524_PoreWater_020	03GC	50.0	POS524_PoreWater_050	06GC/A	280.0
POS524_PoreWater_021	03GC	85.0	POS524_PoreWater_051	07GC/B	47.0
POS524_PoreWater_022	03GC	95	POS524_PoreWater_052	07GC/A	63.0
POS524_PoreWater_023	04GC/C	30.0	POS524_PoreWater_053	07GC/A	80.0
POS524_PoreWater_024	blank	blank	POS524_PoreWater_054	07GC/A	89.0
POS524_PoreWater_025	04GC/C	70.0	POS524_PoreWater_055	07GC/A	101.0
POS524_PoreWater_026	04GC/B	125.0	POS524_PoreWater_056	blank	blank
POS524_PoreWater_027	04GC/B	175.0	POS524_PoreWater_057	07GC/A	110.0
POS524_PoreWater_028	04GC/A	210.0	POS524_PoreWater_058	07GC/A	123.0
POS524_PoreWater_029	04GC/A	240.0	POS524_PoreWater_059	07GC/A	135.0
POS524_PoreWater_030	04GC/A	280.0	POS524_PoreWater_060	08GC/C	24.0
			POS524_PoreWater_061	08GC/C	92.0
			POS524_PoreWater_062	08GC/B	115.0
			POS524_PoreWater_063	08GC/B	142.0
			POS524_PoreWater_064	blank	blank
			POS524_PoreWater_065	08GC/B	156.0
			POS524_PoreWater_066	08GC/B	175.0
			POS524_PoreWater_067	08GC/A	220.0
			POS524_PoreWater_068	08GC/A	250.0
			POS524_PoreWater_069	08GC/A	284.0

GEOMAR Reports

No.	Title
1	FS POSEIDON Fahrtbericht / Cruise Report POS421, 08. – 18.11.2011, Kiel - Las Palmas, Ed.: T.J. Müller, 26 pp, DOI: 10.3289/GEOMAR_REP_NS_1_2012
2	Nitrous Oxide Time Series Measurements off Peru – A Collaboration between SFB 754 and IMARPE –, Annual Report 2011, Eds.: Baustian, T., M. Graco, H.W. Bange, G. Flores, J. Ledesma, M. Sarmiento, V. Leon, C. Robles, O. Moron, 20 pp, DOI: 10.3289/GEOMAR_REP_NS_2_2012
3	FS POSEIDON Fahrtbericht / Cruise Report POS427 – Fluid emissions from mud volcanoes, cold seeps and fluid circulation at the Don- ₂ Kuban deep sea fan (Kerch peninsula, Crimea, Black Sea) – 23.02. – 19.03.2012, Burgas, Bulgaria - Heraklion, Greece, Ed.: J. Bialas, 32 pp, DOI: 10.3289/GEOMAR_REP_NS_3_2012
4	RV CELTIC EXPLORER EUROFLEETS Cruise Report, CE12010 – ECO2@NorthSea, 20.07. – 06.08.2012, Bremerhaven – Hamburg, Eds.: P. Linke et al., 65 pp, DOI: 10.3289/GEOMAR_REP_NS_4_2012
5	RV PELAGIA Fahrtbericht / Cruise Report 64PE350/64PE351 – JEDDAH-TRANSECT –, 08.03. – 05.04.2012, Jeddah – Jeddah, 06.04 - 22.04.2012, Jeddah – Duba, Eds.: M. Schmidt, R. Al-Farawati, A. Al-Aidaros, B. Kürten and the shipboard scientific party, 154 pp, DOI: 10.3289/GEOMAR_REP_NS_5_2013
6	RV SONNE Fahrtbericht / Cruise Report SO225 - MANIHIKI II Leg 2 The Manihiki Plateau - Origin, Structure and Effects of Oceanic Plateaus and Pleistocene Dynamic of the West Pacific Warm Water Pool, 19.11.2012 - 06.01.2013 Suva / Fiji – Auckland / New Zealand, Eds.: R. Werner, D. Nürnberg, and F. Hauff and the shipboard scientific party, 176 pp, DOI: 10.3289/GEOMAR_REP_NS_6_2013
7	RV SONNE Fahrtbericht / Cruise Report SO226 – CHRIMP CHatham RIse Methane Pockmarks, 07.01. - 06.02.2013 / Auckland – Lyttleton & 07.02. – 01.03.2013 / Lyttleton – Wellington, Eds.: Jörg Bialas / Ingo Klaucke / Jasmin Mögeltönder, 126 pp, DOI: 10.3289/GEOMAR_REP_NS_7_2013
8	The SUGAR Toolbox - A library of numerical algorithms and data for modelling of gas hydrate systems and marine environments, Eds.: Elke Kossel, Nikolaus Bigalke, Elena Piñero, Matthias Haeckel, 168 pp, DOI: 10.3289/GEOMAR_REP_NS_8_2013
9	RV ALKOR Fahrtbericht / Cruise Report AL412, 22.03.-08.04.2013, Kiel – Kiel. Eds: Peter Linke and the shipboard scientific party, 38 pp, DOI: 10.3289/GEOMAR_REP_NS_9_2013
10	Literaturrecherche, Aus- und Bewertung der Datenbasis zur Meerforelle (<i>Salmo trutta trutta</i> L.) Grundlage für ein Projekt zur Optimierung des Meerforellenmanagements in Schleswig-Holstein. Eds.: Christoph Petereit, Thorsten Reusch, Jan Dierking, Albrecht Hahn, 158 pp, DOI: 10.3289/GEOMAR_REP_NS_10_2013
11	RV SONNE Fahrtbericht / Cruise Report SO227 TAIFLUX, 02.04. – 02.05.2013, Kaohsiung – Kaohsiung (Taiwan), Christian Berndt, 105 pp, DOI: 10.3289/GEOMAR_REP_NS_11_2013
12	RV SONNE Fahrtbericht / Cruise Report SO218 SHIVA (Stratospheric Ozone: Halogens in a Varying Atmosphere), 15.-29.11.2011, Singapore - Manila, Philippines, Part 1: SO218- SHIVA Summary Report (in German), Part 2: SO218- SHIVA English reports of participating groups, Eds.: Birgit Quack & Kirstin Krüger, 119 pp, DOI: 10.3289/GEOMAR_REP_NS_12_2013
13	KIEL276 Time Series Data from Moored Current Meters. Madeira Abyssal Plain, 33°N, 22°W, 5285 m water depth, March 1980 – April 2011. Background Information and Data Compilation. Eds.: Thomas J. Müller and Joanna J. Waniek, 239 pp, DOI: 10.3289/GEOMAR_REP_NS_13_2013

GEOMAR Reports

No.	Title
14	RV POSEIDON Fahrtbericht / Cruise Report POS457: ICELAND HAZARDS Volcanic Risks from Iceland and Climate Change: The Late Quaternary to Anthropogenic Development Reykjavík / Iceland – Galway / Ireland, 7.-22. August 2013. Eds.: Reinhard Werner, Dirk Nürnberg and the shipboard scientific party, 88 pp, DOI: 10.3289/GEOMAR_REP_NS_14_2014
15	RV MARIA S. MERIAN Fahrtbericht / Cruise Report MSM-34 / 1 & 2, SUGAR Site, Varna – Varna, 06.12.13 – 16.01.14. Eds: Jörg Bialas, Ingo Klauke, Matthias Haeckel, 111 pp, DOI: 10.3289/GEOMAR_REP_NS_15_2014
16	RV POSEIDON Fahrtbericht / Cruise Report POS 442, "AUVinTYS" High-resolution geological investigations of hydrothermal sites in the Tyrrhenian Sea using the AUV "Abyss", 31.10. – 09.11.12, Messina – Messina, Ed.: Sven Petersen, 32 pp, DOI: 10.3289/GEOMAR_REP_NS_16_2014
17	RV SONNE, Fahrtbericht / Cruise Report, SO 234/1, "SPACES": Science or the Assessment of Complex Earth System Processes, 22.06. – 06.07.2014, Walvis Bay / Namibia - Durban / South Africa, Eds.: Reinhard Werner and Hans-Joachim Wagner and the shipboard scientific party, 44 pp, DOI: 10.3289/GEOMAR_REP_NS_17_2014
18	RV POSEIDON Fahrtbericht / Cruise Report POS 453 & 458, "COMM3D", Crustal Structure and Ocean Mixing observed with 3D Seismic Measurements, 20.05. – 12.06.2013 (POS453), Galway, Ireland – Vigo, Portugal, 24.09. – 17.10.2013 (POS458), Vigo, Portugal – Vigo, Portugal, Eds.: Cord Papenberg and Dirk Klaeschen, 66 pp, DOI: 10.3289/GEOMAR_REP_NS_18_2014
19	RV POSEIDON, Fahrtbericht / Cruise Report, POS469, "PANAREA", 02. – 22.05.2014, (Bari, Italy – Malaga, Spain) & Panarea shallow-water diving campaign, 10. – 19.05.2014, Ed.: Peter Linke, 55 pp, DOI: 10.3289/GEOMAR_REP_NS_19_2014
20	RV SONNE Fahrtbericht / Cruise Report SO234-2, 08.-20.07.2014, Durban, -South Africa - Port Louis, Mauritius, Eds.: Kirstin Krüger, Birgit Quack and Christa Marandino, 95 pp, DOI: 10.3289/GEOMAR_REP_NS_20_2014
21	RV SONNE Fahrtbericht / Cruise Report SO235, 23.07.-07.08.2014, Port Louis, Mauritius to Malé, Maldives, Eds.: Kirstin Krüger, Birgit Quack and Christa Marandino, 76 pp, DOI: 10.3289/GEOMAR_REP_NS_21_2014
22	RV SONNE Fahrtbericht / Cruise Report SO233 WALVIS II, 14.05-21.06.2014, Cape Town, South Africa - Walvis Bay, Namibia, Eds.: Kaj Hoernle, Reinhard Werner, and Carsten Lüter, 153 pp, DOI: 10.3289/GEOMAR_REP_NS_22_2014
23	RV SONNE Fahrtbericht / Cruise Report SO237 Vema-TRANSIT Bathymetry of the Vema-Fracture Zone and Puerto Rico Trench and Abyssal Atlantic Biodiversity Study, Las Palmas (Spain) - Santo Domingo (Dom. Rep.) 14.12.14 - 26.01.15, Ed.: Colin W. Devey, 130 pp, DOI: 10.3289/GEOMAR_REP_NS_23_2015
24	RV POSEIDON Fahrtbericht / Cruise Report POS430, POS440, POS460 & POS467 Seismic Hazards to the Southwest of Portugal; POS430 - La-Seyne-sur-Mer - Portimao (7.4. - 14.4.2012), POS440 - Lisbon - Faro (12.10. - 19.10.2012), POS460 - Funchal - Portimao (5.10. - 14.10.2013), POS467 - Funchal - Portimao (21.3. - 27.3.2014), Ed.: Ingo Grevemeyer, 43 pp, DOI: 10.3289/GEOMAR_REP_NS_24_2015
25	RV SONNE Fahrtbericht / Cruise Report SO239, EcoResponse Assessing the Ecology, Connectivity and Resilience of Polymetallic Nodule Field Systems, Balboa (Panama) – Manzanillo (Mexico), 11.03. -30.04.2015, Eds.: Pedro Martínez Arbizu and Matthias Haeckel, 204 pp, DOI: 10.3289/GEOMAR_REP_NS_25_2015

GEOMAR Reports

No.	Title
26	RV SONNE Fahrtbericht / Cruise Report SO242-1, JPI OCEANS Ecological Aspects of Deep-Sea Mining, DISCOL Revisited, Guayaquil - Guayaquil (Ecuador), 29.07.-25.08.2015, Ed.: Jens Greinert, 290 pp, DOI: 10.3289/GEOMAR_REP_NS_26_2015
27	RV SONNE Fahrtbericht / Cruise Report SO242-2, JPI OCEANS Ecological Aspects of Deep-Sea Mining DISCOL Revisited, Guayaquil - Guayaquil (Ecuador), 28.08.-01.10.2015, Ed.: Antje Boetius, 552 pp, DOI: 10.3289/GEOMAR_REP_NS_27_2015
28	RV POSEIDON Fahrtbericht / Cruise Report POS493, AUV DEDAVE Test Cruise, Las Palmas - Las Palmas (Spain), 26.01.-01.02.2016, Ed.: Klas Lackschewitz, 17 pp, DOI: 10.3289/GEOMAR_REP_NS_28_2016
29	Integrated German Indian Ocean Study (IGIOS) - From the seafloor to the atmosphere - A possible German contribution to the International Indian Ocean Expedition 2 (IIOE-2) programme - A Science Prospectus, Eds.: Bange, H.W. , E.P. Achterberg, W. Bach, C. Beier, C. Berndt, A. Biastoch, G. Bohrmann, R. Czeschel, M. Dengler, B. Gaye, K. Haase, H. Herrmann, J. Lelieveld, M. Mohtadi, T. Rixen, R. Schneider, U. Schwarz-Schampera, J. Segsneider, M. Visbeck, M. Voß, and J. Williams, 77pp, DOI: 10.3289/GEOMAR_REP_NS_29_2016
30	RV SONNE Fahrtbericht / Cruise Report SO249, BERING – Origin and Evolution of the Bering Sea: An Integrated Geochronological, Volcanological, Petrological and Geochemical Approach, Leg 1: Dutch Harbor (U.S.A.) - Petropavlovsk-Kamchatsky (Russia), 05.06.2016-15.07.2016, Leg 2: Petropavlovsk-Kamchatsky (Russia) - Tomakomai (Japan), 16.07.2016-14.08.2016, Eds.: Reinhard Werner, et al., DOI: 10.3289/GEOMAR_REP_NS_30_2016
31	RV POSEIDON Fahrtbericht/ Cruise Report POS494/2, HIERROSEIS Leg 2: Assessment of the Ongoing Magmatic-Hydrothermal Discharge of the El Hierro Submarine Volcano, Canary Islands by the Submersible JAGO, Valverde – Las Palmas (Spain), 07.02.-15.02.2016, Eds.: Hannington, M.D. and Shipboard Scientific Party, DOI: 10.3289/GEOMAR_REP_NS_31_2016
32	RV METEOR Fahrtbericht/ Cruise Report M127, Extended Version, Metal fluxes and Resource Potential at the Slow-spreading TAG Mid-ocean Ridge Segment (26°N, MAR) – Blue Mining@Sea, Bridgetown (Barbados) – Ponta Delgada (Portugal) 25.05.-28.06.2016, Eds.: Petersen, S. and Shipboard Scientific Party, DOI: 10.3289/GEOMAR_REP_NS_32_2016
33	RV SONNE Fahrtbericht/Cruise Report SO244/1, GeoSEA: Geodetic Earthquake Observatory on the Seafloor, Antofagasta (Chile) – Antofagasta (Chile), 31.10.-24.11.2015, Eds.: Jan Behrmann, Ingo Klaucke, Michal Stipp, Jacob Geersen and Scientific Crew SO244/1, DOI: 10.3289/GEOMAR_REP_NS_33_2016
34	RV SONNE Fahrtbericht/Cruise Report SO244/2, GeoSEA: Geodetic Earthquake Observatory on the Seafloor, Antofagasta (Chile) – Antofagasta (Chile), 27.11.-13.12.2015, Eds.: Heidrun Kopp, Dietrich Lange, Katrin Hannemann, Anne Krabbenhoeft, Florian Petersen, Anina Timmermann and Scientific Crew SO244/2, DOI: 10.3289/GEOMAR_REP_NS_34_2016
35	RV SONNE Fahrtbericht/Cruise Report SO255, VITIAZ – The Life Cycle of the Vitiaz-Kermadec Arc / Backarc System: from Arc Initiation to Splitting and Backarc Basin Formation, Auckland (New Zealand) - Auckland (New Zealand), 02.03.-14.04.2017, Eds.: Kaj Hoernle, Folkmar Hauff, and Reinhard Werner with contributions from cruise participants, DOI: 10.3289/GEOMAR_REP_NS_35_2017

GEOMAR Reports

No.	Title
36	RV POSEIDON Fahrtbericht/Cruise Report POS515, CALVADOS - CALabrian arc mud VolcAnoes: Deep Origin and internal Structure, Dubrovnik (Croatia) – Catania (Italy), 18.06.-13.07.2017, Eds.: M. Riedel, J. Bialas, A. Krabbenhoef, V. Bähre, F. Beeck, O. Candoni, M. Kühn, S. Muff, J. Rindfleisch, N. Stange, DOI: 10.3289/GEOMAR_REP_NS_36_2017
37	RV MARIA S. MERIAN Fahrtbericht/Cruise Report MSM63, PERMO, Southampton – Southampton (U.K.), 29.04.-25.05.2017, Eds.: Christian Berndt and Judith Elger with contributions from cruise participants C. Böttner, R. Gehrmann, J. Karstens, S. Muff, B. Pitcairn, B. Schramm, A. Lichtschlag, A.-M. Völsch, DOI: 10.3289/GEOMAR_REP_NS_37_2017
38	RV SONNE Fahrtbericht/Cruise Report SO258/1, INCON: The Indian - Antarctic Break-up Enigma, Fremantle (Australia) - Colombo (Sri Lanka), 07.06.-09.07.2017, 29.04.-25.05.2017, Eds.: Reinhard Werner, Hans-Joachim Wagner, and Folkmar Hauff with contributions from cruise participants, DOI: 10.3289/GEOMAR_REP_NS_38_2017
39	RV POSEIDON Fahrtbericht/Cruise Report POS509, ElectroPal 2: Geophysical investigations of sediment hosted massive sulfide deposits on the Palinuro Volcanic Complex in the Tyrrhenian Sea, Malaga (Spain) – Catania (Italy), 15.02.-03.03.2017, Ed.: Sebastian Hölz, DOI: 10.3289/GEOMAR_REP_NS_39_2017
40	RV POSEIDON Fahrtbericht/Cruise Report POS518, Baseline Study for the Environmental Monitoring of Subseafloor CO ₂ Storage Operations, Leg 1: Bremerhaven – Bremerhaven (Germany), 25.09.-11.10.2017, Leg 2: Bremerhaven – Kiel (Germany), 12.10.-28.10.2017, Eds.: Peter Linke and Matthias Haeckel, DOI: 10.3289/GEOMAR_REP_NS_40_2018
41	RV MARIA S. MERIAN Fahrtbericht/Cruise Report MSM71, LOBSTER: Ligurian Ocean Bottom Seismology and Tectonics Research, Las Palmas (Spain) – Heraklion (Greece), 07.02.-27.02.2018, Eds.: H. Kopp, D. Lange, M. Thorwart, A. Paul, A. Dannowski, F. Petersen, C. Aubert, F. Beek, A. Beniest, S. Besançon, A. Brotzer, G. Caielli, W. Crawford, M. Deen, C. Lehmann, K. Marquardt, M. Neckel, L. Papanagnou, B. Schramm, P. Schröder, K.-P. Steffen, F. Wolf, Y. Xia, DOI: 10.3289/GEOMAR_REP_NS_41_2018
42	RV METEOR Fahrtbericht/Cruise Report M143, SLOGARO: Slope failures and active gas expulsion along the Romanian margin – investigating relations to gas hydrate distribution, Varna (Romania) – Heraklion (Greece), 12.12.-22.12.2017, Eds.: M. Riedel, F. Gausepohl, I. Gazis, L. Hähnel, M. Kampmeier, P. Urban, J. Bialas, DOI: 10.3289/GEOMAR_REP_NS_42_2018
43	RV POSEIDON Fahrtbericht/Cruise Report POS510, ANYDROS: Rifting and Hydrothermal Activity in the Cyclades Back-arc Basin, Catania (Italy) – Heraklion (Greece), 06.03.-29.03.2017, Ed.: M.D. Hannington, DOI: 10.3289/GEOMAR_REP_NS_43_2018
44	RV POSEIDON Fahrtbericht/Cruise Report POS524, GrimseyEM: Geophysical and geological investigations in the vicinity of the Grimsey Hydrothermal Field offshore Northern Iceland for the assessment of the geothermal potential and the exploration for potential mineralizations within the seafloor, Reykjavik (Iceland) – Bergen (Norway), 7.6 - 26.6.2018, Eds.: Sebastian Hölz and Sofia Martins, DOI: 10.3289/GEOMAR_REP_NS_44_2018

For GEOMAR Reports, please visit:

https://oceanrep.geomar.de/view/series/GEOMAR_Report.html

Reports of the former IFM-GEOMAR series can be found under:

https://oceanrep.geomar.de/view/series/IFM-GEOMAR_Report.html



Das GEOMAR Helmholtz-Zentrum für Ozeanforschung Kiel
ist Mitglied der Helmholtz-Gemeinschaft
Deutscher Forschungszentren e.V.

The GEOMAR Helmholtz Centre for Ocean Research Kiel
is a member of the Helmholtz Association of
German Research Centres

Helmholtz-Zentrum für Ozeanforschung Kiel / Helmholtz Centre for Ocean Research Kiel

GEOMAR
Dienstgebäude Westufer / West Shore Building
Düsternbrooker Weg 20
D-24105 Kiel
Germany

Helmholtz-Zentrum für Ozeanforschung Kiel / Helmholtz Centre for Ocean Research Kiel

GEOMAR
Dienstgebäude Ostufer / East Shore Building
Wischhofstr. 1-3
D-24148 Kiel
Germany

Tel.: +49 431 600-0
Fax: +49 431 600-2805
www.geomar.de